

Global Genetic Cartography of Urban Metagenomes and Anti-Microbial Resistance

David Danko^{1, 2, †}, Daniela Bezdán^{1, 2, †}, Ebrahim Afshinnekoo^{1, 2, *}, Sofia Ahsanuddin^{3, *}, Chandrima Bhattacharya^{1, 2, *}, Daniel J Butler^{1, 2, *}, Kern Rei Chng^{4, *}, Daisy Donnellan^{1, 2, *}, Jochen Hecht^{5, *}, Katelyn Jackson^{1, 2, *}, Katerina Kuchin^{1, 2, *}, Mikhail Karasikov^{6, *}, Abigail Lyons^{1, 2, *}, Lauren Mak^{1, 2, *}, Dmitry Meleshko^{1, 2, *}, Harun Mustafa^{6, *}, Beth Mutai^{8, 9, *}, Russell Y Neches^{7, *}, Amanda Ng^{4, *}, Olga Nikolayeva^{10, *}, Tatyana Nikolayeva^{10, *}, Eileen Png^{4, *}, Krista Ryon^{1, 2, *}, Jorge L Sanchez^{1, 2, *}, Heba Shaaban^{1, 2, *}, Maria A Sierra^{1, 2, *}, Dominique Thomas^{1, 2, *}, Ben Young^{1, 2, *}, Omar O. Abudayyeh^{11, *}, Josue Alicea^{1, 2, *}, Malay Bhattacharyya^{12, 13, *}, Ran Blekhman^{14, *}, Eduardo Castro-Nallar^{15, *}, Ana M Cañas^{1, 2, *}, Aspasia D Chatziefthimiou^{1, 2, *}, Robert W Crawford^{16, *}, Francesca De Filippis^{17, 18, *}, Youping Deng^{19, *}, Christelle Desnues^{20, *}, Emmanuel Dias-Neto^{21, *}, Marius Dybwad^{22, *}, Eran Elhaik^{23, *}, Danilo Ercolini^{17, 18, *}, Alina Frolova^{24, *}, Dennis Gankin^{11, *}, Jonathan S. Gootenberg^{11, *}, Alexandra B Graf^{25, *}, David C Green^{26, *}, Iman Hajirasouliha^{1, 2, *}, Mark Hernandez^{27, *}, Gregorio Iraola^{28, 29, 30, *}, Soojin Jang^{31, *}, Andre Kahles^{6, *}, Frank J Kelly^{26, *}, Kaymisha Knights^{1, 2, *}, Nikos C Kyrpides^{7, *}, Paweł P Łabaj^{59, *}, Patrick K H Lee^{32, *}, Marcus H Y Leung^{32, *}, Per Ljungdahl^{33, *}, Gabriella Mason-Buck^{26, *}, Ken McGrath^{34, *}, Cem Meydan^{1, 2, *}, Emmanuel F Mongodin^{35, *}, Milton Ozorio Moraes^{36, *}, Niranjan Nagarajan^{4, *}, Marina Nieto-Caballero^{27, *}, Houtan Noushmehr^{37, *}, Manuela Oliveira^{38, *}, Stephan Ossowski^{39, 40, *}, Olayinka O Osulale^{41, *}, Orhan Özcan^{45, *}, David Paez-Espino^{7, *}, Nicolas Rascovan^{42, *}, Hugues Richard^{43, *}, Gunnar Rättsch^{6, *}, Lynn M Schriml^{35, *}, Torsten Semmler^{44, *}, Osman U Sezerman^{45, *}, Leming Shi^{46, 47, *}, Tielu Shi^{48, *}, Le Huu Song^{49, *}, Haruo Suzuki^{50, *}, Denise Syndercombe Court^{26, *}, Scott W Tighe^{51, *}, Xinzhao Tong^{32, *}, Klas I Udekwi^{33, *}, Juan A Ugalde^{52, *}, Brandon Valentine^{1, 2, *}, Dimitar I Vassilev^{53, *}, Elena Vayndorf^{54, *}, Thirumalaisamy P Velavan^{55, *}, Jun Wu^{48, *}, María M Zambrano^{56, *}, Jifeng Zhu^{1, 2, *}, Sibozhu^{57, 58, *}, Christopher E Mason^{1, 2, ‡}, and The International MetaSUB Consortium*

†Equal contribution

*Listed alphabetically

‡Corresponding author

*Full list attached

¹Weill Cornell Medicine

²The Bin Talal Bin Abdulaziz Al Saud Institute for Computational Biomedicine

³Icahn School of Medicine at Mount Sinai

⁴Genome Institute of Singapore

⁵Centre for Genomic Regulation (CRG), The Barcelona Institute of Science and Technology, Barcelona, Spain

⁶ETH Zurich, Department of Computer Science, Biomedical Informatics Group

⁷Department of Energy, Joint Genome Institute, Walnut Creek, California 94598, USA.

⁸Kenya Medical Research Institute / US Army medical Research Directorate - Kenya

⁹Centre for Genomic Regulation (CRG), The Barcelona Institute of Science and Technology, Barcelona, Spain.

¹⁰ETH Zurich, Functional Genomics Center Zurich

¹¹Massachusetts Institute of Technology, McGovern Institute for Brain Research

¹²Machine Intelligence Unit, Indian Statistical Institute, Kolkata

¹³Centre for Artificial Intelligence and Machine Learning, Indian Statistical Institute, Kolkata

¹⁴University of Minnesota

¹⁵Universidad Andrés Bello, Center for Bioinformatics and Integrative Biology, Facultad de Ciencias de la Vida

¹⁶California State University Sacramento

- ¹⁷Department of Agricultural Sciences, Division of Microbiology, University of Naples Federico II
¹⁸Task Force on Microbiome Studies, University of Naples Federico II
¹⁹University of Hawaii John A. Burns School of Medicine
²⁰Aix-Marseille Université, Mediterranean Institute of Oceanology, Université de Toulon, CNRS, IRD, UM 110
²¹A.C. Camargo Cancer Center
²²Norwegian Defence Research Establishment FFI, Kjeller, Norway
²³Department of Animal Plant Sciences, University of Sheffield
²⁴Institute of Molecular Biology and Genetics of National Academy of Science of Ukraine
²⁵University of Applied Sciences Vienna
²⁶Department of Analytical, Environmental and Forensic Sciences
²⁷University of Colorado at Boulder
²⁸Microbial Genomics Laboratory, Institut Pasteur de Montevideo, Uruguay
²⁹Center for Integrative Biology, Universidad Mayor, Santiago de Chile, Chile
³⁰Wellcome Sanger Institute, Hinxton, United Kingdom
³¹Institut Pasteur Korea
³²School of Energy and Environment, City University of Hong Kong, Hong Kong SAR, China
³³Stockholm University
³⁴Microba
³⁵University of Maryland School of Medicine, Institute for Genome Sciences
³⁶Fundação Oswaldo Cruz
³⁷University of São Paulo, Ribeirão Preto Medical School
³⁸Instituto de Patologia e Imunologia Molecular da Universidade do Porto
³⁹Institute of Medical Genetics and Applied Genomics, University of Tübingen, Tübingen, Germany
⁴⁰Centre for Genomic Regulation (CRG), The Barcelona Institute of Science and Technology, Barcelona, Spain.
3) Universitat Pompeu Fabra, Barcelona, Spain.
⁴¹Applied Environmental Metagenomics and Infectious Diseases Research (AEMIDR), Department of Biological Sciences, Elizade University
⁴²Aix-Marseille Université, IRD, AP-HM, IHU Méditerranée Infection
⁴³Sorbonne University, Faculty of science, Institute of Biology Paris-Seine, Laboratory of Computational and Quantitative Biology
⁴⁴Robert Koch Institute Berlin
⁴⁵Acibadem Mehmet Ali Aydınlar University
⁴⁶Center for Pharmacogenomics, School of Life Sciences and Shanghai Cancer Center, Fudan University
⁴⁷State Key Laboratory of Genetic Engineering (SKLGE) and MOE Key Laboratory of Contemporary Anthropology, School of Life Sciences
⁴⁸The Center for Bioinformatics and Computational Biology, Shanghai Key Laboratory of Regulatory Biology, the Institute of Biomedical Sciences and School of Life Sciences, East China Normal University
⁴⁹Institute of Tropical Medicine, Vietnamese-German Center of Excellence
⁵⁰Keio University
⁵¹University of Vermont
⁵²Millennium Initiative for Collaborative Research on Bacterial Resistance
⁵³Faculty of Mathematics and Informatics, Sofia University "St. Kliment Ohridski"
⁵⁴Institute of Arctic Biology, University of Alaska Fairbanks
⁵⁵Institute of Tropical Medicine, Univeristätsklinikum Tübingen, Tübingen
⁵⁶Corporación Corpogen
⁵⁷State Key Laboratory of Genetic Engineering (SKLGE) and MOE Key Laboratory of Contemporary Anthropology, School of Life Sciences, Fudan University
⁵⁸. Department of Epidemiology, School of Public Health, Fudan University
⁵⁹Małopolska Centre of Biotechnology, Jagiellonian University

Abstract

1
2
3
4
5
6
7
8
9
10
11
12

We have created a global atlas of 4,728 metagenomic samples from mass-transit systems in 60 cities across 3 years. This is the first systematic, worldwide study cataloging the urban microbial ecosystem. We identify taxonomically-defined microorganisms collected across three years. This atlas provides an annotated, geospatial profile of microbial strains, functional characteristics AMR markers, and novel genetic elements, including 10,928 viral, 1302 bacteria, and 2 archaea novel species. We identify 4,424 species of urban microorganisms and a consistent "core" of 31 species found in nearly all samples that is largely distinct from any human commensal microbiome. Profiles of AMR genes show geographic variation in type and density. Together, these results constitute a high-resolution, global metagenomic atlas, which enables the discovery of new genetic components, highlights potential forensic applications, and provides an essential first draft of the global AMR burden of the world's cities.

13 **Keywords:** Built Environment, metagenome, global health, antimicrobial resistance

14 1 Introduction

15 The high-density urban environment has historically been home to only a fraction of all people, with
16 the majority living in rural areas or small villages. In the last two decades, the situation has reversed;
17 55% of the world’s population now lives in urban areas (Ritchie and Roser, 2020; United Nations, 2018).
18 Since the introduction of germ theory and John Snow’s work on cholera, it has been clear that people in
19 cities interact with microbes in ways that can be markedly different than in rural areas (Neiderud, 2015).
20 Microbes in the built environment have been implicated as a possible source of contagion (Cooley et al.,
21 1998) and certain syndromes, like allergies, are associated with increasing urbanization (Nicolaou et al.,
22 2005). It is now apparent that cities in general have an impact on human health though the mechanisms
23 of this impact are broadly variable and often little understood. Indeed, our understanding of microbial
24 dynamics in the urban environment outside of pandemics has only begun (Gilbert and Stephens, 2018).

25 Technological advances in next-generation sequencing (NGS) and metagenomics have created an
26 unprecedented opportunity for rapid, global studies of microorganisms and their hosts, providing re-
27 searchers, clinicians, and policymakers with a more comprehensive view of the functional dynamics of
28 microorganisms in a city. NGS facilitates culture-independent sampling of the microorganisms in an
29 area with the potential for both taxonomic and functional annotation; this is particularly important
30 for surveillance of microorganisms as they acquire antimicrobial resistance (AMR) (Fresia et al., 2019).
31 Metagenomic methods enable nearly real-time monitoring of organisms, AMR genes, and pathogens as
32 they emerge within a given geographical location, and have the potential to reveal hidden microbial
33 reservoirs and detect microbial transmission routes as they spread around the world (Zhu et al., 2017).
34 There are several different drivers and sources for AMR; including agriculture, farming, and livestock in
35 rural and suburban areas, household and industrial sewage, usage of antimicrobials, hard metals, and
36 biocides, as well as human and animal waste, all these factors contribute to the complexity of AMR
37 transmission (Allen et al., 2009; Martínez, 2008; Singer et al., 2016; Thanner et al., 2016; Venter et al.,
38 2017). A molecular map of urban environments will enable significant new research on the impact of
39 urban microbiomes on human health.

40 The United Nations projects that by 2050, over two-thirds of the world’s population will live in urban
41 areas (Ritchie and Roser, 2020). Consequently, urban transit systems - including subways and buses -
42 are a daily contact interface for billions of people who live in cities. Notably, urban travelers bring their
43 commensal microorganisms with them as they travel and come into contact with organisms and mobile
44 elements present in the environment, including AMR markers. The study of the urban microbiome and
45 the microbiome of the built environment spans several different projects and initiatives including work
46 focused on transit systems (Afshinnekoo et al., 2015; Hsu et al., 2016; Kang et al., 2018; Leung et al.,
47 2014; MetaSUB International Consortium. Mason et al., 2016), hospitals (Brooks et al., 2017; Lax et al.,
48 2017), soil (Hoch et al., 2019; Joyner et al., 2019), and sewage (Fresia et al., 2019; Maritz et al., 2019),
49 among others. However, these efforts for the most part have only been profiled with comprehensive
50 metagenomic methods in a few selected cities on a limited number of occasions. This leaves a gap
51 in scientific knowledge about a microbial ecosystem, with which the global human population readily
52 interacts. Human commensal microbiomes have been found to vary widely based on culture, and thus
53 the geography and geographically constrained studies may to miss key differences (Brito et al., 2016).
54 Moreover, data on urban microbes and AMR genes are urgently needed in developing nations, where
55 antimicrobial drug consumption is expected to rise by 67% by 2030 (United Nations, 2016; Van Boeckel
56 et al., 2015), both from changes in consumer demand for livestock products and an expanding use of
57 antimicrobials - both of which can alter AMR profiles of these cities.

58 The International Metagenomics and Metadesign of Subways and Urban Biomes (MetaSUB) Consor-
59 tium was launched in 2015 to address this gap in knowledge on the density, types, and dynamics of urban
60 metagenomes and AMR profiles. Since then, we have developed standardized collection and sequencing
61 protocols to process 4,728 samples across 60 cities worldwide (Table S1). Sampling took place at three
62 major time points: a pilot study in 2015-16 and two global city sampling days (gCSD, June 21st) in
63 2016 and 2017. Each sample was sequenced with 5-7M 125bp paired-end reads using Illumina NGS
64 sequencers (see Methods). To deal with the challenging analysis of our large dataset, we generated an
65 open-source analysis pipeline (MetaSUB Core Analysis Pipeline, CAP), which includes a comprehensive
66 set of state-of-the-art, peer-reviewed, metagenomic tools for taxonomic identification, k -mer analysis,
67 AMR gene prediction, functional profiling, de novo assembly, annotation of particular microbial species,
68 and geospatial mapping.

69 To our knowledge this study represents the first and largest global metagenomic study of urban
70 microbiomes - with a focus on transit systems - that reveals a consistent “core” urban microbiome across

71 all cities, as well as distinct geographic variation that may reflect epidemiological variation and that
72 enables a new forensic, source-tracking capabilities. More importantly, our data demonstrate that a
73 significant fraction of the urban microbiome remains to be characterized. Though 1,000 samples are
74 sufficient to discover roughly 80% of the observed taxa and AMR markers, we continued to observe
75 taxa and genes at an ongoing discovery rate of approximately one new species (previously non-observed)
76 and one new AMR marker for every 10 samples. Notably, this genetic variation is affected by various
77 environmental factors (e.g., climate, surface type, latitude, etc.) and samples show greater diversity near
78 the equator. Moreover, sequences associated with AMR markers are widespread, though not necessarily
79 abundant, and show geographic specificity. Here, we present the results of our global analyses and a
80 set of tools developed to access and analyze this extensive atlas, including: two interactive map-based
81 visualizations for samples (metasub.org/map) and AMRs (resistanceopen.org), an indexed search tool
82 over raw sequence data (dnaloc.ethz.ch/), a Git repository for all analytical pipelines and figures, and
83 application programming interfaces (APIs) for computationally accessing results ([github.com/metasub/](https://github.com/metasub/metasub_utils)
84 [metasub_utils](https://github.com/metasub/metasub_utils)).

85 2 Results

86 We have collected 4,728 samples from from the mass transit systems of 60 cities around the world
87 (Table 1, Supplementary table S1). These samples were collected from various common surfaces in the
88 mass transit systems such as railings, benches, and ticket kiosks and were subjected to metagenomic
89 sequencing. We use the microbiome of mass transit systems as a proxy for the urban microbiome as a
90 whole and present our key findings here.

91 2.1 A Core Urban Microbiome Centers Global Diversity

92 We first investigated the distribution of microbial species across the global urban environment. Specifi-
93 cally, we asked whether the urban environment represents a singular type of microbial ecosystem or a set
94 of related, but distinct, communities, especially in terms of biodiversity. We observed a bi-modal distri-
95 bution of taxa prevalence across our dataset, which we used to define two separate sets of taxa based on
96 the inflection points of the distribution: the putative “sub-core” set of urban microbial species that are
97 consistently observed (>70% of samples) and the less common “peripheral” (<25% of samples) species.
98 We also defined a set of true “core” taxa which occur in essentially all samples (>97% of samples). Apply-
99 ing these thresholds, we identified 1,145 microbial species (Figure 1C) that make up the sub-core urban
100 microbiome with 31 species in the true core microbiome (Figure 1A). Core and sub-core taxa classifica-
101 tions were further evaluated for sequence complexity and genome coverage on a subset of samples. Of
102 the 1,206 taxa with prevalence greater than 70%, 69 were flagged as being low quality classifications (see
103 methods). The sub-core microbiome was principally bacterial, with just one eukaryotic taxon identified
104 and not flagged: *Saccharomyces cerevisiae*. Notably, no archaea or viruses were identified in the group of
105 sub-core microorganisms (note that this analysis did not include viruses newly discovered in this study).
106 For viruses in particular, this may be affected by the sampling or DNA extraction methods used, by
107 limitations in sequencing depth, or by missing annotations in the reference databases used for taxonomic

Table 1: Sample Counts, The number of samples collected from each region.

Region	Pilot	CSD16	CSD17	Other	Total
North America	28	284	371	276	959
East Asia	34	26	1297	0	1357
Europe	177	310	939	1	1427
Sub Saharan Africa	0	116	192	0	308
South America	20	44	199	68	331
Middle East	0	100	15	0	115
Oceania	0	94	32	0	126
Background Control	0	0	40	0	40
Lab Control	0	0	20	6	26
Positive Control	0	0	33	6	39
Total	259	974	3138	357	4728

108 classification, which is principally problematic with phages. It is worth noting that potentially prevalent
109 RNA viruses are omitted with our DNA-based sampling. The three most common bacterial phyla across
110 the world's cities ordered by the number of species observed were *Proteobacteria*, *Actinobacteria*, and
111 *Firmicutes*. To test for possible geographic bias in our data, we normalized the prevalence for each taxa
112 by the median prevalence within each city. The two normalization methods broadly agreed (Figure ??).

113 Despite their global prevalence, the core taxa are not uniformly abundant across all cities. Many
114 species exhibited a high standard deviation and kurtosis (calculated using Fisher's definition and normal
115 kurtosis of 0) than other species (Figure 1B). Furthermore, some species show distinctly high mean
116 abundance, often higher than the core species, but more heterogeneous global prevalence. For example,
117 *Salmonella enterica* is identified in less than half of all samples but is the 12th most abundant species
118 based on the fraction of DNA that can be ascribed to it. The most relatively abundant microbial species
119 was *Cutibacterium acnes* (Figure 1D) which had a comparatively stable distribution of abundance across
120 all samples; *Cutibacterium acnes* is known as a prominent member of the human skin microbiome. To
121 test for any biases arising from uneven geographic sampling, we measured the relative abundance of
122 each taxon by calculating the fraction of reads classified to each particular taxon, and compared the
123 raw distribution of abundance to the distribution of median abundance within each city (This process
124 is analogous to the one used for Figure 1C, Figure 1B); the two measures closely aligned. Also, an
125 examination of the positive and negative controls indicates that these results are not likely due to
126 contamination or batch effect (Supp. Figure S13). In total, we observed 31 core taxa (>97%), 1,145
127 sub-core taxa (70-97%) 2,466 peripheral taxa (<25%), and 4,424 taxa across all samples. We term the
128 set of all taxa observed *the urban panmicrobiome*.

129 To estimate the number of taxa present in our samples but which were not detected by our experi-
130 mental techniques, we performed a rarefaction analysis on the taxa that were identified. By estimating
131 the number of taxa identified for different numbers of samples, we see a diminishing trend (Figure 1D),
132 which indicates that at some point, the species in every new sample were likely already identified in a
133 previous one. Our rarefaction curve did not reach a plateau and, even after including all samples, it still
134 shows an expected marginal discovery rate of roughly 1 additional species for every 10 samples added
135 to the study. For clarity we note that this analysis only considers taxa already present in reference
136 databases, not newly discovered taxa (below). Despite the remaining unidentified taxa, we estimate
137 that most (80%) of the classifiable taxa in the urban microbiome could be identified with roughly 1,000
138 samples. However, as noted below, this new diversity is likely not evenly distributed across regions.

139 As humans are a major part of the urban environment, the DNA in our samples could be expected to
140 resemble commensal human microbiomes. To investigate this, we compared non-human DNA fragments
141 from our samples to a randomized set of 50 samples from 5 commensal microbiome sites in the Human
142 Microbiome Project (HMP) (Consortium et al., 2012) (stool, skin, airway, gastrointestinal tract, urogen-
143 ital tract). We used MASH to perform a k -mer based comparison of our samples vs. the selected HMP
144 samples, which showed a roughly uniform dissimilarity between MetaSUB samples and those from differ-
145 ent human body sites (Figure 1E, Supp. Figure S2A & B). Samples taken from surfaces that were likely
146 to have been touched more often by human skin, such as doorknobs, buttons, railings, and touchscreens,
147 were indeed more similar to human skin microbiomes than surfaces like bollards, windows, and the floor.
148 Given that a large fraction of DNA in our samples could not be classified and that a k -mer based compar-
149 ison did not find significant body-site specificity, it is possible that the unclassified DNA in our samples
150 is from novel taxa which are not human commensals. Of note, the taxonomic composition of our samples
151 do not closely resemble soil samples. We processed 28 metagenomic soil samples (Bahram et al., 2018)
152 using the same pipeline as the rest of the data and compared soil samples to our samples using MASH.
153 Our samples were very dissimilar from the soil samples (Figure 1F) even in comparison to human skin
154 microbiomes. This suggests that the unclassified DNA may represent heretofore uncharacterized taxa
155 that are not known commensals being shed into the environment.

156 We next estimated the fraction of sequences in our data that did not resemble sequences in known
157 reference databases. We took a subset of 10,000 reads from each sample and aligned these reads to
158 a number of reference databases using BLASTn (Altschul et al., 1990). We then identified reads that
159 mapped to sequences in the reference databases at 80%, 90%, and 95% Average Nucleotide Identity
160 (ANI) (Figure 1G). We used a broad set of databases for reference: RefSeq, NCBI's NT Environmental,
161 a large database of Metagenome Assembled Genomes (MAGs) from Pasolli et al. (2019), and MAGs from
162 MetaSUB itself (Section 2.5). At 80% ANI, the most permissive threshold, 34.6% of reads did not map
163 to any database while 47.3% of reads did not map or only mapped to MAGs from MetaSUB itself. This
164 mirrors results seen by previous urban microbiome works (Afshinnekoo et al., 2015; Hsu et al., 2016).

165 Next, we analyzed the fraction of sequences that aligned to these same databases by region. Sur-

166 prisingly, samples from Europe had the highest fraction of unaligned reads, followed by the middle east,
167 while samples from Sub Saharan Africa had the smallest fraction of unaligned reads (Supp. Figure
168 S1C). The proportion of reads aligned to each database did not vary significantly by region. We fur-
169 ther investigated the relationship between geography and sample composition. In ecology, an increasing
170 distance from the equator is associated with a decrease in taxonomic diversity (O'Hara et al., 2017).
171 The MetaSUB data recapitulates this result and identifies a significant decrease in taxonomic diversity
172 (though with significant noise, $p < 2e16$, $R^2 = 0.06915$) as a function of absolute latitude; samples are
173 estimated to lose 6.9672 species for each degree of latitude away from the equator (Supp. Figure S1A).
174 The effect of latitude on species diversity is not purely monotonic, since several cities have higher species
175 diversity than their latitude would predict. This is expected as latitude is only a rough predictor of a
176 city's climate. While this is an observation consistent with ecological theory, we note that our samples
177 are heavily skewed by the location of the target cities, as well as the prevalence of those cities in specific
178 latitude zones of the northern hemisphere.

179 2.2 Global Diversity Varies According to Covariates

180 Despite the core urban microbiome present in almost all samples, there was also geographic variation
181 in taxonomy and localization. We calculated the Jaccard distance between samples measured by the
182 presence and absence of species (which is robust to noise from relative abundance) and performed a
183 dimensionality reduction of the data using UMAP (Uniform Manifold Approximation and Projection,
184 McInnes et al. (2018)) for visualization (Figure 2A). Jaccard distance was correlated with distance based
185 on Jensen-Shannon Divergence (which accounts for relative abundance) and k -mer distance calculated by
186 MASH (which is based on the k -mer distribution in a sample, so cannot be biased by a database) (Supp.
187 Figure S10A, B, C). In principle, Jaccard distance could be influenced by read depth as low abundance
188 species drop below detection thresholds. However we expect this issue to be minor as the total number
189 of species identified stabilized at 100,000 reads (Supp. Figure S9B) compared to an average of 6.01M
190 reads per sample. Samples collected from North America and Europe were distinct from those collected
191 in East Asia, but the separation between other regions was less clear. A similar trend was found in an
192 analogous analysis based on functional pathways rather than taxonomy (Supp. Fig S5D), which indicates
193 geographic stratification of the metagenomes at both the functional and taxonomic levels. Subclusters
194 identified by UMAP roughly corresponded to city and climate but not surface type (Supp. Figure S5A,
195 B, C). These findings confirm and extend earlier analyses performed on a fraction of the MetaSUB data
196 which were run as a part of CAMDA Challenges in years 2017, 2018, and 2019 (camda.info).

197 We quantified the degree to which metadata covariates influence the taxonomic composition of our
198 samples using MAVRIC, a statistical tool to estimate the sources of variation in a count-based dataset
199 (Moskowitz and Greenleaf, 2018). We identified covariates which influenced the taxonomic composition
200 of our samples: city, population density, average temperature in June, region, elevation above sea-level,
201 surface type, surface material, elevation above or below ground and proximity to the coast. The most
202 important factor, which could explain 19% of the variation in isolation, was the city from which a sample
203 was taken followed by region which explained 11%. The other four factors ranged from explaining 2%
204 to 7% of the possible variation in taxonomy in isolation (Supp. Table S2). We note that many of
205 the factors were confounded with one another, so they can explain less diversity than their sum. One
206 metadata factor tested, the population density of the sampled city, had no significant effect on taxonomic
207 variation overall.

208 To quantify how the principle covariates, climate, continent, and surface material impacted the taxo-
209 nomic composition of samples, we performed a Principal Component Analysis (PCA) on our taxonomic
210 data normalized by proportion and identified principal components (PCs) which were strongly associated
211 with a metadata covariate in a positive or negative direction (PCs were centered so an average direction
212 indicates an association). We found that the first two PCs (representing 28.0% and 15.7% of the variance
213 of the original data, respectively) associated strongly with the city climate while continent and surface
214 material associate less strongly (Figure 2B).

215 Next, we tested whether geographic proximity (in km) of samples to one another had any effect on
216 the variation, since samples taken from nearby locations could be expected to more closely resemble one
217 another. Indeed, for samples taken in the same city, the average JSD (Jensen-Shannon distance) was
218 weakly predictive of the taxonomic distance between samples, with every increase of 1km in distance
219 between two samples representing an increase of 0.056% in divergence ($p < 2e16$, $R^2 = 0.01073$, Supp.
220 Figure S1B). This suggests a "neighborhood effect" for sample similarity analogous to the effect described
221 by Meyer et al. (2018), albeit a very minor one. To reduce bias that could be introduced by samples

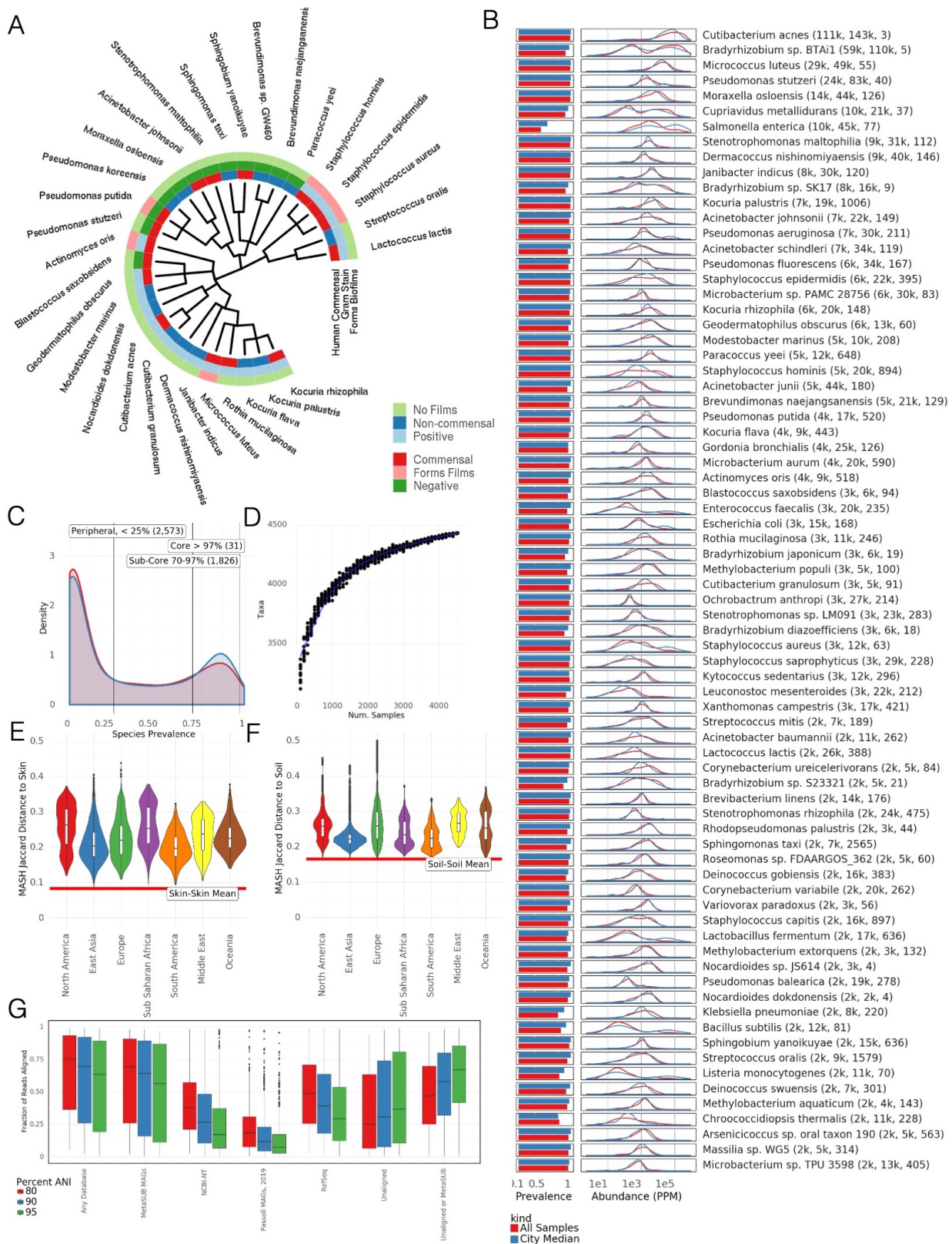


Figure 1: The core microbiome A) Taxonomic tree showing 31 core taxa, colored by phylum and annotated according to gram stain, ability to form biofilms, predicted association with a virus, and whether the bacteria is a human commensal species. B) prevalence and distribution of relative abundances of the 75 most abundant taxa. Mean relative abundance, standard deviation, and kurtosis of the abundance distribution are shown. C) Distribution of species prevalence from all samples and normalized by cities. Vertical lines show defined group cutoffs. D) Rarefaction analysis showing the number of species detected in randomly chosen sets of samples. E) MASH (k -mer based) similarity between MetaSUB samples and HMP skin microbiome samples, by continent. F) MASH (k -mer based) similarity between MetaSUB samples and soil microbiome samples, by continent. G) Fraction of reads aligned (via BLAST) to different databases at different Average Nucleotide Identities.

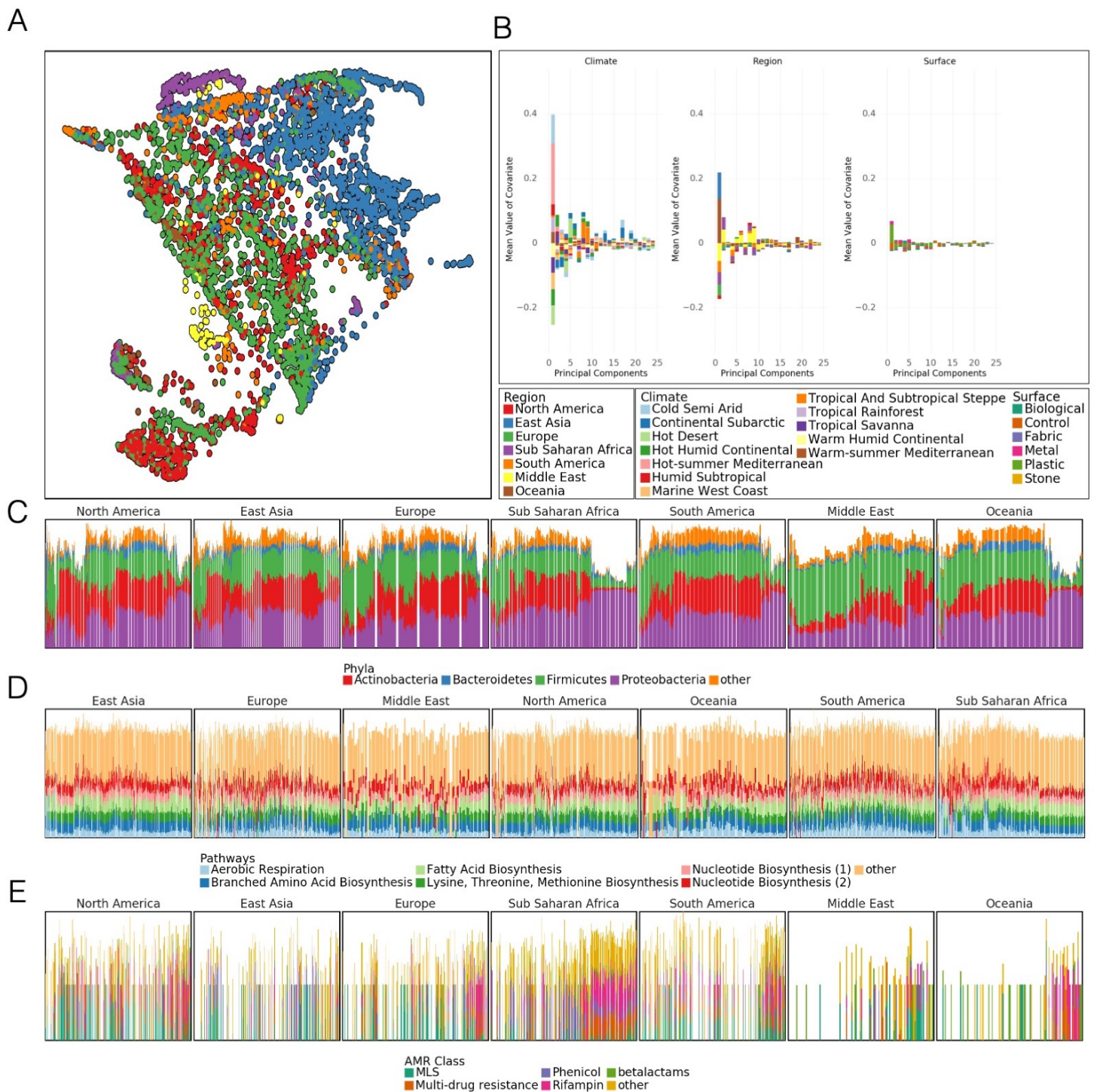


Figure 2: Differences at global scale A) UMAP of taxonomic profiles based on Jaccard distance between samples. Colored by the region of origin for each sample. Axes are arbitrary and without meaningful scale. The color key is shared with panel B. B) Association of the first 25 principal components of sample taxonomy with climate, continent, and surface material. C) Distribution of major phyla, sorted by hierarchical clustering of all samples and grouped by continent. D) Distribution of high-level groups of functional pathways, using the same order as taxa (C). E) Distribution of AMR genes by drug class, using the same order as taxa (C). Note that MLS is macrolide-lincosamide-streptogramin.

222 taken from precisely the same object we excluded all pairs of samples within 1km of one another.

223 At a global level, we examined the prevalence and abundance of taxa and their functional profiles
224 between cities and continents. These data showed a fairly stable phyla distribution across samples, but
225 the relative abundance of these taxa is unstable (Figure 2C) with some continental trends. In contrast
226 to taxonomic variation, functional pathways were much more stable across continents, showing relatively
227 little variation in the abundance of high level categories (Figure 2D). This pattern may also be due to
228 the more limited range of pathway classes and their essential role in cellular function, in contrast to the
229 much more wide-ranging taxonomic distributions examined across metagenomes. Classes of antimicrobial
230 resistance were observed to vary by continent as well. Clusters of AMR classes were observed to occur
231 in groups of taxonomically similar samples (Figure 2E).

232 We quantified the relative variation of taxonomic and functional profiles by comparing the distribution
233 of pairwise distances in taxonomic and functional profiles. Both profiles were equivalently normalized
234 to give the probability of encountering a particular taxon or pathway. Taxonomic profiles have a mean
235 pairwise Jensen-Shannon Divergence (JSD) of 0.61 while pathways have a mean JSD of 0.099. The
236 distributions of distances are significantly different (Welch's *t*-test, unequal variances, $p < 2e - 16$). This
237 is consistent with observations from the Human Microbiome Project, where metabolic function varied
238 less than taxonomic composition (Consortium et al., 2012; Lloyd-Price et al., 2017) within samples from
239 a given body site.

240 2.3 Microbial Signatures Reveal Urban Characteristics

241 To facilitate characterization of novel sequences we created GeoDNA, a high-level web interface (Figure
242 3A) to search raw sequences against our dataset. Users can submit sequences to be processed against
243 a *k*-mer graph-based representation of our data. Query sequences are mapped to samples and a set of
244 likely sample hits is returned to the user. This interface will allow researchers to probe the diversity in
245 this dataset and rapidly identify the range of various genetic sequences.

246 We sought to determine whether a samples taxonomy reflected the environment in which it was
247 collected. To this end we trained a Random Forest Classifier (RFC) to predict a sample's city of origin
248 from its taxonomic profile. We trained an RFC with 100 components on 90% of the samples in our
249 dataset and evaluated its classification accuracy on the remaining 10%. We repeated this procedure with
250 multiple subsamples of our data at various sizes and with 5 replicates per size to achieve a distribution
251 (Fig. 3B). The RFC achieved 88% on held out data which compares favorably to the 7.01% that would
252 be achieved by a randomized classifier. These results from our RFC demonstrate that city specific
253 taxonomic signatures exist and can be predictive.

254 We expanded our analysis of environmental signatures in taxonomy to the prediction of features in
255 cities not present in our training set. To do this we collated a set of 7 features for each city: population,
256 surface material, elevation, proximity to the coast, population density, region, ave June temperature,
257 and Koppen climate classification. We trained a RFCs to predict each feature based on all samples that
258 were not taken from a given city then used the relevant RFC to predict the feature for samples from
259 the held out city and recorded the classification accuracy (Figure 3D). While not all features and cities
260 were equally predictable (in particular features for a number of British cities were roughly similar and
261 could be predicted effectively) in general the predictions exceeded random chance by a significant margin
262 (Supp. Figure S3A). This suggests that certain features of cities generate microbial signatures that are
263 present globally and distinct from city specific signatures. The successful geographic classification of
264 samples demonstrates distinct city-specific trends in the detected taxa, that may enable future forensic
265 biogeographical capacities.

266 However, unique, city-specific taxa are not uniformly distributed (Figure 3B). To quantify this, we
267 developed a score to reflect how endemic a given taxon is within a city, which reflects upon the forensic
268 usefulness of a taxon. We define the Endemicity Score (ES) of a taxa as term-frequency inverse document
269 frequency where the document consists of samples from some metadata defined group such as a city or
270 region. This score is designed to simultaneously reflect the chance that a taxon could identify a given
271 city and that that taxon could be found within the given city. A high ES for a taxon in a given city
272 could be evidence of the evolutionary advantage that the taxon has in a particular cities environment.
273 However, neutral evolution of microbes within a particular niche is also possible and the ES alone does
274 not distinguish between these two hypotheses.

275 Note that while the ES only considers taxa which are found in a city, a forensic classifier could also
276 take advantage of the absence of taxa for a similar metric. ES show a roughly bimodal distribution for
277 regions (Fig. 3C). Each region possesses a number of taxa with ES scores close to 1 and a slightly larger

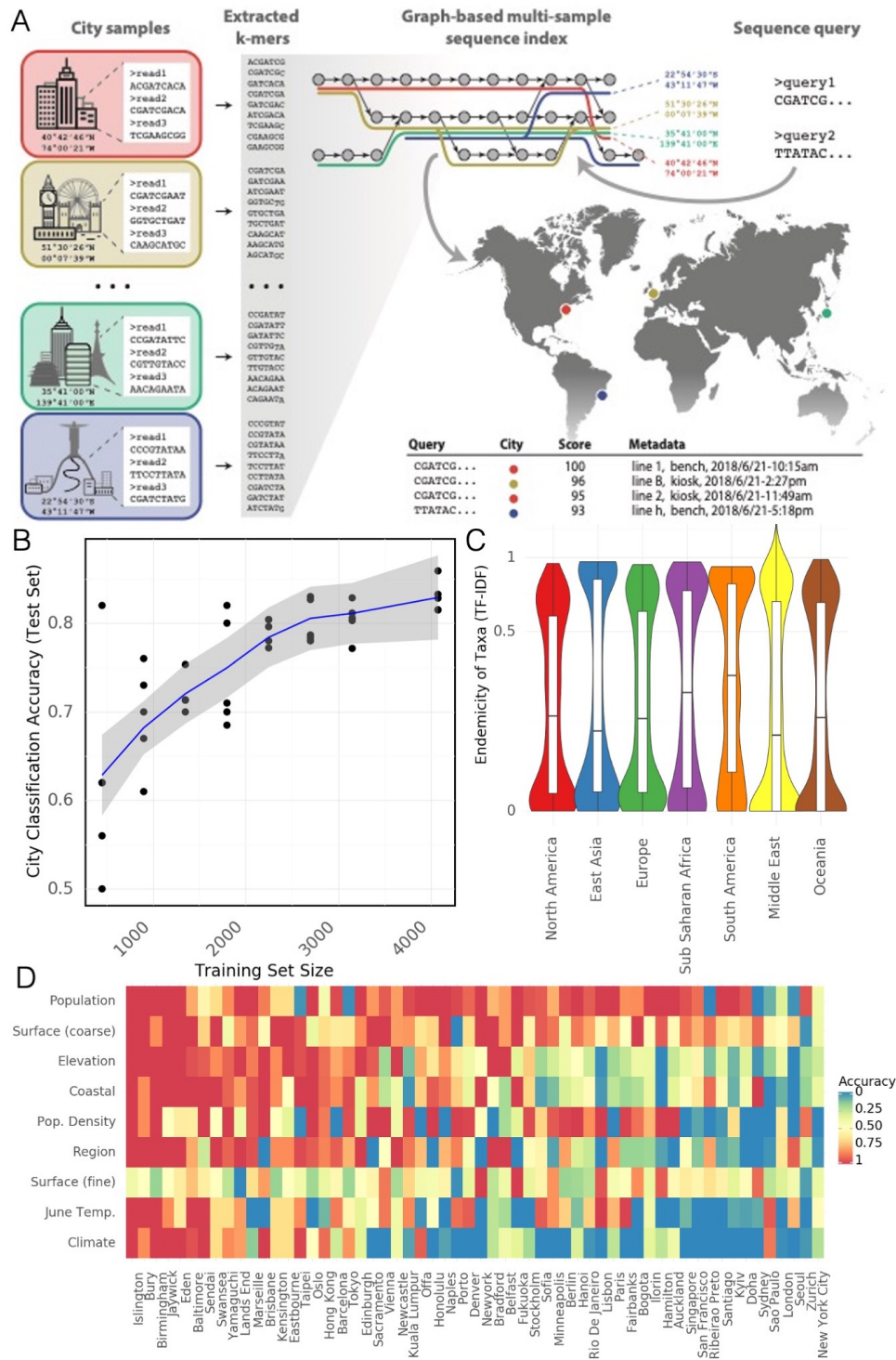


Figure 3: Microbial Signatures A) Schematic of GeoDNA representation generation – Raw sequences of individual samples for all cities are transformed into lists of unique *k*-mers (left). After filtration, the *k*-mers are assembled into a graph index database. Each *k*-mer is then associated with its respective city label and other informative metadata, such as geo-location and sampling information (top middle). Arbitrary input sequences (top right) can then be efficiently queried against the index, returning a ranked list of matching paths in the graph together with metadata and a score indicating the percentage of *k*-mer identity (bottom right). The geo-information of each sample is used to highlight the locations of samples that contain sequences identical or close to the queried sequence (middle right). B) Classification accuracy of a random forest model for assigning city labels to samples as a function of the size of training set. C) Distribution of Endemicity scores (term frequency inverse document frequency) for taxa in each region. D) Prediction accuracy of a random forest model for a given feature (rows) in samples from a city (columns) that was not present in the training set. Rows and columns sorted by average accuracy. Continuous features (e.g. Population) were discretized.

278 number close to 0 (note that ES is not bounded in $[0, 1]$). Some cities, like Offa (Nigeria), host many
279 unique taxa while others, like Zurich (Switzerland), host fewer endemic species (Supp. Figure S3B).
280 Large numbers of endemic species in a city may reflect geographic bias in sampling. However, some
281 cities from well sampled continents (e.g., Lisbon, Hong Kong) also host many endemic species which
282 would suggest that ES may indicate interchangeability and local pockets of microbiome variation for
283 some locations.

284 2.4 Antimicrobial Resistance Genes Form Distinct Clusters

285 Quantification of antimicrobial diversity and AMRs are key components of global antibiotic stewardship.
286 Yet, predicting antibiotic resistance from genetic sequences alone is challenging, and detection accuracy
287 depends on the class of antibiotics (i.e., some AMR genes are associated to main metabolic pathways
288 while others are uniquely used to metabolize antibiotics). As a first step towards a global survey of
289 antibiotic resistance in urban environments, we mapped reads to known antibiotic resistance genes,
290 using the MegaRES ontology and alignment software. We quantified their relative abundance using
291 reads/kilobase/million mapped reads (RPKM) for 20 classes of antibiotic resistance genes detected in
292 our samples (Figure 4A B). 2,210 samples had some sequence which were identified as belonging to an
293 AMR gene, but no consistent core set of genes was identified. The most common classes of antibiotic
294 resistance genes were for macrolides, lincosamides, streptogamines (MLS), and betalactams, yet the most
295 common class of antibiotic resistance genes, MLS was found in only 56% of the samples where AMR
296 sequence was identified.

297 Despite being relatively common, antibiotic resistance genes were universally in low abundance com-
298 pared to functional genes, with RPKM values for resistance classes typically ranging from 0.1 – 1 com-
299 pared to values of 10 - 100 for typical housekeeping genes (AMR classes contain many genes so RPKM
300 values may be lower than they would be for individual genes). In spite of the low abundance of the genes
301 themselves, some samples contained sequences from hundreds of distinct AMR genes. Clusters of high
302 AMR diversity were not evenly distributed across cities (Figure 4C). Some cities had more resistance
303 genes identified on average (15-20X) than others (e.g. Bogota) while other cities had bimodal distribu-
304 tions (e.g. San Francisco) where some samples had hundreds of genes while others very few. We note
305 that 99% of the cases where we detected an AMR genes had an average depth of 2.7x, indicating that
306 our global distribution would not dramatically change with altered read depth (Supp. Figure S6E).

307 As with taxa, AMR genes can be used to classify samples to cities - albeit with much less accuracy.
308 A random forest model analogous to the one trained to predict city classification from taxonomic profiles
309 was trained to predict from profiles of antimicrobial resistance genes. This model achieved 37.6% accuracy
310 on held out test data (Supp. Figure S6A). While poor for actual classification this accuracy far exceeds
311 the 7.01% that would be achieved by randomly assigning labels and indicates that there are possibly
312 weak, city specific signatures for antimicrobial resistance genes.

313 Multiple AMR genes can be carried on a single plasmid and ecological competition may cause mul-
314 tiple taxa in the same sample to develop antimicrobial resistance. As a preliminary analysis into these
315 phenomena we identified clusters of AMR genes that co-occurred in the same samples (Figure 4D).
316 We measured the Jaccard distance between all pairs of AMR genes found in at least 1% of samples and
317 performed agglomerative clustering on the resulting distance matrix. We identified three large clusters of
318 genes and numerous smaller clusters. Of note, these clusters often consist of genes from multiple classes
319 of resistance. At this point we do not posit a specific ecological mechanism for this co-occurrence, but
320 we note that the large clusters contain far more genes than are typically found on plasmids.

321 We performed a rarefaction analysis on the set of all resistance genes in the dataset, which we call
322 the “panresistome” (Figure (Supp. Figure S6B). Similar to the rate of detected species, the panresistome
323 also shows an open slope with an expected rate of discovery of 1 previously unobserved AMR gene per
324 10 samples. Given that AMR gene databases are rapidly expanding and that no AMR genes were found
325 in some samples, it is likely that future analyses will identify many more resistance genes in this data.

326 Additionally, AMR genes show a “neighbourhood” effect within samples that are geographically prox-
327 imal analogous to the effect seen for taxonomic composition (Supp. Figure S6C). Excluding samples
328 where no AMR genes were detected, the Jaccard distance between sets of AMR genes increases with
329 distance for pairs of samples in the same city. As with taxonomic composition. the overall effect is weak
330 and noisy, but significant.

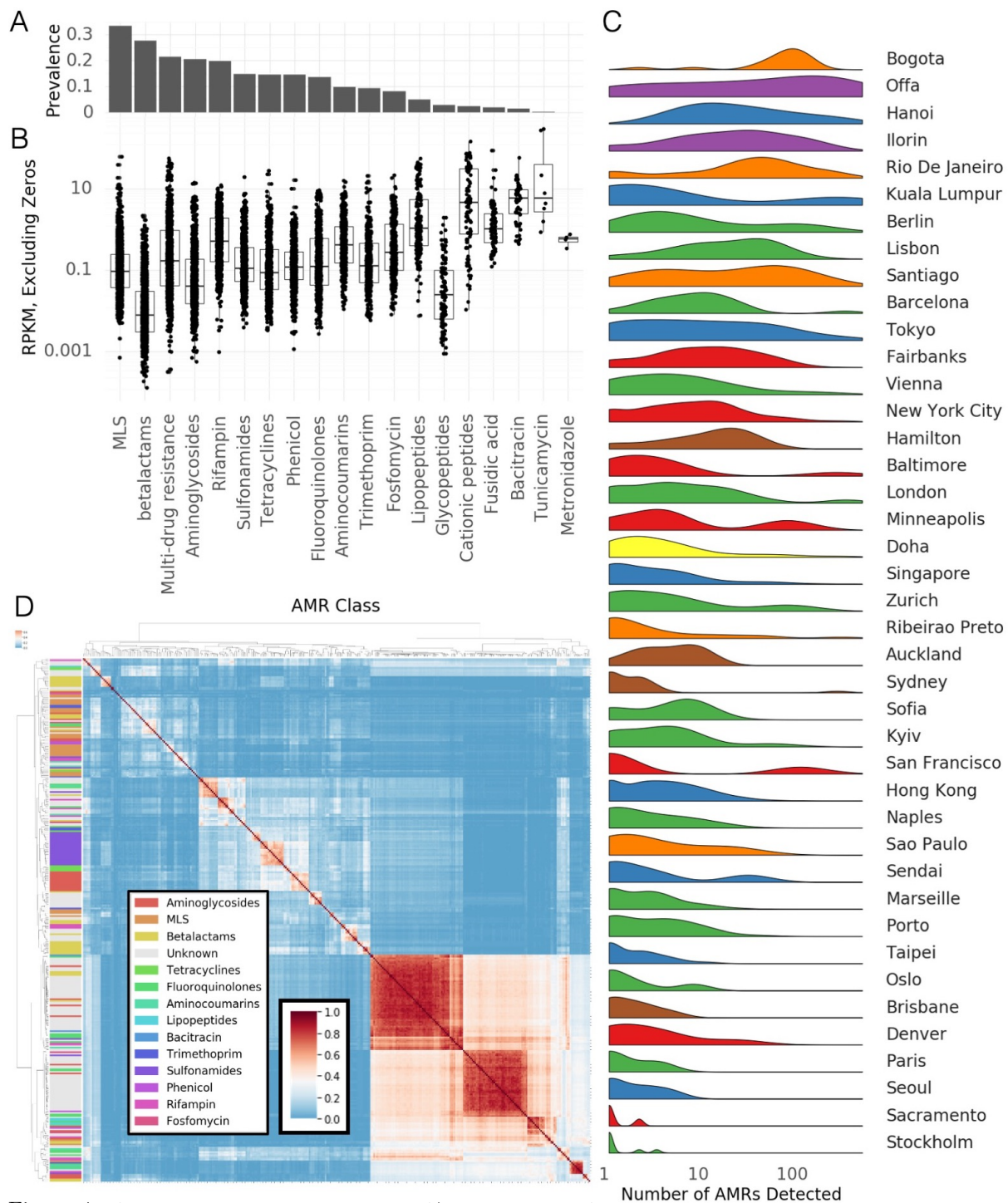


Figure 4: Antimicrobial Resistance Genes. A) Prevalence of AMR genes with resistance to particular drug classes. B) Abundance of AMR gene classes when detected, by drug class. C) Number of detected AMR genes by city. D) Co-occurrence of AMR genes in samples (Jaccard index) annotated by drug class.

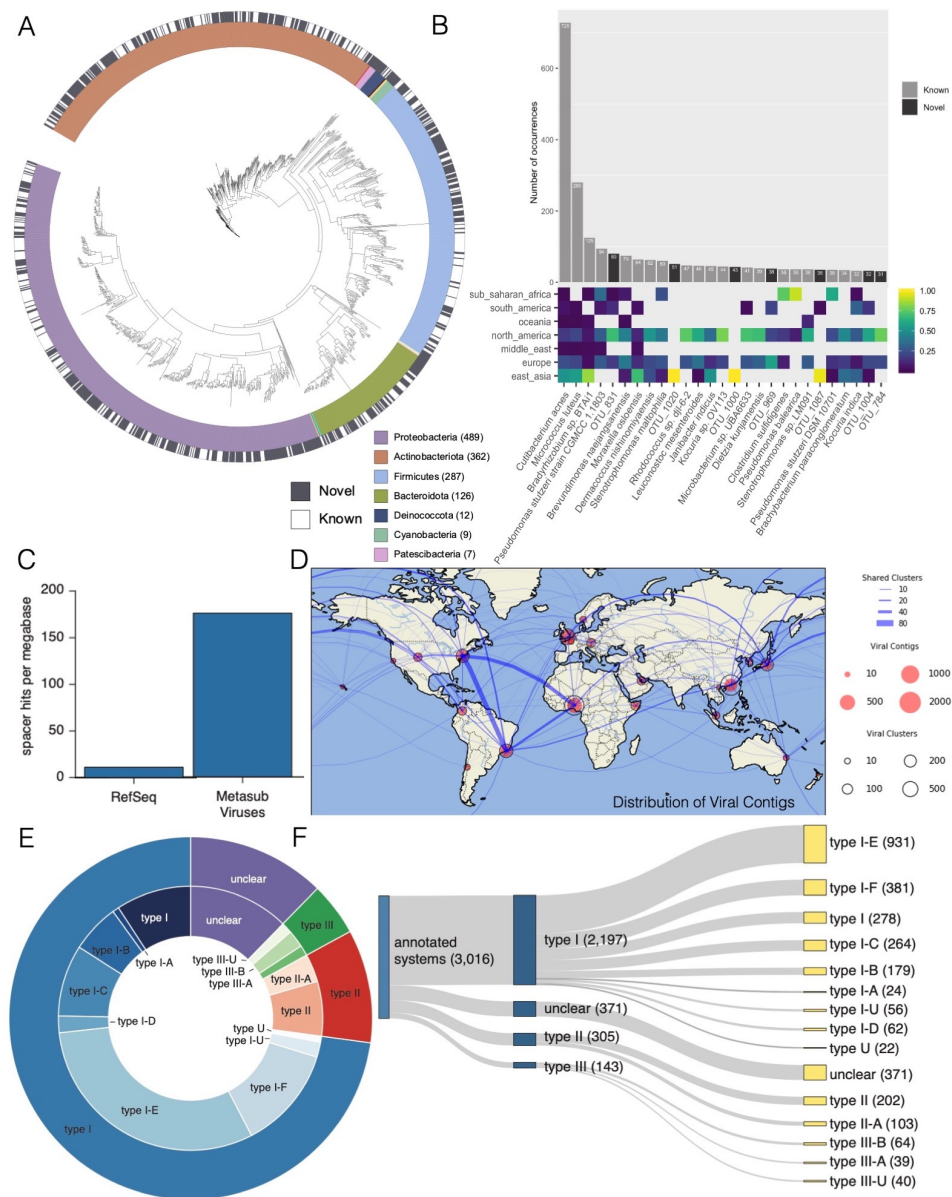


Figure 5: Novel Biology A) Taxonomic tree for Metagenome Assembled Genomes (MAGs) found in the MetaSUB data. Outer black and white ring indicates if the MAG matches a known species, inner ring indicates phyla of the MAG. B) Top: the number of samples where the most prevalent MAGs were found. Bottom: The regional breakdown of samples where the MAG was found. C) Mapping rate of CRISPR Spacers from MetaSUB data to viral genomes in RefSeq and viral genomes found in MetaSUB data. D) Geographic distribution of viral genomes found in MetaSUB data. E & F) Fractional breakdowns of identifiable CRISPR systems found in the MetaSUB data

331 2.5 Widespread Discovery of Novel Biology

332 To examine these samples for novel genetic elements, we assembled and identified Metagenome Assembled
333 Genomes (MAGs) for viruses, bacteria, and archaea and analyzed them with several algorithms. This
334 includes thousands of novel CRISPR arrays that reflect the microbial biology of the cities and 1,304
335 genomes from our data, of which 748 did not match any known reference genome within 95% average
336 nucleotide identity (ANI). 1302 of the genomes were classified as bacteria, and 2 as archaea. Bacterial
337 genomes came predominantly from four phyla: the Proteobacteria, Actinobacteria, Firmicutes, and
338 Bacteroidota. Novel bacteria were evenly spread across these phyla (Figure 5A).

339 Assembled bacterial genomes were often identified in multiple samples. Several of the most prevalent
340 bacterial genomes were novel species (Figure 5B). Some assembled genomes, both novel and not, showed
341 regional specificity while others were globally distributed. The taxonomic composition of identifiable
342 genomes roughly matched the composition of the core urban microbiome (Section 2.1). The number
343 of identified bacterial MAGs was somewhat based on read depth and the sample count per city (Supp.
344 Figure S7A). The number of bacterial MAGs discovered in a city which did not match a known species
345 was closely correlated to the total number of bacterial MAGs discovered in that city (Supp. Figure S7B).
346 Bacterial MAGs were roughly evenly distributed geographically with the notable exception of Offa, which
347 had dramatically more novel bacterial species than other cities.

348 We investigated assembled contigs from our samples to identify 16,584 predicted uncultivated viral
349 genomes (UViGs). Taxonomic analysis of predicted UViGs to identify viral species yielded 2,009 clusters
350 containing a total of 6,979 UViGs and 9,605 singleton UViGs for a total of 11,614 predicted viral species.
351 Predicted viral species from samples collected within 10, 100 and 1000 kilometers of one another were
352 agglomerated to examine their planetary distribution at different scales (Figure 5B). At any scale, most
353 viral clusters appear to be weakly cosmopolitan; the majority of their members are found at or near one
354 location, with a few exceptions.

355 We compared the predicted species to known viral sequences in the JGI IMG/VR system, which
356 contains viral genomes from isolates, a curated set of prophages and 730k viral MAGs from other studies.
357 Of the 11,614 species discovered in our data 94.1% did not match any viral sequence in IMG/VR (*Paez-*
358 *Espino et al., 2019*) at the species level for a total of 10,928 novel viruses. We note that this number is
359 surprisingly high but was obtained using a conservative pipeline (99.6% precision) and corresponded well
360 with our identified CRISPR arrays (below). This suggests that urban microbiomes contain significant
361 diversity not observed in other environments.

362 Next, we attempted to identify possible bacterial and eukaryotic hosts for our predicted viral MAGs.
363 For the 686 species with similar sequences in IMG/VR, we projected known host information onto 2,064
364 MetaSUB viral MAGs. Additionally, we used CRISPR-Cas spacer matches in the IMG/M system to
365 assign possible hosts to a further 1,915 predicted viral species. Finally, we used a database of 20 million
366 metagenome-derived CRISPR spacers to provide further rough taxonomic assignments. Our predicted
367 viral hosts aligned with our taxonomic profiles, 41% of species in the core microbiome (Section 2.1) had
368 predicted viral-host interactions. Many of our viral MAGs were found in multiple locations (Figure 5D).
369 Many viruses were found in South America, North America and Africa. Viral MAGs in Japan often
370 corresponded to those in Europe and North America.

371 We identified 838,532 CRISPR arrays in our data of which 3,245 could be annotated for specific
372 systems. The annotated CRISPR arrays were principally type 1-E and 1-F but a number of type two
373 and three systems were identified as well (Figure 5E, F). A number of arrays had unclear or ambiguous
374 type assignment. Critically the spacers in our identified CRISPR arrays closely matched our predicted
375 viral MAGs. We aligned spacers to both our viral MAGs and all viral sequences in RefSeq. The total
376 fraction of spacers which could be mapped to our viral MAGS and RefSeq was similar (Supp. Figure
377 S7C) but the mapping rate to our viral MAGs dramatically exceeded the mapping rate to RefSeq (Figure
378 5C). We present this as additional evidence supporting these novel viral MAGs.

379 3 Discussion

380 MetaSUB is a global network of scientists and clinicians developing knowledge of urban microbiomes by
381 studying mass transit systems and hospitals within and between cities. We collected and sequenced 4,728
382 samples from 60 cities worldwide (Tables 1 and S1), constituting the first large scale metagenomic study
383 of the urban microbiome. We also identified species that are geographically constrained and showed that
384 these can be used to determine a samples city of origin (Section 2.2). Many of these species are associated
385 with commensal microbiomes from human skin and airways, but we observed that urban microbiomes are

386 nevertheless distinct from both human and soil microbiomes. Notably, no species from the *Bacteroidetes*,
387 a prominent group of human commensal organisms (Eckburg et al., 2005; Qin et al., 2010), was identified
388 in the core urban microbiome. We conclude that there is a consistent urban microbiome core (Figure
389 1, 2), which is supplemented by geographic variation (Figure 2) and microbial signatures based on the
390 specific attributes of a city (Figure 3). Our data also indicates that significant diversity remains to be
391 characterized and that novel taxa may be discovered in the data (Figure 5), that environmental factors
392 affect variation, and that sequences associated with AMR are globally widespread but not necessarily
393 abundant (Figure 4). In addition to these results, we present several ways to access and analyze our
394 data including interactive web based visualizations, search tools over raw sequence data, and high level
395 interfaces to computationally access results.

396 Unique taxonomic composition and association with covariates specific to the urban environment
397 suggest that urban microbiomes should be treated as ecologically distinct from both surrounding soil
398 microbiomes and human commensal microbiomes. Though these microbiomes undoubtedly interact
399 with the urban environment, they nonetheless represent distinct ecological niches with different genetic
400 profiles. While our metadata covariates were associated with the principal variation in our samples, they
401 do not explain a large proportion of the observed variance. It remains to be determined whether variation
402 is essentially a stochastic process or if a deeper analysis of our covariates proves more fruitful. We have
403 observed that less important principal components (roughly PCs 10-100) are generally less associated
404 with metadata covariates but that PCs 1-3 do not adequately describe the data alone. This is a pattern
405 that was observed in the human microbiome project as well, where minor PCs (such as our Figure 2B)
406 were required to separate samples from closely related body sites.

407 Much of the urban microbiome likely represents novel diversity as our samples contain a significant
408 proportion of unclassified DNA. This finding is comparable to many other metagenomic and microbiome
409 studies including other work done in subway environments (Afshinnekoo et al., 2015; Hsu et al., 2016),
410 airborne microbiomes (Yooseph et al., 2013), work done by the Earth Microbiome Project (Thompson
411 et al., 2017), and others. As noted in in Figure 1 more sensitive methodology only marginally increases
412 the proportion of DNA that can be classified. We consider the DNA which would not be classified by
413 a sensitive technique to be true unclassified DNA and postulate that it may derive from novel genes or
414 species. Given that our samples did not closely resemble human commensal microbiomes or soil samples,
415 it is possible this represents novel urban DNA sequences.

416 Additionally, our discovery of a large number of novel viral sequences in our data suggests that there
417 are likely to be additional novel taxa from other domains. The fraction of predicted viral sequences which
418 belonged to previously unobserved taxa was particularly high in our study (94.1%) however taxonomic
419 associations of these viruses to observed microbial hosts suggests these results are not spurious. This
420 rate of discovery may prove prescient for novel taxa in other domains, and novel discovery of taxa may
421 help to reduce the large fraction of DNA which cannot currently be classified.

422 Many of the identified taxa are frequently implicated as infectious agents in a clinical setting including
423 specific *Staphylococcus*, *Streptococcus*, *Corynebacterium*, *Klebsiella* and *Enterobacter* species. There is
424 no clear indication that these species identified in the urban environment are pathogenic, and further in-
425 depth study is necessary to determine the clinical impact of urban microbiomes. This includes microbial
426 culture studies, specifically searching for virulence factors and performing strain-level characterization.
427 Seasonal variation also remains open to study as the majority of the samples collected here were from two
428 global City Sampling Days (June 21, 2016 and 2017). Further studies, some generating novel data, will
429 need to explore whether the core microbiome shifts over the course of the year, with particular interest
430 in the role of the microbiome in flu transmission (Cáliz et al., 2018; Korownyk et al., 2018).

431 The COVID-19 crisis has thrown the need for broad microbial surveillance into sharp relief. Microbial
432 genetic mapping of urban environments will give public health officials tools to assess risk, map outbreaks,
433 and genetically characterize problematic species. This study identifies a large number of novel viruses in
434 the environment as well as antimicrobial resistance genes in bacteria. These data will be an important
435 starting point for mitigating future epidemics.

436 As metagenomics and next-generation sequencing becomes more and more available for clinical (Wil-
437 son et al., 2019) and municipal use (Hendriksen et al., 2019), it is essential to contextualize the AMR
438 markers or presence of new species and strains within a global and longitudinal context. The most
439 common AMR genes were found for two classes of antibiotic: MLS and beta-lactams. MLS represents
440 macrolides, lincosamides and streptogramins, which are three groups of antibiotics with a mechanism
441 of action of inhibiting bacterial protein synthesis. Macrolides, with strong Gram-positive and limited
442 Gram-negative coverage, are prevalently used to treat upper respiratory, skin, soft tissue and sexually
443 transmitted infections amongst others. Beta-lactam antibiotics are a major class of antibiotics including

444 penicillins, cephalosporins, monobactams, carbapenems and carbacephems that are all used to treat a
445 wide array of infections. Antimicrobial resistance has surged due to the selection pressure of widespread
446 use of antibiotics and is now a global health issue plaguing communities and hospitals worldwide. Antimi-
447 crobial resistance genes are thought to spread from a variety of sources including hospitals, agriculture
448 and water (Bougnom and Piddock, 2017; Klein et al., 2018). The antimicrobial classes particularly
449 impacted by resistance include beta-lactamases, glycopeptides and fluoroquinolones (Rice, 2012), all of
450 which we found antimicrobial resistance genes for across our samples. We found that there was uneven
451 distribution of AMR genes across cities. This could be the result of some of combination of different
452 levels of antibiotic use, differences in the urban geography between cities (population density, presence
453 of untreated wastewater etc), or reflect the background microbiome in different places in the world.
454 Techniques to estimate antibiotic resistance from sequencing data remain an area of intense research as
455 certain classes of AMR gene (ie. fluoroquinolones) are sensitive to small mutations and it is possible that
456 our methods may not fully reflect true resistance. Further research is needed to fully explore AMR genes
457 in the urban environment, including culture studies which directly measure the phenotype of resistance.

458 One of the challenges in the field of metagenomics of the built environment is dealing with low
459 biomass samples. Not only does it introduce the challenge of contamination (Kim et al., 2017) which
460 requires standardized sample preparation and the use of positive and negative controls, but there is
461 also the challenge in biases and data interpretation (McLaren et al., 2019). Metagenomic studies rely
462 on bioinformatics analyses that predict relative abundances of taxa, functional genes, antimicrobial
463 resistance genes, etc. When you have low biomass samples, these relative abundances may appear high
464 when their absolute abundance is in fact low when considering where the samples came from. However,
465 this is an inherent component of metagenomics that studies and examines microbiomes and communities
466 based on the metrics and measurements of relative abundances. There are important considerations to
467 be made from sample collection to bioinformatics analysis to ensure limited biases are introduced to a
468 study (McLaren et al., 2019). Moreover, the overall findings must be interpreted with the proper context
469 and scope of the experiment and samples collected.

470 In summary, this study presents a first molecular atlas of urban and mass-transit metagenomics from
471 across the world. By facilitating large scale epidemiological comparisons, it is a first critical step to-
472 wards quantifying the clinical role of environmental microbiomes and provides requisite data for tracking
473 changes in ecology or virulence. Moreover, in order to study the transmission of AMRs on a global scales
474 this dataset represents only focuses on some of the sources and vectors of the built environment. Indeed,
475 datasets from rural and suburban areas with livestock and farms, sewage from cities (Fresia et al., 2019;
476 Joseph et al., 2019), and other notable sources of AMRs need to be integrated together to truly capture
477 AMR mechanisms at the global scale (Singer et al., 2016; Thanner et al., 2016). Previous studies have
478 already demonstrated a role for precision clinical metagenomics in managing infectious disease and global
479 health (Afshinnkoo et al., 2017; Gardy and Loman, 2018; Ladner et al., 2019). As demonstrated by the
480 coronavirus disease 2019 (COVID-19) pandemic, as an atlas this data has the potential to aid physicians,
481 public health officers, government officials, and others in tracing, diagnosis, clinical decision making, and
482 policy within their communities.

483 3.1 Open Science

484 The MetaSUB dataset is built and organized for full accessibility to other researchers. This is consistent
485 with the concept of Open Science. Specifically, we built our study with the FAIR principles in mind:
486 Findable, Accessible, Interoperable and Reusable.

487 To make our study reproducible, we released an open source version-controlled pipeline called the
488 MetaSUB Core Analysis Pipeline (CAP). The CAP is intended to improve the reproducibility of our
489 findings by making it easy to apply a number of analyses consistently to a large dataset. This pipeline
490 includes all steps from extracting data from raw sequence data to producing refined results like taxonomic
491 and functional profiles. The CAP itself is principally composed of other open peer-reviewed scientific
492 tools, with only a few custom scripts for mundane tasks. Every tool in the CAP is open source with a
493 permissive license. The CAP is available as a docker container for easier installation in some instances
494 and all databases used in the CAP are available for public download. The CAP is versioned and includes
495 all necessary databases allowing researchers to replicate results. The CAP is not designed to produce
496 highly novel results but is meant to be a good practice agglomeration of open source tools.

497 However, the output of the CAP still consists of a number of different output formats with multiple
498 files for each sample. To make our results more reproducible and accessible, we have developed a program
499 to condense the outputs of the Core Analysis Pipeline into a condensed data-packet. This data packet

500 contains results as a series of Tidy-style data tables with descriptions. The advantage of this set-up is
501 that result tables for an entire dataset can be parsed with a single command in most high level analysis
502 languages like Python and R. This package also contains Python utilities for parsing and analyzing data
503 packets which streamlines most of the boilerplate tasks of data analysis. All development of the CAP
504 and data packet builder (Capalyzer) package is open source and permissively licensed.

505 In addition to general purpose data analysis tools essentially all analysis in this paper is available
506 as a series of Jupyter notebooks. Our hope is that these notebooks allow researchers to reproduce our
507 results, build upon our results in different contexts, and better understand precisely how we arrived at
508 our conclusions. By providing the exact source used to generate our analyses and figures, we also hope
509 to be able to quickly incorporate new data or correct any mistakes that might be identified.

510 For less technical purposes, we also provide web-based interactive visualizations of our dataset (typ-
511 ically broken into city-specific groups). These visualizations are intended to provide a quick reference
512 for major results as well as an exploratory platform for generating novel hypotheses and serendipitous
513 discovery. The web platform used, MetaGenScope, is open source, permissively licensed, and can be run
514 on a moderately powerful machine (though its output relies on results from the MetaSUB CAP).

515 Our hope is that by making our dataset open and easily accessible to other researchers the scientific
516 community can more rapidly generate and test hypotheses. One of the core goals of the MetaSUB
517 consortium is to build a dataset that benefits public health. As the project develops we want to make
518 our data easy to use and access for clinicians and public health officials who may not have computational
519 or microbiological expertise. We intend to continue to build tooling that supports these goals.

520 3.2 CAMDA

521 Since 2017 MetaSUB has partnered with the Critical Assessment of Massive Data Analysis (CAMDA)
522 camda.info, a full conference track at the Intelligent Systems for Molecular Biology (ISMB) Conference.
523 At this venue a subset of the MetaSUB data were released to the CAMDA community in the form
524 of annual challenge addressing the issue of geographically locating samples: ‘The MetaSUB Inter-City
525 Challenge’ in 2017 and ‘The MetaSUB Forensics Challenge’ in 2018 and 2019. In the latter challenge
526 the MetaSUB data has been complemented by data from EMP ([Thompson et al., 2017](#)) and other
527 studies ([Delgado-Baquerizo et al., 2018](#); [Hsu et al., 2016](#)). This Open Science approach of CAMDA
528 has generated multiple interesting results and concepts relating to urban microbiomics, resulting in
529 several publications biologydirect.biomedcentral.com/articles/collections/camdaproc as well
530 as perspective manuscript about moving towards metagenomics in the intelligence ([Mason-Buck et al.,](#)
531 [2020](#)). The partnership is continued in 2020 with ‘The Metagenomic Geolocation Challenge’ where the
532 MetaSUB data has been complemented by the climate/weather data in order to construct multi-source
533 microbiome fingerprints and predict the originating ecological niche of the sample.

534 4 Data Access

535 Raw sequencing reads from this study contain significant amounts of human DNA and cannot yet be
536 made public. However, reads with the majority of human DNA filtered and low quality bases removed are
537 available for download from Wasabi (an Amazon S3 clone) with individual URLs located here: [https:](https://github.com/MetaSUB/metasub_utils)
538 [//github.com/MetaSUB/metasub_utils](https://github.com/MetaSUB/metasub_utils). In addition to raw reads higher level results (e.g. taxonomic
539 profiles, functional pathways, etc.) are available in the MetaSUB data packet also available for download
540 from Wasabi. For instructional purposes we also provide a simplified data packet for teaching which
541 includes balanced numbers of samples from each city and completely filled metadata tables.

542 Interactive data visualizations are available on <https://pangea.gimmebio.com/contrib/metasub>,
543 <https://www.metagenscope.com> and GeoDNA, an interface to search query DNA sequences against
544 MetaSUB samples, is available at (dnaloc.ethz.ch/). MetaSUB data may be downloaded from [https:](https://pangea.gimmebio.com)
545 [//pangea.gimmebio.com](https://pangea.gimmebio.com). MetaSUB metadata is available in the data-packet, on Pangea, or may
546 be downloaded from <https://github.com/MetaSUB/MetaSUB-metadata>. Programs used for analy-
547 sis of data may be found at https://github.com/MetaSUB/MetaSUB_CAP and [https://github.com/](https://github.com/dcdanko/capalyzer)
548 [dcdanko/capalyzer](https://github.com/dcdanko/capalyzer). Jupyter notebooks used to generate the figures and statistics in this study can be
549 found at https://www.github.com/MetaSUB/main_paper_figures. Additional tools and resources are
550 described here https://github.com/MetaSUB/bioinformatics_management.

551 5 Acknowledgement

552 DCD was supported by the Tri-Institutional Training Program in Computational Biology and Medicine
553 (CBM) funded by the NIH grant 1T32GM083937.

554 We thank GitHub for providing private repositories to the MetaSUB consortium at no cost.

555 We thank XSEDE and Philip Blood for their support of this project.

556 We would like to thank the Epigenomics and Genomics Core Facilities at Weill Cornell Medicine, fund-
557 ing from the Irma T. Hirschl and Monique Weill-Caulier Charitable Trusts, Bert L and N Kuggie Vallee
558 Foundation, the WorldQuant Foundation, Igor Tulchinsky, The Pershing Square Sohn Cancer Research
559 Alliance, NASA (NNX14AH50G, NNX17AB26G), the National Institutes of Health (R01ES021006,
560 R25EB020393, 1R21AI129851, 1R01MH117406), TRISH (NNX16AO69A:0107, NNX16AO69A:0061),
561 the NSF (1840275), the Bill and Melinda Gates Foundation (OPP1151054) and the Alfred P. Sloan Foun-
562 dation (G-2015-13964), Swiss National Science Foundation grant #407540_167331 “Scalable Genome
563 Graph Data Structures for Metagenomics and Genome Annotation” as part of Swiss National Research
564 Programme (NRP) 75 “Big Data”

565 Discovery of novel viral sequences was work conducted by the US Department of Energy Joint Genome
566 Institute, a DOE Office of Science User Facility, under contract number DE-AC02-05CH11231 and used
567 resources of the National Energy Research Scientific Computing Center, supported by the Office of
568 Science of the US Department of Energy.

569 MetaSUB Sweden was supported by Stockholm Health Authority (Region Stockholm) grant SLL
570 20160933 awarded to KIU.

571 MetaSUB Seoul was supported by the Institut Pasteur Korea (2015MetaSUB) and a National Re-
572 search Foundation of Korea (NRF) grant (NRF-2014K1A4A7A01074645, 2017M3A9G6068246).

573 Metasub Chile was supported by funding from CONICYT Fondecyt Iniciación grant 11140666 and
574 11160905, as well as funding from the Millennium Science Initiative of the Ministry of Economy, Devel-
575 opment and Tourism, Government of Chile.

576 MetaSUB Japan was supported by research funds from Keio University, the Yamagata prefectural
577 government and the City of Tsuruoka.

578 MetaSUB Austria and Ukraine acknowledge the bilateral AT-UA collaboration fund (WTZ:UA
579 02/2019; Ministry of Education and Science of Ukraine, UA:M/84-2019).

580 MetaSUB Ukraine was supported by research funds from Kyiv Academic Univeristy, Ministry of
581 Education and Science of Ukraine grant 0118U100290. MetaSUB Ukraine would like to express gratitude
582 to Kyiv Metro for the support of sampling days.

583 MetaSUB Barcelona was supported by the Spanish Ministry of Economy and Competitiveness, ‘Cen-
584 tro de Excelencia Severo Ochoa 2013-2017, the CERCA Programme / Generalitat de Catalunya, the “la
585 Caixa” Foundation, the CRG-Novartis-Africa mobility programme 2016 and TMB Director Eladio De
586 Miguel Sainz

587 Work in Colombia was partially funded by Colciencias (project No. 639677758300).

588 Work in Sao Paulo, Brazil was partially funded by CNPq (EDN - 309973/2015-5)

589 Sampling was carried out in compliance with regulations and permissions from local authorities
590 (Azienda Napoletana Mobilitàà s.p.a. in Naples, Italy; Régie des Transports Métropolitains in Marseille,
591 France; Transmilenio and ANLA permit 1484 in Bogotá, Colombia; Nigerian Railway Corporation (NRC)
592 [Ilorin and Offa Branch] and Kwara Express Transport)

593 We thank the many volunteers who made this study possible. Sara Abdul Majid, Natasha Abdullah,
594 Ait-hamlat Adel, Nayra Aguilar Rojas, Affifah Saadah Ahmad Kassim, Faisal S Al-Quaddoomi, Alex
595 Alexiev, Muhammad Al-Fath Amran, Watson Andrew, Harilanto Andrianjakarivony, Álvaro Aranguren,
596 Carme Arnan, Freddy Asenjo, Juliette Auvinet, Nuria Aventin, Erdenetsetseg Batdelger, François Baudon,
597 Carla Bello, Médine Benchouaia, Hannah Benisty, Anne-Sophie Benoiston, Diego Benítez, Juliana Bernardes,
598 Tristan Bitard-Feildel, Lucie Bittner, Guillaume Blanc, Julia Boeri, Kevin Bolzli, Alexia Bordigoni, Ciro
599 Borrelli, Sonia Bouchard, Jean-Pierre Bouly, Alessandra Breschi, Alan Briones, Aszia Burrell, Alina Bu-
600 tova, Dayana Calderon, Angela Cantillo, Miguel Carbajo, Katerine Carrillo, Laurie Casalot, Sofia Castro,
601 Jasna Chalangal, Starr Chatziefthimiou, Francisco Chavez, Allaeddine Chettouh, Erika Cifuentes, Sylvie
602 Collin, Romain Conte, Flavia Corsi, Cecilia N Cossio, Bruno D’Alessandro, Ophélie Da Silva, Katherine
603 E Dahlhausen, Natalie R Davidson, Eleonora De Lazzari, Stéphane Delmas, Chloé Dequeker, Alexandre
604 Desert, Clara N. Dias, Valeriia Dotsenko, Cassie L Ettinger, Emile Faure, Fazlina Fauzi, Aubin Fleiss,
605 Juan Carlos Forero, Mathilde Garcia, Catalina García, Sonia L Ghose, Liliana Godoy, Andrea Gon-
606 zalez, Camila Gonzalez-Poblete, Charlotte Greselle, Sophie Guasco, Nika Gurianova, Sebastien Halary,
607 Eric Helfrich, Aliaksei Holik, Chiaki Homma, Michael Huber, Stephanie Hyland, Andrea Hässig, Roland

608 Häusler, Nathalie Hüsser, Badamnyambuu Iderzorig, Mizuki Igarashi, Shino Ishikawa, Sakura Ishizuka,
609 Kohei Ito, Sota Ito, Tomoki Iwashiro, Marisano James, Marianne Jaubert, Marie-Laure Jerier, Guill-
610 laume Jospin, Nao Kato, Inderjit Kaur, Akash Keluth Chavan, Mahshid Khavari, Maryna Korshevniuk,
611 Jonas Krebs, Andrii Kuklin, Antonietta La Stora, Juliana Lago, Elodie Laine, Olha Lakhneko, Ger-
612 ardo de Lamotte, Romain Lannes, Madeline Leahy, Vincent Lemaire, Dagmara Lewandowska, Manon
613 Loubens, Olexandr Lykhenko, Salah Mahmoud, Natalka Makogon, Dimitri Manoir, German Marchan-
614 don, Natalia Marciniak, Vincent Matthys, Arif Asyraf Md Supie, Irène Mauricette Mendy, Roy Meoded,
615 Mathilde Mignotte, Ryusei Miura, Kunihiko Miyake, Maria D Moccia, Mauricio Moldes, Jennifer Mo-
616 linet, Orgil-Erdene Molomjamts, Mario Moreno, Maureen Muscat, Cristina Muñoz, Francesca Nadalin,
617 Dorottya Nagy-Szakal, Ashanti Narce, Hiba Naveed, Thomas Neff, Wan Chiew Ng, Elsy Ngwa, Agier
618 Nicolas, Pierre Nicolas, Abdollahi Nika, Javier Quilez Oliete, Nils Ordioni, Mitsuki Ota, Francesco Oteri,
619 Yuya Oto, Coral Pardo-Este, Young-Ja Park, Jananan Pathmanathan, Manuel Perez, Melissa P Pizzi,
620 María Gabriela Portilla, Leonardo Posada, Catherine E. Pugh, Kyrylo Pyrshev, Sreya Ray Chaudhuri,
621 Hubert Rehrauer, Renee Richer, Paula Rodríguez, Paul Roldán, Sandra Roth, Maria Ruiz, Mariia Ry-
622 bak, Ikuto Saito, Yoshitaka Saito, Khaliun Sanchir, Kai Sasaki, Kaisei Sato, Masaki Sato, Ryo Sato,
623 Seisuke Sato, Yuma Sato, Oli Schacher, Christian Schori, Felipe Sepulveda, Juan C Severyn, Sarah
624 Shalaby, Hikaru Shirahata, Jordana M Silva, Gwenola Simon, Kasia Sluzek, Rebecca Smith, Yuya Sono-
625 hara, Nicolas Sprinsky, Stefan G Stark, Chisato Suzuki, Sora Takagi, Kou Takahashi, Naoya Takahashi,
626 Tomoki Takeda, Soma Tanaka, Andrea Tassinari, Eunice Thambiraja, Antonin Thiébaud, Takumi To-
627 gashi, Yuto Togashi, Anna Tomaselli, Itsuki Tomita, Nora C Toussaint, Takafumi Tsurumaki, Yelyzaveta
628 Tymoshenko, Mariko Usui, Sophie Vacant, Laura E Vann, Jhovana L Velasco Flores, Fabienne Velter,
629 Riccardo Vicedomini, Tomoro Warashina, Ayuki Watanabe, Tina Wunderlin, Olena Yemets, Tetiana
630 Yeskova, Shusei Yoshikawa, Stas Zubenko.

631 **6 Declaration of Interests**

632 The authors declare they have no competing interests that impacted this study. CEM is co-founder of
633 Biotia and Onegevity.

634 **7 Methods**

635 **7.1 Metadata Collection and Cleaning**

636 Metadata from individual cities was collected from a standardized form and set of data fields. The
637 principle fields collected were the location of sampling, the material being sampled, the type of object
638 being sampled, the elevation above or below ground, and the station or line where the sample was
639 collected. However, several cities were unable to use the provided apps for various reasons and submitted
640 their metadata as separate spreadsheets. Additionally, certain metadata features, such as those related
641 to sequencing and quality control, were added after initial sample collection.

642 To collate various metadata sources, we built a publicly available program which assembled a large
643 master spreadsheet with consistent sample UUIDs. After assembling the originally collected data at-
644 tributes we added normalized attributes based on the original metadata to account for surface material,
645 control status, and features of individual cities. A full description of ontologies used is provided as part
646 of the collating program.

647 **7.2 Sample Collection and Preparation**

648 To obtain a comprehensive picture of microbial communities within a sample it is essential to choose
649 a sampling method which absorbs and preserves biological materials during sampling, transport and
650 storage until DNA extraction. The effectiveness of a swab may be influenced by a number of factors,
651 including most importantly the material of the swab tip affecting the rate at which bacteria are absorbed
652 during the sampling process. Furthermore, the design of the transport tube and DNA preserving liquids
653 affect the integrity of the material during transport. Finally, the amount of background contamination
654 identified for different products should be taken into account.

655 7.2.1 Swab Comparisons

656 Surface samples were collected and preserved using a flocked swab with a DNA preservation tube. Two
657 different sets of materials were used for collection. The Copan Liquid Amies Elution Swab (ESwab, Copan
658 Diagnostics, Cat.:480C) paired with a 1mL of Liquid Amies in a plastic, screw cap tube, referred to as
659 'copan swab' and the Isohelix Swabs (Mini-Swab, Isohelix Cat.:MS-02) referred to as 'isohelix swabs',
660 which were combined with 2D Thermo Scientific™ Matrix™ storage tubes (3741-WP1D-BR/Matrix 1.0
661 ml/EA) referred to as 'matrix tube'. The matrix tubes were prefilled with the preservative liquid Zymo
662 Research DNA/RNA Shield reagent™ (R1100-250) referred to as 'Zymo shield'. After samples were
663 collected with Copan swabs they were transported at room temperature and stored at -80C until DNA
664 extraction. Isohelix swabs have been stored in matrix tubes containing 400µl Zymo shield preservative.
665 Matrix tubes were also transported at room temperature and stored at -80C until DNA extraction. We
666 tested the absorption strength of Copan and Isohelix swabs for various biological and surface materials
667 encountered when sampling subway stations. A single surface was selected for a designated sampling
668 area to test the absorption strength. Both swabs were moistened by submerging the swab for a few
669 seconds in their preservative media. The area was then swabbed for 3 min. covering the selected surface.
670 It was determined that a moistened swab would lead to greater absorption strength.

671 7.2.2 Sampling Protocol

672 A standard operating procedure (SOP) was developed for the sample collection to be followed by all
673 members of the MetaSUB consortium participating in CSD. This protocol was adapted from work by
674 Afshinneko et al. (2015). The goal was to standardize as much of the sampling procedure and ensure
675 high quality control across the various cities and sampling teams. Thus it was recommended that teams
676 collect samples from surfaces that are present throughout most subway and transit stations and systems
677 around the world. These included ticket kiosks, turnstiles, railings, seats or benches, etc. Some cities
678 had to adapt the SOP according to their city especially if they did not have a subway system and were
679 collecting samples from other transit systems. Changes to the SOP involved the types of surfaces being
680 sampled, not the sampling procedure itself. However, the vast majority of sampling teams collected
681 samples from these surfaces. Moreover, a significant amount of metadata was recorded throughout
682 sample collections to ensure as much information regarding the samples was captured. All cities also
683 developed sampling plans for their collections and submitted them for review to have swabs sent to them,
684 this was to ensure consistency across the various sites.

685 All principal investigators and MetaSUB city leaders were trained in the sampling instructions and
686 this training was further disseminated to the respective sampling teams to ensure consistent and quality
687 control sampling. Swabbers were instructed to put on gloves before each sample collection. The swab
688 was dipped in the preservative medium to be pre-moistened before collection and sampling was timed
689 to 3 minutes to ensure highest yield. Sample collectors used Copan swabs in 2016 and Isohelix swabs
690 in 2017. Other key points in training included ensure highest surface area was used for collection (i.e.
691 swab entire bench, not just one area) and avoiding any areas that appeared wet, contaminated, and not
692 consistent with a subway surface. Any other observations or important notes during sample collection
693 that could add more context to data analysis and interpretation were recorded on the notes section of
694 the metadata collection apps.

695 7.2.3 In-Lab controls CSD2016

696 As positive lab control we used 30µl ZymoBiOMICS Microbial Community standard (Catalog #D6300),
697 which we added to an empty sterile urine cap, followed by swabbing with Copan Liquid Amies Elution
698 Swab (ESwab, Copan Diagnostics, Cat.:480C) for 1.5min / 3 minutes. As negative (background) lab
699 control we used 50µl of the final resuspension buffer (MoBio PowerSoil®DNA Isolation Kit, Cat.:12888-
700 100), which we have added to an empty sterile urine cup followed by swabbing for 3 min (Fig.S1).
701 Furthermore, the working space has been swabbed for 1.5 min / 3 min before and after treatment with
702 10% bleach (Fig. S2) to test for background contamination rates. To identify the background levels of
703 biological material in the air at sample areas, a Copan swab has been held for 1.5 min - 3 min in the
704 air. To estimate the source and amount of contamination in commercial swab and tube products used
705 for MetaSUB, we tested all consumables in triplicates in the sterilized hood (UV light and 10% bleach
706 wiped with ethanol).

707 **7.2.4 DNA Extraction and Library Preparation**

708 Different extraction methods were benchmarked on the samples collected across 2015-2017, these in-
709 cluded the MoBio Powersoil DNA, Promega Maxwell, and ZymoBiomics 96 MagBead kits. Samples
710 were processed per the protocol with modifications highlighted in the Supplemental Methods. Library
711 preparation for NGS analysis were prepped at HudsonAlpha Genome Center by the same methods as de-
712 scribed in [Afshinnekoo et al. \(2015\)](#). Pilot samples collected in Barcelona and Stockholm were prepared
713 using the QIAGEN QIAseq FX DNA Library Kit.

714 **7.3 Quality Control**

715 **7.3.1 Sequencing quality**

716 We measured sequencing quality based on 5 metrics: number of reads obtained from a sample, GC
717 content, Shannon's entropy of k -mers, post PCR Qubit score, and recorded DNA concentration before
718 PCR. The number of reads in each sample was counted both before and after quality control, we used
719 the number of reads after quality control for our results though the difference was slight. GC content
720 was estimated from 100,000 reads in each sample after low quality DNA and human reads had been
721 removed. Shannon's entropy of k -mers was estimated from 10,000 reads taken from each samples. PCR
722 Qubit score and DNA concentration are described in the wet lab methods.

723 **7.3.2 Sequencing quality scores show expected trends**

724 We measured sequencing quality based on 5 metrics: number of reads obtained from a sample, GC
725 content (taken after removing human reads), Shannon's entropy of k -mers (from 10,000 reads sampled
726 from each sample), post PCR Qubit score, and recorded DNA concentration before PCR. We observed
727 good separation of negative and positive controls based on both PCR Qubit and k -mer entropy (Supp.
728 Figure [S14](#)). Distributions of DNA concentration and the number of reads were as expected. GC content
729 was broadly distributed for negative controls while positive controls were tightly clustered, expected since
730 positive controls have a consistent taxonomic profile. Comparing the number of reads before and after
731 quality control did not reveal any major outliers.

732 **7.3.3 Batch effect appears minimal**

733 A major concern for this low-biomass studies and large-scale studies are batch effects. The median flowcell
734 used in our study contained samples from 3 cities and 2 continents. However, two flowcells covered 18
735 cities from 5 or 6 continents respectively. When samples from these flowcells were plotted using UMAP
736 (see Section [2.2](#) for details) the major global trends we described were recapitulated (Supp. Figure
737 [S15A](#)). Further, when plotting samples by PCR qubit and k -mer entropy (the two metrics that most
738 reliably separated our positive and negative controls) and overlaying the flowcell used to sequence each
739 sample only one outlier flowcell was identified and this flowcell was used to sequence a large number of
740 background control samples (Supp. Figure [S15B](#)). Plots of the number of reads against city of origin and
741 surface material (Supp. Figure [S15C & D](#)) showed a stable distribution of reads across cities. Analogous
742 plots of PCR Qubit scores were less stable than the number of reads but showed a clear drop for control
743 samples (Supp. Figure [S15E & F](#)). These results led us to conclude that batch effects are likely to be
744 minimal.

745 **7.3.4 Strain Contamination**

746 We used BLASTn to align nucelotide assemblies from case samples to control samples. We used a
747 threshold of 8,000 base pairs and 99.99% identity as a minimum to consider two sequences homologous.
748 This threshold was chosen to be sensitive without solely capturing conserved regions. We identified all
749 connected groups of homologous sequences and found approximate taxonomic identifications by aligning
750 contigs to NCBI-NT using BLASTn searching for 90% nucleotide identity over half the length of the
751 longest contig in each group.

752 **7.3.5 Strain contamination is rare or absent**

753 Despite good separation of positive and negative controls (see Section [7.3.1](#)) we identified several species
754 in our negative controls which were also identified as prominent taxa in the data-set as a whole (See

755 Section 2.1). Our dilemma was that a microbial species that is common in the urban environment
756 might also reasonably be expected to be common in the lab environment. In general, negative controls
757 had lower k -mer complexity, fewer reads, and lower post PCR Qubit scores than case samples and
758 no major flowcell specific species were observed. Similarly, positive control samples were not heavily
759 contaminated. These results suggest samples are high quality but do not systematically exclude the
760 possibility of contamination.

761 Previous studies have reported that microbial species whose relative abundance is negatively cor-
762 related with DNA concentration may be contaminants. We observed a number of species that were
763 negatively correlated with DNA concentration (Supp. Figure S13A) but this distribution followed the
764 same shape (but had a greater magnitude) as a null distribution of uniformly randomly generated rela-
765 tive abundances (Supp. Figure S13B) leading us to conclude that negative correlation may simply be a
766 statistical artifact. We also plotted correlation with DNA concentration against each species mean rela-
767 tive abundance across the entire data-set (Supp. Figure S13C). Species that were negatively correlated
768 with DNA concentration were clearly more abundant than uncorrelated species, this suggests that there
769 may be a jackpot effect for prominent species in samples with lower concentrations of DNA but is not
770 generally consistent with contamination.

771 We analyzed the total complexity of case samples in comparison to control samples. Case samples
772 had a significantly higher taxonomic diversity (Supp. Figure S12A) than any type of negative control
773 sample. We also compared the confidence of taxonomic assignments to control assignments for prominent
774 taxa (Supp. Figure S12B) using the number of unique marker k -mers to compare assignments. We found
775 that case samples had more and higher quality assignments than could be found in controls. One species,
776 *Bradyrhizobium sp. BTAi1*, was not clearly better in case samples than controls but in this case we were
777 able to assemble genomes for this species in several unique samples so we feel it is ambiguous.

778 Finally, we compared assemblies from negative controls to assemblies from our case samples searching
779 for regions of high similarity that could be from the same microbial strain. We reasoned that uncon-
780 taminated samples may contain the same species as negative controls but were less likely to contain
781 identical strains. Only 137 case samples were observed to have any sequence with high similarity to
782 an assembled sequence from a negative control (8,000 base pairs minimum of 99.99% identity). The
783 identified sequences were principally from *Bradyrhizobium* and *Cutibacterium*. Since these genera are
784 core taxa (See Section 2.1) observed in nearly every sample but high similarity was only identified in a
785 few samples, we elected not to remove species from these genera from case samples.

786 7.3.6 K-Mer Based Analyses

787 We generated 31-mer profiles for raw reads using Jellyfish. All k -mers that occurred at least twice in
788 a given sample were retained. We also generated MASH sketches from the non-human reads of each
789 sample with 10 million unique minimizers per sketch.

790 We calculated the Shannon's entropy of k -mers by sampling 31-mers from a uniform 10,000 reads per
791 sample. Shannon's entropy of taxonomic profiles was calculated using the CAPalyzer package (Section
792 4).

793 7.3.7 K-Mer based metrics correlate with taxonomic metrics

794 We found clear correlations between three pairwise distance metrics (Supp. Figure S10A, B, C): k -mer
795 based Jaccard distance (MASH), taxonomic Jaccard distance, and taxonomic Jensen-Shannon diver-
796 gence. This suggests that taxonomic variation reflects meaningful variation in the underlying sequence
797 in a sample.

798 We also compared alpha diversity metrics (Supp. Figure S10D): Shannon entropy of k -mers, and
799 Shannon entropy of taxonomic profiles. As with pairwise distances these metrics were correlated though
800 noise was present. This noise may reflect sub-species taxonomic variation in our samples.

801 7.3.8 Sequence Preprocessing

802 Sequence data were processed with AdapterRemoval (v2.17, Schubert et al. (2016)) to remove low quality
803 reads and reads with ambiguous bases. Subsequently reads were aligned to the human genome (hg38,
804 including alternate contigs) using Bowtie2 (v2.3.0, fast preset, Langmead and Steven L Salzberg (2013)).
805 Read pairs where both ends mapped to the human genome were separated from read pairs where neither
806 mate mapped. Read pairs where only one mate mapped were discarded. Hereafter, we refer to the read
807 sets as human reads and non-human reads.

808 7.3.9 Unmapped DNA is not similar to any known sequence

809 A large proportion of the reads in our samples were not mapped to any references sequences. There
810 are three major reasons why a fragment of DNA would not be classified in our analysis 1) The DNA
811 originated from a non-human and non-microbial species which would not be present in the databases
812 we used for classification 2) Our classifier (KrakenUniq) failed to classify a DNA fragment that was in
813 the database due to slight mismatch 3) The DNA fragment is novel and not represented in any existing
814 database. Explanations (1) and (2) are essentially drawbacks of the database and computational model
815 used, and we can quantify them by mapping reads using a more sensitive aligner to a larger database,
816 such as BLASTn (Altschul et al., 1990), or ensemble methods for analysis (McIntyre et al., 2017). To
817 estimate the proportion of reads which could be assigned, we took 10k read subsets from each sample
818 and mapped these to a set of large database using BLASTn (see 2.1 for details). This resulted in 34.6%
819 reads which could not be mapped to any external database compared to 41.3% of reads mapped using
820 our approach with KrakenUniq. We note that our approach to estimate the fraction of reads that could
821 be classified using BLASTn does not account for hits to low quality taxa which would ultimately be
822 discarded in our pipeline, and so represents a worst-case comparison. Explanation (3) is altogether more
823 interesting and we refer to this DNA as true unclassified DNA. In this analysis we do not seek to quantify
824 the origins of true unclassified DNA except to postulate that it may derive from novel species as have
825 been identified in other similar studies.

826 7.4 Computational Analysis

827 We processed raw reads from all samples into taxonomic, functional and AMR profiles for each sample
828 using the MetaSUB Core Analysis Pipeline (Danko and Mason, 2020) (v1.0.0). This includes a prepro-
829 cessing stage that consists of AdapterRemoval (Schubert et al., 2016) and Human sequence removal with
830 Bowtie2 (Langmead and Steven L Salzberg, 2013). Pre-processed reads were subsequently processed
831 according to the methods below.

832 7.4.1 Taxonomic Analysis

833 We generated taxonomic profiles by processing non-human reads with KrakenUniq (v0.3.2 Breitwieser
834 et al. (2018)) using a database based on all draft and reference genomes in NCBI/RefSeq Microbial (bacter-
835 ia/archaea, fungi and virus) ca. March 2017. KrakenUniq was selected because its high performance,
836 as it has been demonstrated to be comparable or having higher sensitivity than the best tools identified
837 in a recent benchmarking study (McIntyre et al. (2017)) on the same comparative dataset. In addition,
838 KrakenUniq allows for tunable specificity and identifies k -mers that are unique to particular taxa in a
839 database. Reads are broken into k -mers and searched against this database. Finally, the taxonomic
840 makeup of a sample is given by identifying the taxa with the greatest leaf to ancestor weight.

841 KrakenUniq reports the number of unique marker k -mers assigned to each taxon, as well as the total
842 number of reads, the fraction of available marker k -mers found, and the mean copy number of those
843 k -mers. We found that requiring more k -mers to identify a species resulted in a roughly linear decrease
844 in the total number of species identified without a plateau or any other clear point to set a threshold
845 (Supp. Figure S9A). In an ongoing but unpublished clinical study we have used a threshold of 512
846 marker k -mers to accurately recapitulate the results of culturing while identifying few species which were
847 not cultured. Since false positives are less problematic in the current study than in a clinical study and
848 because we could use our large number of samples as a partially orthogonal confirmation we chose less
849 strict thresholds for KrakenUniq in this study.

850 At a minimum we required three reads assigned to a taxa with 64 unique marker k -mers. This setting
851 captures a group of taxa with low abundance but reasonable (~ 10 -20%) coverage of the k -mers in their
852 marker set (Supp. Figure S9C). However, this also allows for a number of taxa with very high (105)
853 duplication of the identified marker k -mers and very few k -mers per read which we believe is biologically
854 implausible (Supp. Figure S9D). We filtered these taxa by applying a further filter which required that
855 the number of reads not exceed $\frac{10}{25}$ times the number of unique k -mers, unless the set of unique k -mers
856 was saturated ($> 90\%$ completeness). We include a full list of all taxonomic calls from all samples
857 including diagnostic values for each call. We do not attempt to classify reads below the species level in
858 this study.

859 We further evaluated prominent taxonomic classifications for sequence complexity and genome cov-
860 erage. For each microbe evaluated we calculated two indices generated using a random subset of 152
861 samples: the average topological entropy of reads assigned to the microbe and the Gini-coefficient of read

862 positions on the microbial genome. For brevity we refer to these as *mean sequence entropy* (MSE) and
863 *coverage equality* (CE). The formula for topological entropy of a DNA sequence is described by [Koslicki](#)
864 [\(2011\)](#). Values close to 0 correspond to low-complexity sequences and values near 1 are high complexity.
865 In this work we use a word size of 3 with an overall sequence length of 64 since this readily fits into
866 our reads. To find the MSE of a microbial classification we take the arithmetic mean of the topological
867 entropy of all reads that map to a given microbial genome in a sample. The Gini-coefficient is a classic
868 economic measure of income inequality. We repurpose it here to evaluate the evenness of read coverage
869 over a microbial classification. Reads mapping to a microbial genome are assigned to a contiguous 10kbp
870 bin and the Gini-coefficient of all bins is calculated. Like MSE, the Gini-coefficient is bounded in $[0, 1]$.
871 Lower values indicate greater inequality, very low values indicate that a taxon may be misidentified from
872 conserved and near conserved regions. We downloaded one representative genome per species evaluated
873 and mapped all reads from samples to using Bowtie2 (sensitive-local preset). Indices were processed
874 from alignments using a custom script. Species classifications with an average MSE less than 0.75 or CE
875 less than 0.1 were flagged.

876 To determine relative abundance of taxa where applicable we rarefied samples to 100,000 classified
877 reads, computed the proportion of reads assigned to each taxon, and took the distribution of values from
878 all samples. This was the minimum number of reads sufficient to maintain taxonomic richness (Supp.
879 Figure S9B). We chose sub-sampling (sometimes referred to as rarefaction in the literature) based on the
880 study by [Weiss et al. \(2017\)](#), showing that sub-sampling effectively estimates relative abundance. Note
881 that we use the term prevalence to describe the fraction of samples where a given taxon is found at any
882 abundance and we use the term relative abundance to describe the fraction of DNA in a sample from a
883 given taxon.

884 We compared our samples to metagenomic samples from the Human Microbiome Project and a
885 metagenomic study of European soil samples using MASH ([Ondov et al., 2016](#)), a fast k -mer based
886 comparison tool. We built MASH sketches from all samples with 10 million unique k -mers to ensure
887 a sensitive and accurate comparison. We used MASH's built-in Jaccard distance function to generate
888 distances between our samples and HMP samples. We then took the distribution of distances to each
889 particular human commensal community as a proxy for the similarity of our samples to a given human
890 body site.

891 We also compared our samples to HMP and soil samples using taxonomic profiles generated by
892 MetaPhlAn v2.0 ([Segata et al., 2012](#)). We generated taxonomic profiles from non-human reads using
893 MetaPhlAn v2.0 and found the cosine similarity between all pairs of samples.

894 We used the Microbe Directory ([Shaaban et al., 2018](#)) to annotate taxonomic calls. The Microbe
895 Directory is a hand curated, machine readable, database of functional annotations for 5,000 microbial
896 species.

897 7.4.2 Functional Analysis

898 We analyzed the metabolic functions in each of our samples by processing non-human reads with HU-
899 MAnN2 ([Franzosa et al., 2018](#)). We aligned all reads to UniRef90 using DIAMOND (v0.8.36, ([Buchfink](#)
900 [et al., 2014](#))) and used HUMAnN2 to produce estimate of pathway abundance and completeness. We
901 filtered all pathways that were less than 50% covered in a given sample but otherwise took the reported
902 pathway abundance as is after relative abundance normalization (using HUMAnN2's attached script).

903 High level categories of functional pathways were found by grouping positively correlated pathways
904 and manually annotating resulting clusters.

905 7.5 Assembly and Plasmid Annotations

906 All samples were assembled using metaSPAdes (v3.8.1 [Nurk et al. \(2017\)](#)) with default settings. Assem-
907 bled scaffolds of at least 1,500bp of length were annotated using PlasFlow (v1.1 [Krawczyk et al. \(2018\)](#))
908 using default settings. PlasFlow predicts whether a contig is likely from a chromosome or a plasmid and
909 gives a rough taxonomic annotation. Predicting which sequences are from plasmids is a difficult problem
910 and some annotations may be incorrect.

911 7.5.1 Analysis of Antimicrobial Resistance Genes

912 We generated profiles of antimicrobial resistance genes using MegaRes (v1.0.1, [Lakin et al. \(2017\)](#)). To
913 generate profiles from MegaRes, we mapped non-human reads to the MegaRes database using Bowtie2
914 (v2.3.0, very-sensitive presets, [Langmead and Steven L Salzberg \(2013\)](#)). Subsequently, alignments

915 were analyzed using ResistomeAnalyzer (commit 15a52dd github.com/cdeanj/resistomeanalyzer)
916 and normalized by total reads per sample and gene length to give RPKMs. MegaRes includes an ontology
917 grouping resistance genes into gene classes, AMR mechanisms, and gene groups. AMR detection remains
918 a difficult problem and we note that detection of a homologous sequence to a known AMR gene does
919 not necessarily imply an equivalent resistance in our samples. Currently, the gold standard for detecting
920 AMR is via culturing.

921 Known AMR genes can come from gene families with homologous regions of sequence. To reduce
922 spurious mapping from gene homology we used BLASTn to align all MegaRes AMR genes against
923 themselves. We considered any connected group of genes with an average nucleotide identity of 80%
924 across 50% of the gene length as a set of potentially confounded genes. We collapsed all such groups
925 into a single pseudo-gene with the mean abundance of all constituent genes. Before clustering genes we
926 removed all genes which were annotated as requiring SNP verification to predict resistance.

927 In addition to MegaRes we mapped non-human reads from all samples to the amino acid gene se-
928 quences in the Comprehensive Antibiotic Resistance Database ([McArthur et al., 2013](#)) using DIAMOND.
929 While we do not use this analysis explicitly in this study we provide the results as a data table.

930 Assembled contigs were annotated for AMR genes using metaProdigal ([Hyatt et al., 2010](#)), HMMER3
931 ([Eddy, 2011](#)), and ResFam ([Gibson et al., 2015](#)) as described by [Rahman et al. \(2018\)](#). All predicted
932 gene annotations with an e-value higher than 10^{-10} were discarded.

933 7.5.2 Beta Diversity

934 Inter-sample (beta) diversity was measured by using Jaccard distances. We note that Jaccard distances
935 do not use relative abundance information. Matrices of Jaccard distances were produced using built in
936 SciPy functions treating all elements greater than 0 as present. Hierarchical clustering (average linkage)
937 was performed on the matrix of Jaccard distances using SciPy (<https://www.scipy.org/>).

938 Dimensionality reduction of taxonomic and functional profiles was performed using UMAP ([McInnes
939 et al., 2018](#)) on the matrix of Jaccard distances with 100 neighbours (UMAP-learn package, random
940 seed of 42). We did not use Principal Component Analysis as a preprocessing step before UMAP as it
941 is sometimes done for high dimensional data.

942 7.5.3 Alpha Diversity

943 Intra-sample (alpha) diversity was measured by using Species Richness and Shannon’s Entropy. We
944 took species richness as the total number of detected species in a sample after rarefaction to 1 million
945 reads. Shannon’s entropy is robust to sample read depth and accounts for the relative size of each
946 group in diversity estimation. Shannon’s entropy is typically defined as $H = -\sum a_i \log_2 a_i$ where a_i is the
947 relative abundance of taxon i in the sample. For alpha diversity based on k -mers or pathways, we simply
948 substitute the relative abundance of a species for the relative abundance of the relevant type of object.

949 7.5.4 GeoDNA Sequence Search

950 For building the sequence graph index, each sample was processed with KMC (version 3, [1]) to convert
951 the reads in FASTA format into lists of k -mer counts, using different values of k ranging from 13 to 19 in
952 increments of 2. All k -mers that contained the character “N” or occurred in a sample less than twice were
953 removed. For each value of k , we built a separate index, consisting of a labeled de Bruijn graph, using an
954 implicit representation of the complete graph and a compressed label representation based on Multiary
955 Binary Relation Wavelet Trees (Multi-BRWT). For further details, we refer to the manuscript [2]. To
956 build the index, for each sample the KMC k -mer count lists were transformed into de Bruijn graphs, from
957 which path covers in the form of contig sets were extracted and stored as intermediate FASTA files. The
958 contig sets of each sample were then transformed into annotation columns (one column per sample) by
959 mapping them onto an implicit complete de Bruijn graph of order k . All annotation columns were then
960 merged into a joint annotation matrix and transformed into Multi-BRWT format. Finally, the topology
961 of the Multi-BRWT representation was optimized by relaxing its internal tree arity constraints to allow
962 for a maximum arity of 40.

963 7.6 Novel Biology

964 7.7 Identifying Bacteria and Archaea

965 **Metagenomic Assembly and Binning** All samples were re-assembled with metaSPAdes (v3.10.1
966 Nurk et al., 2017); generated contigs with length <1000nt were excluded from further analysis. Remaining
967 contigs were binned with MetaBAT2 (v2.12.1 Kang et al. (2019)) with default parameters, resulting in
968 14,080 bins. As MetaBAT2 uses contig abundance (mean base coverage) in its analysis, we mapped reads
969 back to their respective contigs via Bowtie2 (v2.3.4.1 Langmead and Steven L Salzberg (2013)) with the
970 flags `-local -very-sensitive-local` to provide accurate coverage metrics. Draft genome quality was assessed
971 via CheckM (v1.0.13 Parks et al. (2015)) lineage_wf workflow with default parameters. Using the
972 strategy proposed by Parks et al. (2018) we filtered bins by quality score, defined as $QS = completeness -$
973 $5 * contamination$; bins with $QS < 50$ were removed from consideration. The remaining 6,107 bins were
974 labeled by quality based on the MIMAG standard (Bowers et al. (2018)), with some modification: 1,448
975 high quality (completeness >90%, contamination <5%, strain heterogeneity <0.5%) bins, 4,532 medium
976 quality (completeness >50%, contamination <5%) bins, all others low quality. Bins of at least medium
977 quality were selected as acceptable MAGs (5,980 total).

978 **MAG Dereplication** OTUs (MAG representatives) were chosen with a two-step clustering strategy.
979 Single-linkage clustering formed primary clusters of MAGs based on Mash ANI (v2.1.1), with intra-cluster
980 identity at 90%. Though Mash ANI can be inaccurate for potentially incomplete genomes (Olm et al.
981 (2017)), we can leverage the technique's speed for the many pairwise comparisons needed in this granular
982 step. Within primary clusters, MAGs were compared pairwise by a more accurate whole-genome ANI
983 (gANI) via dnadiff (v1.3) from MUMmer (v3.23 Kurtz et al. (2004)). Secondary, more refined clusters
984 were grouped based on gANI using average-linkage hierarchical clustering from the R package dendextend
985 (v1.12.0 Galili (2015)). A gANI cut-off of 95% resulted in 1,304 representative OTUs.

986 **OTU to Reference Genome Matching** OTUs were compared against reference genomes from Ref-
987 Seq (release 96 from November 2019, complete bacterial and archaeal genomes only, with "Exclude
988 anomalous" and "Exclude derived from surveillance project" applied) as well as the full Integrated Gut
989 Genomes (IGG) dataset (v1.0 Nayfach et al. (2019); 23,790 representative genomes). A MinHash sketch
990 was created for each reference genome via Mash (v2.1.1) with default parameters to find Mash distances
991 and select candidate "best matches" from each reference database. Then, dnadiff (v1.3) was used to
992 further quantify differences between each OTU and its best match from either database. ANI between
993 OTUs and their matches was found as "M-to-M AvgIdentity" in the query report column (ANI 95% over
994 60% OTU sequence qualified as a match).

995 **OTU Taxonomic Assignment** OTUs were placed into a bacterial or archaeal reference tree (based
996 on the Genome Database Taxonomy, GTDB) and then assigned taxonomic classifications using GTDB-
997 Tk (v1.0.2 Chaumeil et al. (2019)). GTDB-Tk relies on 120 bacterial and 122 archaeal marker genes;
998 domain assignment is chosen based on domain-specific marker content of the OTU sequence. Using the
999 GTDB-Tk placements, we built an OTU-only bacterial phylogeny with FastTree (v2.1.10 Price et al.
1000 (2010)). The tree was visualized using iTOL (v5.5 Letunic and Bork (2019)).

1001 7.7.1 Viral Discovery

1002 We followed the protocol described by Paez-Espino et al. (2017). Briefly, we used an expanded and
1003 curated set of viral protein families (VPFs) as bait in combination with recommended filtering steps to
1004 identify 16,584 UViGs directly from all MetaSUB metagenomic assemblies greater than 5kb. Then, the
1005 UViGs were clustered with the content of the IMG/VR system (a total of over 730k viral sequences
1006 including isolate viruses, prophages, and UViGs from all kind of habitats). The clustering step relied on
1007 a sequence-based classification framework (based on 95% sequence identity across 85% of the shortest
1008 sequence length) followed by the markov clustering (mcl). This approach yielded 2,009 viral clusters
1009 (ranging from 2-611 members) and 9,605 singletons (or viral clusters of 1 member), sequences that failed
1010 to cluster with any sequence from the dataset or the references from IMG/VR, resulting in a total of
1011 11,614 vOTUs. We define viral species from vOTUs as sequences sharing at least 95% identity over 85%
1012 of their length. Out of this total MetaSUB viral diversity, only 686 vOTUs clustered with any known
1013 viral sequence in IMG/VR.

1014 7.7.2 Identifying Host Virus Interactions

1015 We used two computational methods to reveal putative host-virus connections (Paez-Espino et al., 2016a).
1016 (1) For the 686 vOTUs that clustered with viral sequences from the IMG/VR system, we projected the
1017 known host information to all the members of the group (total of 2,064 MetaSUB UViGs). (2) We used
1018 bacterial/archaeal CRISPR-Cas spacer matches (from the IMG/M 1.1 million isolate spacer database) to
1019 the UViGs (allowing only for 1 SNP over the whole spacer length) to assigned a host to 1,915 MetaSUB
1020 vOTUs. Additionally, we also used a database of over 20 million CRISPR-Cas spacers identified from
1021 metagenomic contigs from the IMG/M system with taxonomy assigned. Since some of these spacers may
1022 derive from short contigs these results should be interpreted with caution.

1023 7.7.3 CRISPR Array Detection and Annotation

1024 Using CRISPRCasFinder the MetaSUB database was investigated to predict CRISPR arrays and an-
1025 notate them with their corresponding predicted type based on CRISPR-Cas genes in their vicinity.
1026 CRISPRCasFinder was run with default parameters, “-so” and “-cas” options to identify cas genes. The
1027 precision and recall of the virus detection was 99.6% and 37.5% respectively, as previously reported by
1028 (Paez-Espino et al., 2016b).

1029 CRISPR-Cas types were assigned to arrays based on detected cas genes within a 10 kilobases vicinity.
1030 Cases where CRISPRCasFinder associated several cas genes of contradicting CRISPR-Cas types with
1031 the same CRISPR array were regarded as unclear annotation. This procedure yielded 838,532 predicted
1032 CRISPR arrays (with additional CRISPR arrays predicted with default parameters for PILER-CR), of
1033 which, 3,245 CRISPR arrays had unambiguous annotation, resulting in 43,656 unique spacers queried
1034 against genomic databases using BLASTN.

1035 7.8 Organisms/BLAST Databases

1036 In order to associate detected spacers within defined groups (plasmids, prophages, viruses) four different
1037 genomic databases were aggregated to be searched with BLASTN. The aggregated database consisted
1038 of IMG/VR, PHASTER, and PLSDB alongside bacterial and archaeal genomic sequences from the
1039 National Center for Biotechnology Information (NCBI). All database downloads were made on the 28th
1040 January 2020. Detected and annotated spacers were searched against the databases mentioned above
1041 using BLASTN with the following additional arguments, which correspond to the default parameters of
1042 CRISPRtarget: word_size=7, evalue=1, gapopen=10, gapextend=2, penalty=-1, reward=1.

1043 7.9 MetaSUB Genomic Database and Statistical Analysis

1044 Genomic data was acquired from the MetaSUB database and matched by sample names to the cor-
1045 responding metadata downloaded from the MetaSUB-metadata github repository (<https://github.com/MetaSUB/MetaSUB-metadata>). All data derived from MetaSUB and the subsequent steps described
1046 above was then analysed using Python 3.6. Python packages plotnine, plotly, matplotlib and seaborn
1047 where used for plotting as well as pandas to create and manage dataframes. The heatmap is clustered
1048 by Euclidean distance on the columns.
1049

1050

References

- 1051
- 1052 Afshinnkoo, E., Chou, C., Alexander, N., Ahsanuddin, S., Schuetz, A. N., and Mason, C. E. (2017).
1053 Precision metagenomics: Rapid metagenomic analyses for infectious disease diagnostics and public
1054 health surveillance. *Journal of Biomolecular Techniques*, 28(1):40–45.
- 1055 Afshinnkoo, E., Meydan, C., Chowdhury, S., Jaroudi, D., Boyer, C., Bernstein, N., Maritz, J. M.,
1056 Reeves, D., Gandara, J., Chhangawala, S., Ahsanuddin, S., Simmons, A., Nessel, T., Sundaresh, B.,
1057 Pereira, E., Jorgensen, E., Kolokotronis, S. O., Kirchberger, N., Garcia, I., Gandara, D., Dhanraj, S.,
1058 Nawrin, T., Saletore, Y., Alexander, N., Vijay, P., Hénaff, E. M., Zumbo, P., Walsh, M., O'Mullan,
1059 G. D., Tighe, S., Dudley, J. T., Dunaif, A., Ennis, S., O'Halloran, E., Magalhaes, T. R., Boone, B.,
1060 Jones, A. L., Muth, T. R., Paolantonio, K. S., Alter, E., Schadt, E. E., Garbarino, J., Prill, R. J.,
1061 Carlton, J. M., Levy, S., and Mason, C. E. (2015). Geospatial Resolution of Human and Bacterial
1062 Diversity with City-Scale Metagenomics. *Cell Systems*, 1(1):72–87.
- 1063 Allen, H. K., Moe, L. A., Rodbumrer, J., Gaarder, A., and Handelsman, J. (2009). Functional metage-
1064 nomics reveals diverse β -lactamases in a remote alaskan soil. *The ISME journal*, 3(2):243–251.
- 1065 Altschul, S. F., Gish, W., Miller, W., Myers, E. W., and Lipman, D. J. (1990). Altschul et al.. 1990.
1066 Basic Local Alignment Search Tool.pdf.
- 1067 Bahram, M., Hildebrand, F., Forslund, S. K., Anderson, J. L., Soudzilovskaia, N. A., Bodegom, P. M.,
1068 Bengtsson-Palme, J., Anslan, S., Coelho, L. P., Harend, H., Huerta-Cepas, J., Medema, M. H., Maltz,
1069 M. R., Mundra, S., Olsson, P. A., Pent, M., Pölme, S., Sunagawa, S., Ryberg, M., Tedersoo, L., and
1070 Bork, P. (2018). Structure and function of the global topsoil microbiome.
- 1071 Bougnom, B. P. and Piddock, L. J. (2017). Wastewater for Urban Agriculture: A Significant Factor in
1072 Dissemination of Antibiotic Resistance.
- 1073 Bowers, R. M., Kyrpides, N. C., Stepanauskas, R., Harmon-Smith, M., Doud, D., Reddy, T. B. K.,
1074 Schulz, F., Jarett, J., Rivers, A. R., Eloie-Fadrosch, E. A., Tringe, S. G., Ivanova, N. N., Copeland,
1075 A., Clum, A., Becraft, E. D., Malmstrom, R. R., Birren, B., Podar, M., Bork, P., Weinstock, G. M.,
1076 Garrity, G. M., Dodsworth, J. A., Yooseph, S., Sutton, G., Glöckner, F. O., Gilbert, J. A., Nelson,
1077 W. C., Hallam, S. J., Jungbluth, S. P., Ettema, T. J. G., Tighe, S., Konstantinidis, K. T., Liu, W. T.,
1078 Baker, B. J., Rattei, T., Eisen, J. A., Hedlund, B., McMahon, K. D., Fierer, N., Knight, R., Finn, R.,
1079 Cochrane, G., Karsch-Mizrachi, I., Tyson, G. W., Rinke, C., Lapidus, A., Meyer, F., Yilmaz, P., Parks,
1080 D. H., Eren, A. M., Schriml, L., Banfield, J. F., Hugenholtz, P., and Woyke, T. (2018). Corrigendum:
1081 Minimum information about a single amplified genome (MISAG) and a metagenome-assembled genome
1082 (MIMAG) of bacteria and archaea. *Nat. Biotechnol.*, 36(7):660.
- 1083 Breitwieser, F. P., Baker, D. N., and Salzberg, S. L. (2018). KrakenUniq: confident and fast metagenomics
1084 classification using unique k-mer counts. *Genome biology*, 19(1):198.
- 1085 Brito, I. L., Yilmaz, S., Huang, K., Xu, L., Jupiter, S. D., Jenkins, A. P., Naisilisili, W., Tamminen, M.,
1086 Smillie, C. S., Wortman, J. R., Birren, B. W., Xavier, R. J., Blainey, P. C., Singh, A. K., Gevers, D.,
1087 and Alm, E. J. (2016). Mobile genes in the human microbiome are structured from global to individual
1088 scales. *Nature*, 535(7612):435–439.
- 1089 Brooks, B., Olm, M. R., Firek, B. A., Baker, R., Thomas, B. C., Morowitz, M. J., and Banfield, J. F.
1090 (2017). Strain-resolved analysis of hospital rooms and infants reveals overlap between the human and
1091 room microbiome. *Nature communications*, 8(1):1–7.
- 1092 Buchfink, B., Xie, C., and Huson, D. H. (2014). Fast and sensitive protein alignment using DIAMOND.
1093 *Nature Methods*, 12(1):59–60.
- 1094 Cáliz, J., Triadó-Margarit, X., Camarero, L., and Casamayor, E. O. (2018). A long-term survey unveils
1095 strong seasonal patterns in the airborne microbiome coupled to general and regional atmospheric
1096 circulations. *Proceedings of the National Academy of Sciences*, 115(48):12229–12234.
- 1097 Chaumeil, P. A., Mussig, A. J., Hugenholtz, P., and Parks, D. H. (2019). GTDB-Tk: a toolkit to classify
1098 genomes with the Genome Taxonomy Database. *Bioinformatics*.

- 1099 Consortium, T. H. M. P., Human, T., Project, M., Consortium, T. H. M. P., Human, T., and Project, M.
1100 (2012). Structure, function and diversity of the healthy human microbiome. *Nature*, 486(7402):207–14.
- 1101 Cooley, J. D., Wong, W. C., Jumper, C. A., and Straus, D. C. (1998). Correlation between the prevalence
1102 of certain fungi and sick building syndrome. *Occupational and Environmental Medicine*, 55(9):579–584.
- 1103 Danko, D. C. and Mason, C. (2020). The metasub microbiome core analysis pipeline enables large scale
1104 metagenomic analysis.
- 1105 Delgado-Baquerizo, M., Oliverio, A. M., Brewer, T. E., Benavent-González, A., Eldridge, D. J., Bardgett,
1106 R. D., Maestre, F. T., Singh, B. K., and Fierer, N. (2018). A global atlas of the dominant bacteria
1107 found in soil. *Science*, 359(6373):320–325.
- 1108 Eckburg, P. B., Mian, M. F., Surette, M. G., Bienenstock, J., Forsythe, P., and Sargent, M. (2005).
1109 Diversity of the Human Intestinal Microbial Flora. *Science*, 308(5728):1635–1638.
- 1110 Eddy, S. R. (2011). Accelerated profile HMM searches. *PLoS Computational Biology*, 7(10).
- 1111 Franzosa, E. A., McIver, L. J., Rahnavard, G., Thompson, L. R., Schirmer, M., Weingart, G., Lipson,
1112 K. S., Knight, R., Caporaso, J. G., Segata, N., and Huttenhower, C. (2018). Species-level functional
1113 profiling of metagenomes and metatranscriptomes. *Nature methods*, 15(11):962–968.
- 1114 Fresia, P., Antelo, V., Salazar, C., Giménez, M., D’Alessandro, B., Afshinnekoo, E., Mason, C., Gonnet,
1115 G. H., and Iraola, G. (2019). Urban metagenomics uncover antibiotic resistance reservoirs in coastal
1116 beach and sewage waters. *Microbiome*, 7(1).
- 1117 Galili, T. (2015). dendextend: an R package for visualizing, adjusting and comparing trees of hierarchical
1118 clustering. *Bioinformatics*, 31(22):3718–3720.
- 1119 Gardy, J. L. and Loman, N. J. (2018). Towards a genomics-informed, real-time, global pathogen surveil-
1120 lance system.
- 1121 Gibson, M. K., Forsberg, K. J., and Dantas, G. (2015). Improved annotation of antibiotic resistance
1122 determinants reveals microbial resistomes cluster by ecology. *ISME Journal*, 9(1):207–216.
- 1123 Gilbert, J. A. and Stephens, B. (2018). Microbiology of the built environment.
- 1124 Hendriksen, R. S., Munk, P., Njage, P., van Bunnik, B., McNally, L., Lukjancenko, O., Röder, T.,
1125 Nieuwenhuijse, D., Pedersen, S. K., Kjeldgaard, J., Kaas, R. S., Clausen, P. T. L. C., Vogt, J. K.,
1126 Leekitcharoenphon, P., van de Schans, M. G. M., Zuidema, T., de Roda Husman, A. M., Rasmussen,
1127 S., Petersen, B., Bego, A., Rees, C., Cassar, S., Coventry, K., Collignon, P., Allerberger, F., Rahube,
1128 T. O., Oliveira, G., Ivanov, I., Vuthy, Y., Sopheak, T., Yost, C. K., Ke, C., Zheng, H., Baisheng,
1129 L., Jiao, X., Donado-Godoy, P., Coulibaly, K. J., Jergović, M., Hrenovic, J., Karpíšková, R., Villacis,
1130 J. E., Legesse, M., Eguale, T., Heikinheimo, A., Malania, L., Nitsche, A., Brinkmann, A., Saba,
1131 C. K. S., Kocsis, B., Solymosi, N., Thorsteinsdottir, T. R., Hatha, A. M., Alebouyeh, M., Morris,
1132 D., Cormican, M., O’Connor, L., Moran-Gilad, J., Alba, P., Battisti, A., Shakenova, Z., Kiiyukia, C.,
1133 Ng’eno, E., Raka, L., Avsejenko, J., Bērziņš, A., Bartkevics, V., Penny, C., Rajandas, H., Parimannan,
1134 S., Haber, M. V., Pal, P., Jeunen, G.-J., Gemmell, N., Fashae, K., Holmstad, R., Hasan, R., Shakoor,
1135 S., Rojas, M. L. Z., Wasyl, D., Bosevska, G., Kochubovski, M., Radu, C., Gassama, A., Radosavljevic,
1136 V., Wuertz, S., Zuniga-Montanez, R., Tay, M. Y. F., Gavačová, D., Pastuchova, K., Truska, P., Trkov,
1137 M., Esterhuyse, K., Keddy, K., Cerdà-Cuellar, M., Pathirage, S., Norrgren, L., Örn, S., Larsson,
1138 D. G. J., Heijden, T. V. d., Kumburu, H. H., Sanneh, B., Bidjada, P., Njanpop-Lafourcade, B.-M.,
1139 Nikiema-Pessinaba, S. C., Levent, B., Meschke, J. S., Beck, N. K., Van, C. D., Phuc, N. D., Tran,
1140 D. M. N., Kwenda, G., Tabo, D.-a., Wester, A. L., Cuadros-Orellana, S., Amid, C., Cochrane, G.,
1141 Sicheritz-Ponten, T., Schmitt, H., Alvarez, J. R. M., Aidara-Kane, A., Pamp, S. J., Lund, O., Hald,
1142 T., Woolhouse, M., Koopmans, M. P., Vigre, H., Petersen, T. N., Aarestrup, F. M., and project
1143 consortium, T. G. S. S. (2019). Global monitoring of antimicrobial resistance based on metagenomics
1144 analyses of urban sewage. *Nature Communications*, 10(1):1124.
- 1145 Hoch, J. M., Rhodes, M. E., Shek, K. L., Dinwiddie, D., Hiebert, T. C., Gill, A. S., Salazar Estrada,
1146 A., Griffin, K. L., Palmer, M. I., and McGuire, K. L. (2019). Soil microbial assemblages are linked to
1147 plant community composition and contribute to ecosystem services on urban green roofs. *Front. Ecol.*
1148 *Evol. 7: 198. doi: 10.3389/fevo.*

- 1149 Hsu, T., Joice, R., Vallarino, J., Abu-Ali, G., Hartmann, E. M., Shafquat, A., DuLong, C., Baranowski,
1150 C., Gevers, D., Green, J. L., Morgan, X. C., Spengler, J. D., and Huttenhower, C. (2016). Urban
1151 Transit System Microbial Communities Differ by Surface Type and Interaction with Humans and the
1152 Environment. *mSystems*, 1(3):e00018–16.
- 1153 Hyatt, D., Chen, G. L., LoCascio, P. F., Land, M. L., Larimer, F. W., and Hauser, L. J. (2010). Prodigal:
1154 Prokaryotic gene recognition and translation initiation site identification. *BMC Bioinformatics*, 11.
- 1155 Joseph, S. M., Battaglia, T., Maritz, J. M., Carlton, J. M., and Blaser, M. J. (2019). Longitudinal
1156 comparison of bacterial diversity and antibiotic resistance genes in new york city sewage. *MSystems*,
1157 4(4):e00327–19.
- 1158 Joyner, J. L., Kerwin, J., Deeb, M., Lozefski, G., Paltseva, A., Prithiviraj, B., McLaughlin, J., Cheng,
1159 Z., Groffman, P., and Muth, T. R. (2019). Green infrastructure design influences urban soil bacteria
1160 communities. *Frontiers in microbiology*, 10:982.
- 1161 Kang, D. D., Li, F., Kirton, E., Thomas, A., Egan, R., An, H., and Wang, Z. (2019). MetaBAT
1162 2: an adaptive binning algorithm for robust and efficient genome reconstruction from metagenome
1163 assemblies. *PeerJ*, 7:e7359.
- 1164 Kang, K., Ni, Y., Li, J., Imamovic, L., Sarkar, C., Kobler, M. D., Heshiki, Y., Zheng, T., Kumari, S.,
1165 Wong, J. C. Y., Archana, A., Wong, C. W. M., Dingle, C., Denizen, S., Baker, D. M., Sommer, M.
1166 O. A., Webster, C. J., and Panagiotou, G. (2018). The Environmental Exposures and Inner- and
1167 Intercity Traffic Flows of the Metro System May Contribute to the Skin Microbiome and Resistome.
1168 *Cell Reports*, 24(5):1190–1202.e5.
- 1169 Kim, D., Hofstaedter, C. E., Zhao, C., Mattei, L., Tanes, C., Clarke, E., Lauder, A., Sherrill-Mix,
1170 S., Chehoud, C., Kelsen, J., et al. (2017). Optimizing methods and dodging pitfalls in microbiome
1171 research. *Microbiome*, 5(1):52.
- 1172 Klein, E. Y., Van Boeckel, T. P., Martinez, E. M., Pant, S., Gandra, S., Levin, S. A., Goossens, H.,
1173 and Laxminarayan, R. (2018). Global increase and geographic convergence in antibiotic consumption
1174 between 2000 and 2015. *Proceedings of the National Academy of Sciences*, 115(15):E3463–E3470.
- 1175 Korownyk, C., Liu, F., and Garrison, S. (2018). Population level evidence for seasonality of the human
1176 microbiome. *Chronobiology International*, 35(4):573–577.
- 1177 Koslicki, D. (2011). Topological entropy of DNA sequences. *Bioinformatics*, 27(8):1061–1067.
- 1178 Krawczyk, P. S., Lipinski, L., and Dziembowski, A. (2018). PlasFlow: predicting plasmid sequences in
1179 metagenomic data using genome signatures. *Nucleic Acids Research*, 46(6):e35–e35.
- 1180 Kurtz, S., Phillippy, A., Delcher, A. L., Smoot, M., Shumway, M., Antonescu, C., and Salzberg, S. L.
1181 (2004). Versatile and open software for comparing large genomes. *Genome Biol.*, 5(2):R12.
- 1182 Ladner, J. T., Grubaugh, N. D., Pybus, O. G., and Andersen, K. G. (2019). Precision epidemiology for
1183 infectious disease control.
- 1184 Lakin, S. M., Dean, C., Noyes, N. R., Dettenwanger, A., Ross, A. S., Doster, E., Rovira, P., Abdo, Z.,
1185 Jones, K. L., Ruiz, J., Belk, K. E., Morley, P. S., and Boucher, C. (2017). MEGARes: An antimicrobial
1186 resistance database for high throughput sequencing. *Nucleic Acids Research*, 45(D1):D574–D580.
- 1187 Langmead and Steven L Salzberg (2013). Bowtie2. *Nature methods*, 9(4):357–359.
- 1188 Lax, S., Sangwan, N., Smith, D., Larsen, P., Handley, K. M., Richardson, M., Guyton, K., Krezalek,
1189 M., Shogan, B. D., Defazio, J., et al. (2017). Bacterial colonization and succession in a newly opened
1190 hospital. *Science translational medicine*, 9(391):eaah6500.
- 1191 Letunic, I. and Bork, P. (2019). Interactive Tree Of Life (iTOL) v4: recent updates and new develop-
1192 ments. *Nucleic Acids Res.*, 47(W1):W256–W259.
- 1193 Leung, M. H., Wilkins, D., Li, E. K., Kong, F. K., and Lee, P. K. (2014). Indoor-air microbiome in an
1194 urban subway network: diversity and dynamics. *Appl. Environ. Microbiol.*, 80(21):6760–6770.

- 1195 Lloyd-Price, J., Mahurkar, A., Rahnavard, G., Crabtree, J., Orvis, J., Hall, A. B., Brady, A., Creasy,
1196 H. H., McCracken, C., Giglio, M. G., McDonald, D., Franzosa, E. A., Knight, R., White, O., and
1197 Huttenhower, C. (2017). Strains, functions and dynamics in the expanded Human Microbiome Project.
1198 *Nature*, 550(7674):61–66.
- 1199 Maritz, J. M., Ten Eyck, T. A., Alter, S. E., and Carlton, J. M. (2019). Patterns of protist diversity
1200 associated with raw sewage in new york city. *The ISME journal*, 13(11):2750–2763.
- 1201 Martínez, J. L. (2008). Antibiotics and antibiotic resistance genes in natural environments. *Science*,
1202 321(5887):365–367.
- 1203 Mason-Buck, G., Graf, A., Elhaik, E., Robinson, J., Pospiech, E., Oliveira, M., Moser, J., Lee, P. K. H.,
1204 Githae, D., Ballard, D., Bromberg, Y., Casimiro-Soriguer, C. S., Dhungel, E., Ahn, T.-H., Kawulok,
1205 J., Loucera, C., Ryan, F., Walker, A. R., Zhu, C., Mason, C. E., Amorim, A., Syndercombe Court,
1206 D., Branicki, W., and Łabaj, P. (2020). DNA based methods in intelligence - moving towards metage-
1207 nomics. *Preprints*, page 2020020158.
- 1208 McArthur, A. G., Waglechner, N., Nizam, F., Yan, A., Azad, M. A., Baylay, A. J., Bhullar, K., Canova,
1209 M. J., De Pascale, G., Ejim, L., Kalan, L., King, A. M., Koteva, K., Morar, M., Mulvey, M. R.,
1210 O’Brien, J. S., Pawlowski, A. C., Piddock, L. J., Spanogiannopoulos, P., Sutherland, A. D., Tang, I.,
1211 Taylor, P. L., Thaker, M., Wang, W., Yan, M., Yu, T., and Wright, G. D. (2013). The comprehensive
1212 antibiotic resistance database. *Antimicrobial Agents and Chemotherapy*, 57(7):3348–3357.
- 1213 McInnes, L., Healy, J., Saul, N., and Großberger, L. (2018). UMAP: Uniform Manifold Approximation
1214 and Projection. *Journal of Open Source Software*, 3(29):861.
- 1215 McIntyre, A. B., Ounit, R., Afshinnekoo, E., Prill, R. J., Hénaff, E., Alexander, N., Minot, S. S., Danko,
1216 D., Foon, J., Ahsanuddin, S., Tighe, S., Hasan, N. A., Subramanian, P., Moffat, K., Levy, S., Lonardi,
1217 S., Greenfield, N., Colwell, R. R., Rosen, G. L., and Mason, C. E. (2017). Comprehensive benchmarking
1218 and ensemble approaches for metagenomic classifiers. *Genome Biology*, 18(1).
- 1219 McLaren, M. R., Willis, A. D., and Callahan, B. J. (2019). Consistent and correctable bias in metage-
1220 nomic sequencing measurements. *BioRxiv*, page 559831.
- 1221 MetaSUB International Consortium. Mason, C., Afshinnekoo, E., Ahsannudin, S., Ghedin, E., Read,
1222 T., Fraser, C., Dudley, J., Hernandez, M., Bowler, C., Stolovitzky, G., Chernonetz, A., Gray, A.,
1223 Darling, A., Burke, C., ?abaj, P. P., Graf, A., Noushmehr, H., Moraes, S., Dias-Neto, E., Ugalde, J.,
1224 Guo, Y., Zhou, Y., Xie, Z., Zheng, D., Zhou, H., Shi, L., Zhu, S., Tang, A., Ivankovi?, T., Siam, R.,
1225 Rascovan, N., Richard, H., Lafontaine, I., Baron, C., Nedunuri, N., Prithiviraj, B., Hyat, S., Mehr,
1226 S., Banihashemi, K., Segata, N., Suzuki, H., Alpuche Aranda, C. M., Martinez, J., Christopher Dada,
1227 A., Osuolale, O., Oguntoyinbo, F., Dybwad, M., Oliveira, M., Fernandes, A., Oliveira, M., Fernandes,
1228 A., Chatziefthimiou, A. D., Chaker, S., Alexeev, D., Chuvelev, D., Kurilshikov, A., Schuster, S., Siwo,
1229 G. H., Jang, S., Seo, S. C., Hwang, S. H., Ossowski, S., Bezdan, D., Udekwu, K., Udekwu, K., Lungj-
1230 dahl, P. O., Nikolayeva, O., Sezerman, U., Kelly, F., Mestrstry, S., Elhaik, E., Gonnet, G., Schriml,
1231 L., Mongodin, E., Huttenhower, C., Gilbert, J., Hernandez, M., Vayndorf, E., Blaser, M., Schadt,
1232 E., Eisen, J., Beitel, C., Hirschberg, D., Schriml, L., and Mongodin, E. (2016). The Metagenomics
1233 and Metadesign of the Subways and Urban Biomes (MetaSUB) International Consortium inaugural
1234 meeting report. *Microbiome*, 4(1):24.
- 1235 Meyer, K. M., Memiaghe, H., Korte, L., Kenfack, D., Alonso, A., and Bohannan, B. J. (2018). Why do
1236 microbes exhibit weak biogeographic patterns? *ISME Journal*, 12(6):1404–1413.
- 1237 Moskowitz, D. M. and Greenleaf, W. J. (2018). Nonparametric analysis of contributions to variance in
1238 genomics and epigenomics data. *bioRxiv*.
- 1239 Nayfach, S., Shi, Z. J., Seshadri, R., Pollard, K. S., and Kyrpides, N. C. (2019). New insights from
1240 uncultivated genomes of the global human gut microbiome. *Nature*, 568(7753):505–510.
- 1241 Neiderud, C. J. (2015). How urbanization affects the epidemiology of emerging infectious diseases. *African*
1242 *Journal of Disability*, 5(1).
- 1243 Nicolaou, N., Siddique, N., and Custovic, A. (2005). Allergic disease in urban and rural populations:
1244 Increasing prevalence with increasing urbanization. *Allergy: European Journal of Allergy and Clinical*
1245 *Immunology*, 60(11):1357–1360.

- 1246 Nurk, S., Meleshko, D., Korobeynikov, A., and Pevzner, P. A. (2017). MetaSPAdes: A new versatile
1247 metagenomic assembler. *Genome Research*, 27(5):824–834.
- 1248 O’Hara, N. B., Reed, H. J., Afshinnkoo, E., Harvin, D., Caplan, N., Rosen, G., Frye, B., Woloszynek, S.,
1249 Ounit, R., Levy, S., Butler, E., and Mason, C. E. (2017). Metagenomic characterization of ambulances
1250 across the USA. *Microbiome*, 5(1):125.
- 1251 Olm, M. R., Brown, C. T., Brooks, B., and Banfield, J. F. (2017). dRep: a tool for fast and accurate ge-
1252 nomic comparisons that enables improved genome recovery from metagenomes through de-replication.
1253 *ISME J*, 11(12):2864–2868.
- 1254 Ondov, B. D., Treangen, T. J., Melsted, P., Mallonee, A. B., Bergman, N. H., Koren, S., and Phillippy,
1255 A. M. (2016). Mash: fast genome and metagenome distance estimation using MinHash. *Genome*
1256 *biology*, 17(1):132.
- 1257 Paez-Espino, D., Eloë-Fadrosh, E. A., Pavlopoulos, G. A., Thomas, A. D., Huntemann, M., Mikhailova,
1258 N., Rubin, E., Ivanova, N. N., and Kyrpides, N. C. (2016a). Uncovering Earth’s virome. *Nature*,
1259 536(7617):425–430.
- 1260 Paez-Espino, D., Eloë-Fadrosh, E. A., Pavlopoulos, G. A., Thomas, A. D., Huntemann, M., Mikhailova,
1261 N., Rubin, E., Ivanova, N. N., and Kyrpides, N. C. (2016b). Uncovering earth’s virome. *Nature*,
1262 536(7617):425–430.
- 1263 Paez-Espino, D., Pavlopoulos, G. A., Ivanova, N. N., and Kyrpides, N. C. (2017). Nontargeted virus
1264 sequence discovery pipeline and virus clustering for metagenomic data. *Nature Protocols*, 12(8):1673–
1265 1682.
- 1266 Paez-Espino, D., Roux, S., Chen, I. M. A., Palaniappan, K., Ratner, A., Chu, K., Huntemann, M.,
1267 Reddy, T. B., Pons, J. C., Llabrés, M., Eloë-Fadrosh, E. A., Ivanova, N. N., and Kyrpides, N. C.
1268 (2019). IMG/VR v.2.0: An integrated data management and analysis system for cultivated and
1269 environmental viral genomes. *Nucleic Acids Research*, 47(D1):D678–D686.
- 1270 Parks, D. H., Imelfort, M., Skennerton, C. T., Hugenholtz, P., and Tyson, G. W. (2015). CheckM:
1271 assessing the quality of microbial genomes recovered from isolates, single cells, and metagenomes.
1272 *Genome Res.*, 25(7):1043–1055.
- 1273 Parks, D. H., Rinke, C., Chuvochina, M., Chaumeil, P. A., Woodcroft, B. J., Evans, P. N., Hugenholtz,
1274 P., and Tyson, G. W. (2018). Author Correction: Recovery of nearly 8,000 metagenome-assembled
1275 genomes substantially expands the tree of life. *Nat Microbiol*, 3(2):253.
- 1276 Pasolli, E., Asnicar, F., Manara, S., Zolfo, M., Karcher, N., Armanini, F., Beghini, F., Manghi, P.,
1277 Tett, A., Ghensi, P., et al. (2019). Extensive unexplored human microbiome diversity revealed by over
1278 150,000 genomes from metagenomes spanning age, geography, and lifestyle. *Cell*, 176(3):649–662.
- 1279 Price, M. N., Dehal, P. S., and Arkin, A. P. (2010). FastTree 2—approximately maximum-likelihood trees
1280 for large alignments. *PLoS ONE*, 5(3):e9490.
- 1281 Qin, J., Li, R., Raes, J., and Arumugam, M. (2010). A human gut microbial gene catalogue established
1282 by metagenomic sequencing: Commentary.
- 1283 Rahman, S. F., Olm, M. R., Morowitz, M. J., and Banfield, J. F. (2018). Machine Learning Leverag-
1284 ing Genomes from Metagenomes Identifies Influential Antibiotic Resistance Genes in the Infant Gut
1285 Microbiome. *mSystems*, 3(1).
- 1286 Rice, L. B. (2012). Mechanisms of resistance and clinical relevance of resistance to β -lactams, glycopep-
1287 tides, and fluoroquinolones. In *Mayo Clinic Proceedings*, volume 87, pages 198–208. Elsevier.
- 1288 Ritchie, H. and Roser, M. (2020). Urbanization. *Our World in Data*.
1289 <https://ourworldindata.org/urbanization>.
- 1290 Schubert, M., Lindgreen, S., and Orlando, L. (2016). AdapterRemoval v2: Rapid adapter trimming,
1291 identification, and read merging. *BMC Research Notes*, 9(1).

- 1292 Segata, N., Waldron, L., Ballarini, A., Narasimhan, V., Jousson, O., and Huttenhower, C. (2012).
1293 Metagenomic microbial community profiling using unique clade-specific marker genes. *Nature Methods*,
1294 9(8):811.
- 1295 Shaaban, H., Westfall, D. A., Mohammad, R., Danko, D., Bezdán, D., Afshinnekoo, E., Segata, N.,
1296 and Mason, C. E. (2018). The Microbe Directory: An annotated, searchable inventory of microbes'
1297 characteristics. *Gates Open Research*, 2:3.
- 1298 Singer, A. C., Shaw, H., Rhodes, V., and Hart, A. (2016). Review of antimicrobial resistance in the
1299 environment and its relevance to environmental regulators. *Frontiers in microbiology*, 7:1728.
- 1300 Thanner, S., Drissner, D., and Walsh, F. (2016). Antimicrobial resistance in agriculture. *MBio*,
1301 7(2):e02227–15.
- 1302 Thompson, L. R., Sanders, J. G., McDonald, D., Amir, A., Ladau, J., Locey, K. J., Prill, R. J., Tripathi,
1303 A., Gibbons, S. M., Ackermann, G., Navas-Molina, J. A., Janssen, S., Kopylova, E., Vazquez-Baeza,
1304 Y., Gonzalez, A., Morton, J. T., Mirarab, S., Xu, Z. Z., Jiang, L., Haroon, M. F., Kanbar, J., Zhu, Q.,
1305 Song, S. J., Kosciulek, T., Bokulich, N. A., Lefler, J., Brislawn, C. J., Humphrey, G., Owens, S. M.,
1306 Hampton-Marcell, J., Berg-Lyons, D., McKenzie, V., Fierer, N., Fuhrman, J. A., Clauset, A., Stevens,
1307 R. L., Shade, A., Pollard, K. S., Goodwin, K. D., Jansson, J. K., Gilbert, J. A., and Knight, R. (2017).
1308 A communal catalogue reveals Earth's multiscale microbial diversity. *Nature*, 551(7681):457–463.
- 1309 United Nations (2016). Political declaration of the high-level meeting of the General Assembly on
1310 antimicrobial resistance. Technical report.
- 1311 United Nations (2018). World Urbanization Prospects: The 2018 Revision. Key facts. Technical report.
- 1312 Van Boeckel, T. P., Brower, C., Gilbert, M., Grenfell, B. T., Levin, S. A., Robinson, T. P., Teillant, A.,
1313 and Laxminarayan, R. (2015). Global trends in antimicrobial use in food animals. *Proceedings of the*
1314 *National Academy of Sciences of the United States of America*, 112(18):5649–54.
- 1315 Venter, H., Henningsen, M. L., and Begg, S. L. (2017). Antimicrobial resistance in healthcare, agriculture
1316 and the environment: the biochemistry behind the headlines. *Essays in biochemistry*, 61(1):1–10.
- 1317 Weiss, S., Xu, Z. Z., Peddada, S., Amir, A., Bittinger, K., Gonzalez, A., Lozupone, C., Zaneveld, J. R.,
1318 Vázquez-Baeza, Y., Birmingham, A., Hyde, E. R., and Knight, R. (2017). Normalization and microbial
1319 differential abundance strategies depend upon data characteristics. *Microbiome*, 5(1):27.
- 1320 Wilson, M. R., Sample, H. A., Zorn, K. C., Arevalo, S., Yu, G., Neuhaus, J., Federman, S., Stryke,
1321 D., Briggs, B., Langelier, C., Berger, A., Douglas, V., Josephson, S. A., Chow, F. C., Fulton, B. D.,
1322 DeRisi, J. L., Gelfand, J. M., Naccache, S. N., Bender, J., Dien Bard, J., Murkey, J., Carlson, M.,
1323 Vespa, P. M., Vijayan, T., Allyn, P. R., Campeau, S., Humphries, R. M., Klausner, J. D., Ganzon,
1324 C. D., Memar, F., Ocampo, N. A., Zimmermann, L. L., Cohen, S. H., Polage, C. R., DeBiasi, R. L.,
1325 Haller, B., Dallas, R., Maron, G., Hayden, R., Messacar, K., Dominguez, S. R., Miller, S., and Chiu,
1326 C. Y. (2019). Clinical Metagenomic Sequencing for Diagnosis of Meningitis and Encephalitis. *New*
1327 *England Journal of Medicine*, 380(24):2327–2340.
- 1328 Yooseph, S., Andrews-Pfannkoch, C., Tenney, A., McQuaid, J., Williamson, S., Thiagarajan, M., Bami,
1329 D., Zeigler-Allen, L., Hoffman, J., Goll, J. B., et al. (2013). A metagenomic framework for the study
1330 of airborne microbial communities. *PLoS One*, 8(12):e81862.
- 1331 Zhu, Y.-G., Gillings, M., Simonet, P., Stekel, D., Banwart, S., and Penuelas, J. (2017). Microbial mass
1332 movements. *Science*, 357(6356):1099–1100.

1333 8 Contributing Members of the MetaSUB Consortium

1334 Marcos Abraao, Muhammad Afaq, Ireen Alam, Gabriela E Albuquerque, Kalyn Ali, Lucia E Alvarado-
1335 Arnez, Sarh Aly, Jennifer Amachee, Maria G. Amorim, Majelia Ampadu, Nala An, Núria Andreu So-
1336 mavilla, Michael Angelov, Verónica Antelo, Catharine Aquino, Mayra Arauco Livia, Luiza F Araujo,
1337 Jenny Arevalo, Lucia Elena Alvarado Arnez, Fernanda Arredondo, Matthew Arthur, Sadaf Ayaz, Silva
1338 Baburyan, Abd-Manaaf Bakere, Katrin Bakhil, Thais F. Bartelli, Kevin Becher, Joseph Benson, Denis
1339 Bertrand, Silvia Beurmann, Christina Black, Brittany Blyther, Bazartseren Boldgiv, Gabriela P Branco,
1340 Christian Brion, Paulina Buczanska, Catherine M Burke, Irvind Buttar, Jalia Bynoe, Sven Bönigk, Kari
1341 O Bøifot, Hiram Caballero, Alessandra Carbone, Anais Cardenas, Ana V Castro, Ana Valeria B Castro,
1342 Astred Castro, Simone Cawthorne, Jonathan Cedillo, Salama Chaker, Allison Chan, Anastasia I Chas-
1343 api, Gregory Chem, Jenn-Wei Chen, Michelle Chen, Xiaoqing Chen, Ariel Chernomoretz, Daisy Cheung,
1344 Diana Chicas, Hira Choudhry, Carl Chrispin, Kianna Ciaramella, Jake Cohen, David A Coil, Colleen
1345 Conger, Ana F. Costa, Delisia Cuebas, Aaron E Darling, Pujita Das, Lucinda B Davenport, Laurent
1346 David, Gargi Dayama, Paola F De Sessions, Chris K Deng, Monika Devi, Felipe S Dezem, Sonia Dorado,
1347 LaShonda Dorsey, Steven Du, Alexandra Dutan, Naya Eady, Stephen Eduard Boja Ruiz, Jonathan A
1348 Eisen, Miar Elaskandrany, Lennard Epping, Juan P Escalera-Antezana, Iqra Faiz, Luce Fan, Nadine
1349 Farhat, Kelly French, Skye Felice, Laís Pereira Ferreira, Gabriel Figueroa, Denisse Flores, Marcos AS
1350 Fonseca, Jonathan Fook, Aaishah Francis, Pablo Fresia, Jacob Friedman, Jaime J Fuentes, Josephine
1351 Galipon, Laura Garcia, Annie Geiger, Samuel M Gerner, Dao Phuong Giang, Matías Giménez, Donato
1352 Giovannelli, Dedan Githae, Samantha Goldman, Gaston H Gonnet, Juana Gonzalez, Irene González
1353 Navarrete, Tranette Gregory, Felix Hartkopf, Arya Hawkins-Zafarnia, Nur Hazlin Hazrin-Chong, Tam-
1354 era Henry, Samuel Hernandez, David Hess-Homeier, Yui Him Lo, Lauren E Hittle, Nghiem Xuan Hoan,
1355 Irene Hoxie, Elizabeth Humphries, Shaikh B Iqbal, Riham Islam, Sharah Islam, Takayuki Ito, Tomislav
1356 Ivankovic, Sarah Jackson, JoAnn Jacobs, Esmeralda Jiminez, Ayantu Jinfessa, Takema Kajita, Amrit
1357 Kaur, Fernanda de Souza Gomes Kehdy, Vedbar S Khadka, Shaira Khan, Michelle Ki, Gina Kim, Hyung
1358 Jun Kim, Sangwan Kim, Ryan J King, Kaymisha Knights, Ellen Koag, Nadezhda Kobko-Litskevitch,
1359 Giuseppe KoLoMonaco, Michael Kozhar, Nanami Kubota, Sheelta S Kumar, Lawrence Kwong, Rachel
1360 Kwong, Ingrid Lafontaine, Manolo Laiola, Isha Lamba, Hyunjung Lee, Lucy Lee, Yunmi Lee, Emily
1361 Leong, Marcus H Y Leung, Chenhao Li, Weijun Liang, Moses Lin, Yan Ling Wong, Priscilla Lisboa,
1362 Anna Litskevitch, Tracy Liu, Sonia Losim, Jennifer Lu, Simona Lysakova, Gustavo Adolfo Malca Salas,
1363 Denisse Maldonado, Krizzy Mallari, Tathiane M Malta, Maliha Mamun, Yuk Man Tang, Sonia Mari-
1364 novic, Brunna Marques, Nicole Mathews, Yuri Matsuzaki, Madelyn May, Elias McComb, Adiel Melamed,
1365 Wayne Menary, Ambar Mendez, Katterinne N Mendez, Irene Meng, Ajay Menon, Mark Menor, Nancy
1366 Merino, Cem Meydan, Karishma Miah, Tanja Miketic, Eric Minwei Liu, Wilson Miranda, Athena Mit-
1367 sios, Natasha Mohan, Mohammed Mohsin, Karobi Moitra, Laura Molina, Eftar Moniruzzaman, Sookwon
1368 Moon, Isabelle de Oliveira Moraes, Maritza S Mosella, Maritza S Mosella, Josef W Moser, Christopher
1369 Mozsary, Amanda L Muehlbauer, Oasima Muner, Muntaha Munia, Naimah Munim, Tatjana Mustac,
1370 Kaung Myat San, Areeg Naeem, Mayuko Nakagawa, Masaki Nasu, Bryan Nazario, Narasimha Rao
1371 Nedunuri, Aida Nesimi, Aida Nesimi, Gloria Nguyen, Hosna Noorzi, Avigdor Nosrati, Houtan Noush-
1372 mehr, Diana N. Nunes, Kathryn O'Brien, Niamh B O'Hara, Gabriella Oken, Rantimi A Olawoyin, Kiara
1373 Olmeda, Itunu A Oluwadare, Tolulope Oluwadare, Jenessa Orpilla, Jacqueline Orrego, Melissa Ortega,
1374 Princess Osma, Israel O Osuolale, Oluwatosin M Osuolale, Rachid Ounit, Christos A Ouzounis, Sub-
1375 hamitra Pakrashi, Rachel Paras, Andrea Patrignani, Ante Peros, Sabrina Persaud, Anisia Peters, Robert
1376 A Petit III, Adam Phillips, Lisbeth Pineda, Alketa Plaku, Alma Plaku, Brianna Pompa-Hogan, Max
1377 Priestman, Bharath Prithiviraj, Sambhawa Priya, Phanthira Pugdeethosal, Benjamin Pulatov, Angelika
1378 Pupiec, Tao Qing, Saher Rahiel, Savlatjon Rahmatulloev, Kannan Rajendran, Aneisa Ramcharan, Adan
1379 Ramirez-Rojas, Shahryar Rana, Prashanthi Ratnanandan, Timothy D Read, Hugues Richard, Alexis
1380 Rivera, Michelle Rivera, Alessandro Robertiello, Courtney Robinson, Anyelic Rosario, Kaitlan Russell,
1381 Timothy Ryan Donahoe, Krista Ryon, Thais S Sabedot, Thais S Sabedot, Mahfuza Sabina, Cecilia
1382 Salazar, Jorge Sanchez, Ryan Sankar, Paulo Thiago de Souza Santos, Zulena Saravi, Thomas Saw Aung,
1383 Thomas Saw Aung, Nowshin Sayara, Steffen Schaaf, Anna-Lena M Schinke, Ralph Schlapbach, Jason R
1384 Schriml, Felipe Segato, Marianna S. Serpa, Heba Shaaban, Maheen Shakil, Hyenah Shim, Yuh Shiwa,
1385 Shaleni K Singh, Eunice So, Camila Souza, Jason Sperry, Kiyoshi Sukanuma, Hamood Suliman, Jill
1386 Sullivan, Jill Sullivan, Fumie Takahara, Isabella K Takenaka, Anyi Tang, Emilio Tarcitano, Mahdi Taye,
1387 Alexis Terrero, Andrew M Thomas, Sade Thomas, Masaru Tomita, Xinzhao Tong, Jennifer M Tran,
1388 Catalina Truong, Stefan I Tsonev, Kazutoshi Tsuda, Michelle Tuz, Carmen Urgiles, Brandon Valentine,
1389 Hitler Francois Vasquez Arevalo, Valeria Ventorino, Patricia Vera-Wolf, Sierra Vincent, Renee Vivancos-

1390 Koopman, Andrew Wan, Cindy Wang, Samuel Weekes, Xiao Wen Cai, Johannes Werner, David Westfall,
1391 Lothar H Wieler, Michelle Williams, Silver A Wolf, Brian Wong, Tyler Wong, Hyun Woo Joo, Rasheena
1392 Wright, Ryota Yamanaka, Jingcheng Yang, Hirokazu Yano, George C Yeh, Tsoi Ying Lai, Laraib Zafar,
1393 Amy Zhang, Shu Zhang, Yang Zhang, Yuanting Zheng,

1394 9 Supplemental Materials

1395 9.1 Supplemental Methods

1396 9.1.1 DNA Extraction from Isohelix swabs using ZymoBiomics 96 MagBead

1397 The Isohelix swab head and the entire 400 μ l of DNA/RNA Shield-solubilized sample were transferred
1398 into ZR BashingBead Lysis Tubes (0.1 & 0.5 mm) (Cat# S6012-50) to which an additional 600 μ l of
1399 DNA/RNA Shield was added. Mechanical lysis using bead beating was performed on a maximum of 18
1400 samples simultaneously using the Scientific Industries Vortex-Genie 2 with Horizontal-(24) Microtube
1401 Adapter (Cat # SI-0236 and SI-H524) at maximum power for 40 minutes. The resulting lysate (400 μ l)
1402 was transferred to NuncTM 96-Well Polypropylene DeepWell Storage Plates (Cat # 278743), followed
1403 by DNA extraction using the ZymoBIOMICS 96 MagBead Kit (Lysis Tubes) (Catalog # D4308) on the
1404 Hamilton Star according to manufacturer instructions.

1405 9.1.2 DNA extraction from Copan swabs using MoBio PowerSoil®DNA

1406 Droplets in the Copan Liquid Amies Elution Swab tube (ESwab, Copan Diagnostics, Cat.:480C (<http://goo.gl/8a9uCP>)) were spun down at 300rpm/1min. Next, the swab pad was transferred to a Mo-
1407 Bio PowerSoil®DNA vial containing beads using sterile scissors, which we sterilized by flaming with
1408 100% ethanol. The remaining 400-500 μ l Copan Amines liquid has been transferred into an Eppen-
1409 dorf tube and centrifuged at full speed to collect bacteria and debris in a pellet. The pellet was
1410 finally transferred to the same MoBio PowerSoil®DNA vial also containing the corresponding swab
1411 pad. MoBio PowerSoil®DNA Isolation Kit, Cat.:12888-100 (<https://www.qiagen.com/us/resources/resourcedetail?id=5c00f8e4-c9f5-4544-94fa-653a5b2a6373&lang=en>) was used according to man-
1412 ufacturer's instructions except for the following modifications:
1413

1414 Both swab and pellet have been re-suspended with 135 μ l C1 buffer (MoBio PowerSoil®DNA). Sample
1415 homogenization was performed using either TissueLyser II (Qiagen) with 2 cycles of 3 minutes at 30Hz
1416 (<https://goo.gl/hBg8Lb>), or using the Vortex-Genie 2 (Vortex Catalog #13000-V1-24) adaptor and
1417 vortex at maximum speed for 10 minutes. The sequencing centers in Stockholm and Shanghai used
1418 different procedures for homogenization. Stockholm used a method based on MPI FASTPREP, while
1419 Shanghai added 0.6 grams of 100-micron zirconium-silica beads to 2ml tubes containing the swab pad
1420 and the media, followed by bead beating for 1 min. The eluted samples have been additionally purified
1421 and concentrated by Beckmann Coulter Agencourt AMPure XP (Cat.:A63881) purification (1.8X) and
1422 eluted into 12 μ l - 50 μ l elution buffer. Subsequently, DNA was quantified using Qubit® dsDNA HS
1423 Assay (Catalog #Q32854).
1424

1425 9.1.3 DNA extraction using Promega Maxwell

1426 We added 300 μ l Promega Maxwell Lysis buffer and 30 μ l Promega Maxwell Proteinase K to Copan swab
1427 heads or Isohelix swab heads and transferred the swabs back to their respective collection tube. For lysis
1428 the sample tubes containing the swabs and the lysis mixture were incubated in a water bath at 54C for
1429 30min. Following lysis, Copan swab heads were cut off their stem using sterile scissors and transferred
1430 into a filter tube (Promega V4745). The filter containing the swab was placed into a 2ml Eppendorf tube
1431 and spun down at full speed for 2min. This step is necessary since the Copan swab material consists of a
1432 foam, which harbors the main liquid containing the extracted DNA. Next, the eluate has been combined
1433 with the corresponding sample tube media and added to the first well of the cartridge (Maxwell® RSC
1434 Buccal Swab kit AS1640). Cartridges were processed using the Maxwell® RSC Instrument (AS4500)
1435 following the manufacturer's default instructions. Extracted DNA was eluted in 50 μ l Promega Elution
1436 Buffer and stored at -80C.

1437 The matrix tubes containing the Isohelix swabs and the lysis buffer have been vortexed at full speed for
1438 one minute. The Isohelix swab head material is a non-porous material, which allows for easy collection of
1439 the lysate. We transferred the lysate to the first cartridge of the Maxwell® RSC Blood DNA KitAS1400
1440 using syringes (BD 3 mL Syringes with 18G x 1.5" Luer Lok Tip Blunt Fill Needles) and ran the Promega
1441 Maxwell using the Blood program according to manufacturer's instructions. Samples were subsequently
1442 eluted in 50 μ l elution buffer and stored at -80C.

Table S1: Sample Counts

Region	project city	Pilot	CSD16	CSD17	Other	Total
Control	Background Control	0.0	40	0	0.0	40
	Lab Control	0.0	20	6	0.0	26
	Positive Control	0.0	33	6	0.0	39
East Asia	Region Total	26.0	1297	0	34.0	1357
	Hanoi	0.0	16	0	0.0	16
	Hong Kong	0.0	712	0	12.0	724
	Kuala Lumpur	0.0	30	0	0.0	30
	Sendai	0.0	32	0	0.0	32
	Seoul	0.0	80	0	12.0	92
	Shanghai	0.0	0	0	10.0	10
	Singapore	0.0	192	0	0.0	192
	Taipei	0.0	94	0	0.0	94
	Tokyo	26.0	132	0	0.0	158
	Yamaguchi	0.0	9	0	0.0	9
	Europe	Region Total	310.0	939	1	177.0
Barcelona		99.0	0	0	25.0	124
Belfast		0.0	5	0	0.0	5
Berlin		55.0	1	0	0.0	56
Birmingham		0.0	5	1	0.0	6
Bradford		0.0	4	0	0.0	4
Bury		0.0	6	0	0.0	6
Eastbourne		0.0	6	0	0.0	6
Eden		0.0	5	0	0.0	5
Edinburgh		0.0	6	0	0.0	6
Islington		0.0	5	0	0.0	5
Jaywick		0.0	6	0	0.0	6
Kensington		0.0	6	0	0.0	6
Kyiv		0.0	97	0	0.0	97
Lands End		0.0	5	0	0.0	5
Lisbon		60.0	0	0	28.0	88
London		0.0	534	0	0.0	534
Marseille		96.0	16	0	0.0	112
Naples		0.0	16	0	0.0	16
Newcastle		0.0	5	0	0.0	5
Oslo		0.0	16	0	12.0	28
Paris		0.0	16	0	0.0	16
Porto	0.0	0	0	112.0	112	
Sofia	0.0	16	0	0.0	16	
Stockholm	0.0	62	0	0.0	62	
Swansea	0.0	6	0	0.0	6	
Vienna	0.0	16	0	0.0	16	
Zurich	0.0	79	0	0.0	79	
Middle East	Region Total	100.0	15	0	0.0	115
	Doha	100.0	15	0	0.0	115

Table S1: Sample Counts Cont.

continent	project city	Pilot	CSD16	CSD17	Other	Total
North America	Region Total	284.0	371	276	28.0	959
	Baltimore	0.0	23	0	0.0	23
	Denver	24.0	23	0	0.0	47
	Fairbanks	141.0	0	0	0.0	141
	Mexico City	0.0	0	0	10.0	10
	Minneapolis	0.0	16	0	0.0	16
	New York City	103.0	279	276	0.0	658
	Sacramento	16.0	0	0	18.0	34
	San Francisco	0.0	30	0	0.0	30
	Oceania	Region Total	94.0	32	0	0.0
Auckland		16.0	0	0	0.0	16
Brisbane		0.0	16	0	0.0	16
Hamilton		16.0	0	0	0.0	16
Honolulu		0.0	16	0	0.0	16
Sydney		62.0	0	0	0.0	62
South America		Region Total	44.0	199	68	20.0
	Bogota	17.0	0	0	0.0	17
	Montevideo	0.0	0	0	20.0	20
	Ribeirao Preto	0.0	93	0	0.0	93
	Rio De Janeiro	0.0	77	68	0.0	145
	Santiago	27.0	0	0	0.0	27
	Sao Paulo	0.0	29	0	0.0	29
	Sub Saharan Africa	Region Total	116.0	192	0	0.0
Ilorin		90.0	134	0	0.0	224
Offa		26.0	58	0	0.0	84

Table S2: Covariate Variance. The sample variance that can be explained by each factor, in isolation.

Factor	Variance Explained
City	19%
City Population Density	0%
City Ave June Temp	4%
City Elevation	2%
Coastal City	1%
Surface Material	4%
Koppen Climate Classification	8%
Setting	2%
Above/Below Ground	7%
Continent	11%

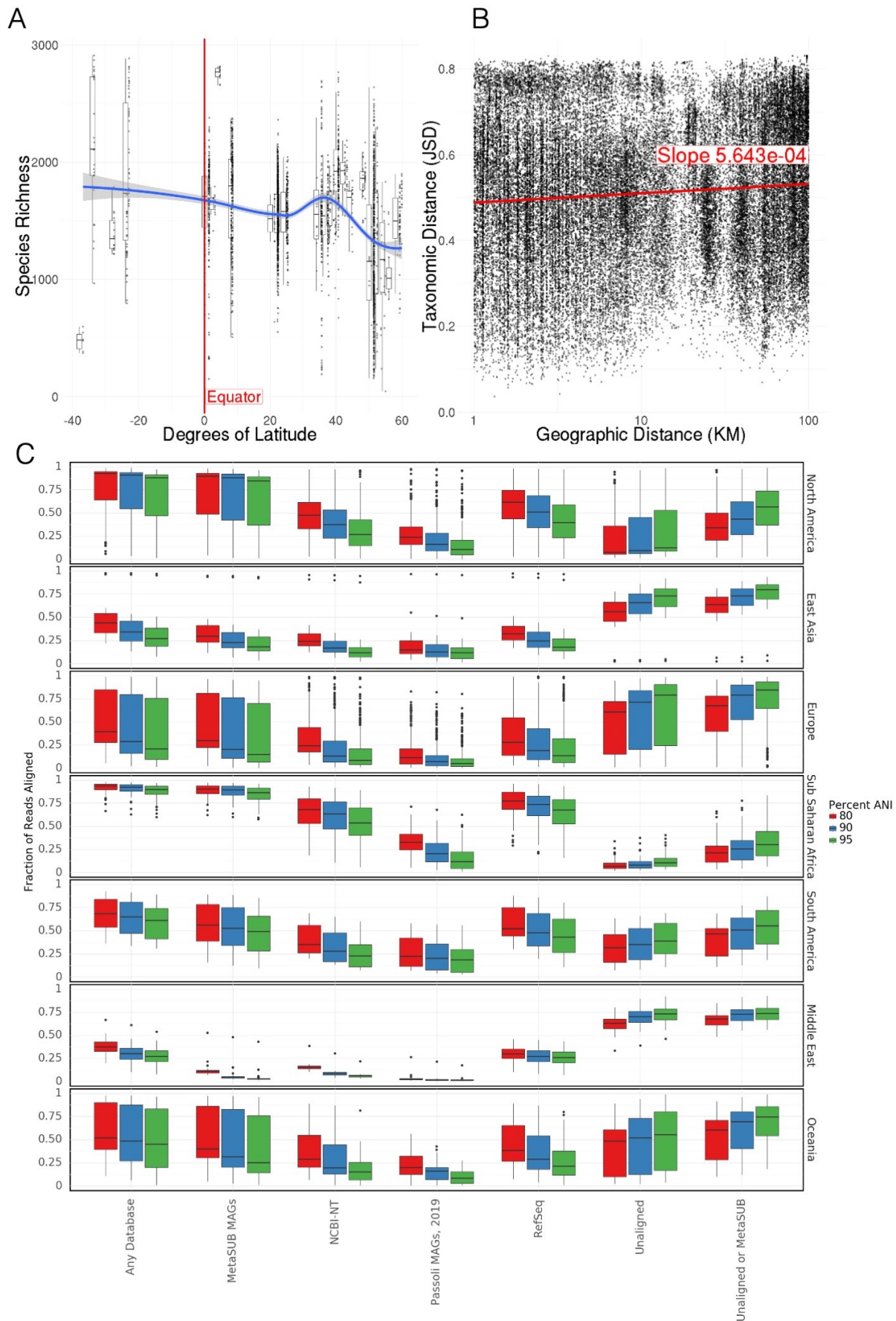


Figure S1: Ecological relationships with taxa. A) Correlation between species richness and latitude. Richness decreases significantly with latitude B) Neighbourhood effect. Taxonomic distance weakly correlates with geographic distance within cities. C) Fraction of reads assigned to different databases by BLAST for each region, at different levels of average nucleotide identity

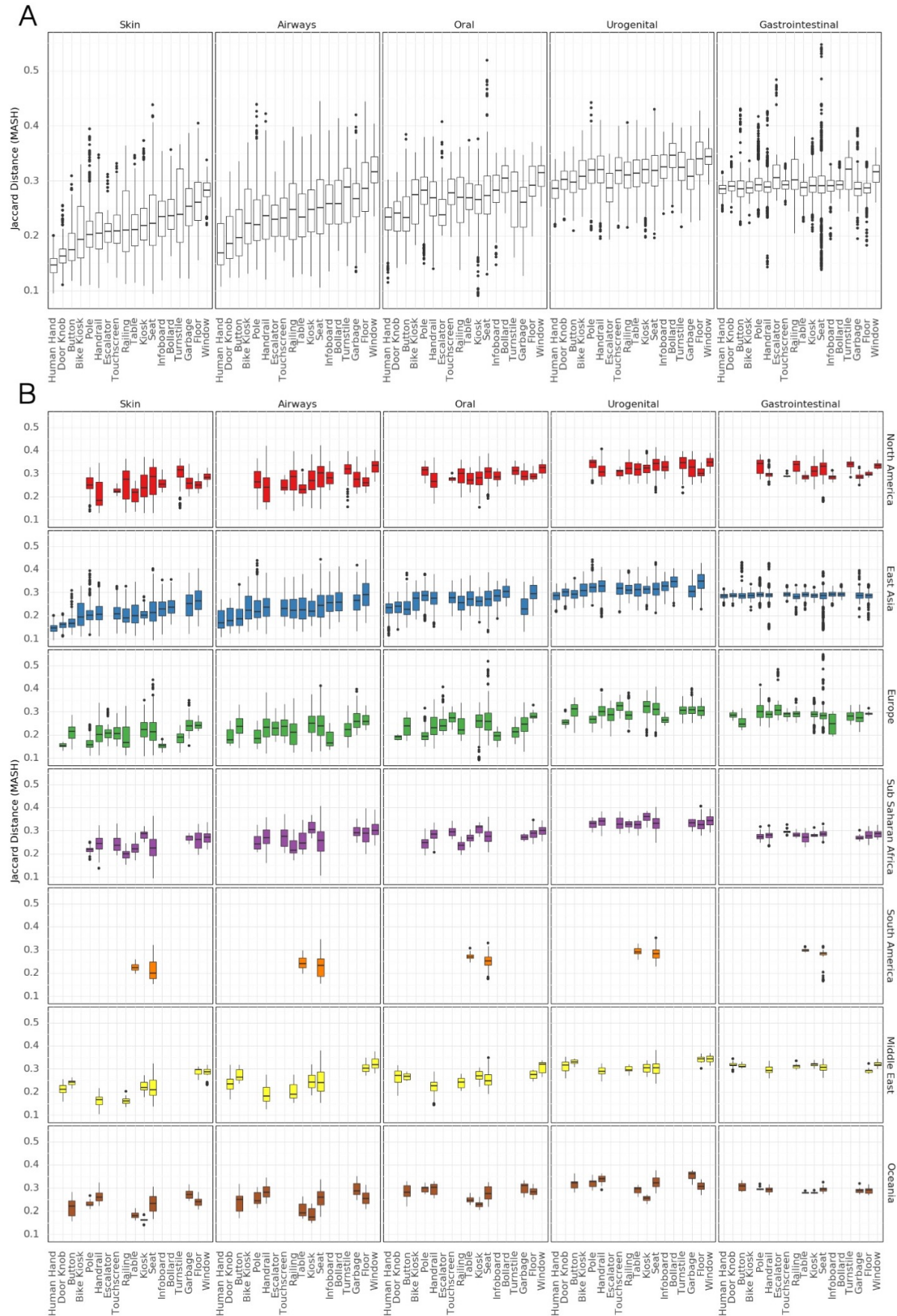


Figure S2: Comparison to Human Microbiome Project. A) Jaccard similarity of MASH indices to HMP samples for different surface types. B) Jaccard similarity of MASH indices to HMP samples for different surface types by region.

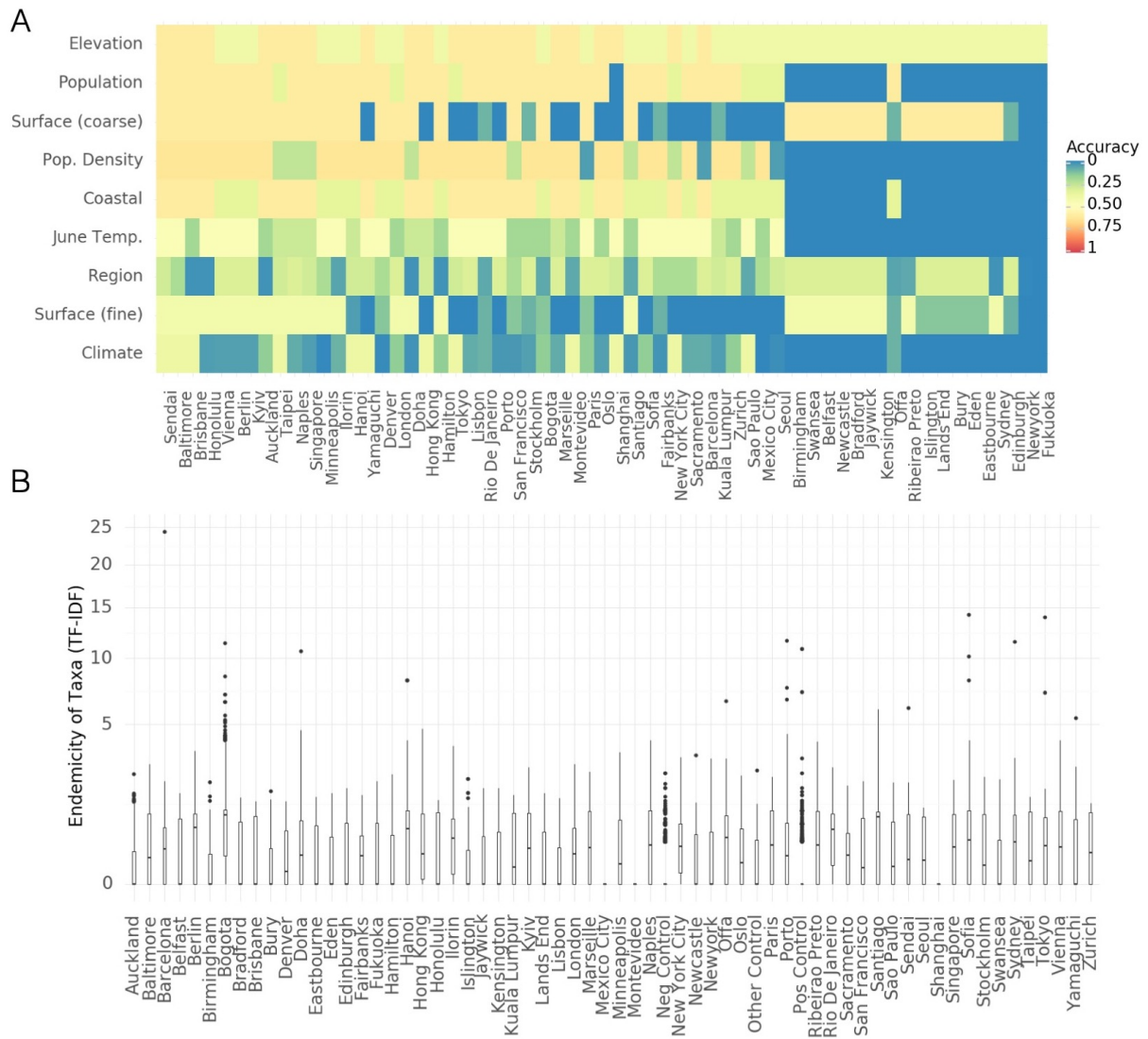


Figure S3: Microbial Signatures, supplemental. A) Classification accuracy that would be achieved by a random model predicting features (rows) for held out cities (columns) B) Endemicity Score (Term Frequency Inverse Document Frequency) for taxa in cities

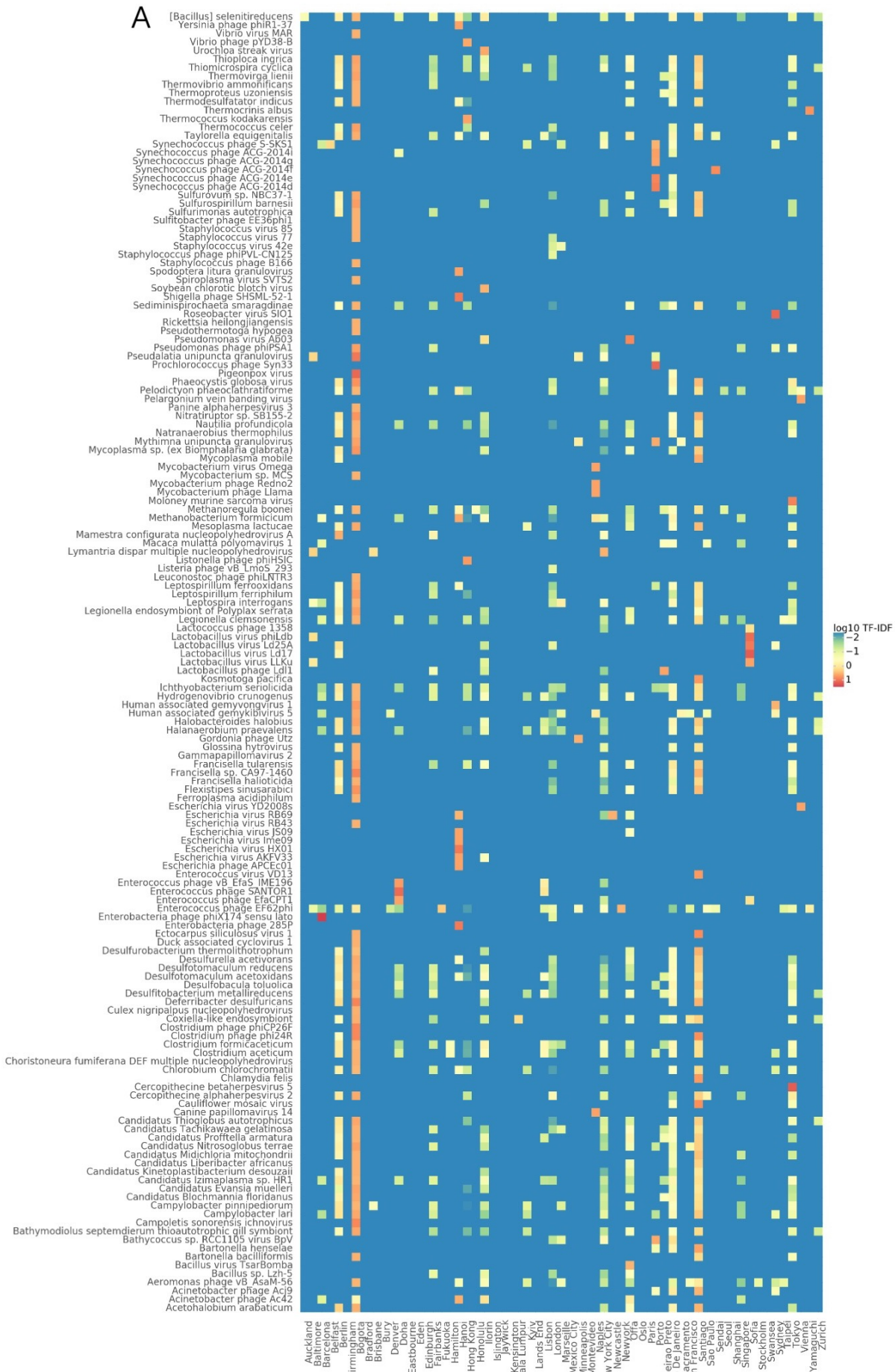


Figure S4: Endemicity scores of particular taxa. A) Heatmap showing the endemicity scores (term-frequency inverse document frequency) for taxa in different cities. This table is filtered to show only taxa with high endemicity scores in at least one city.

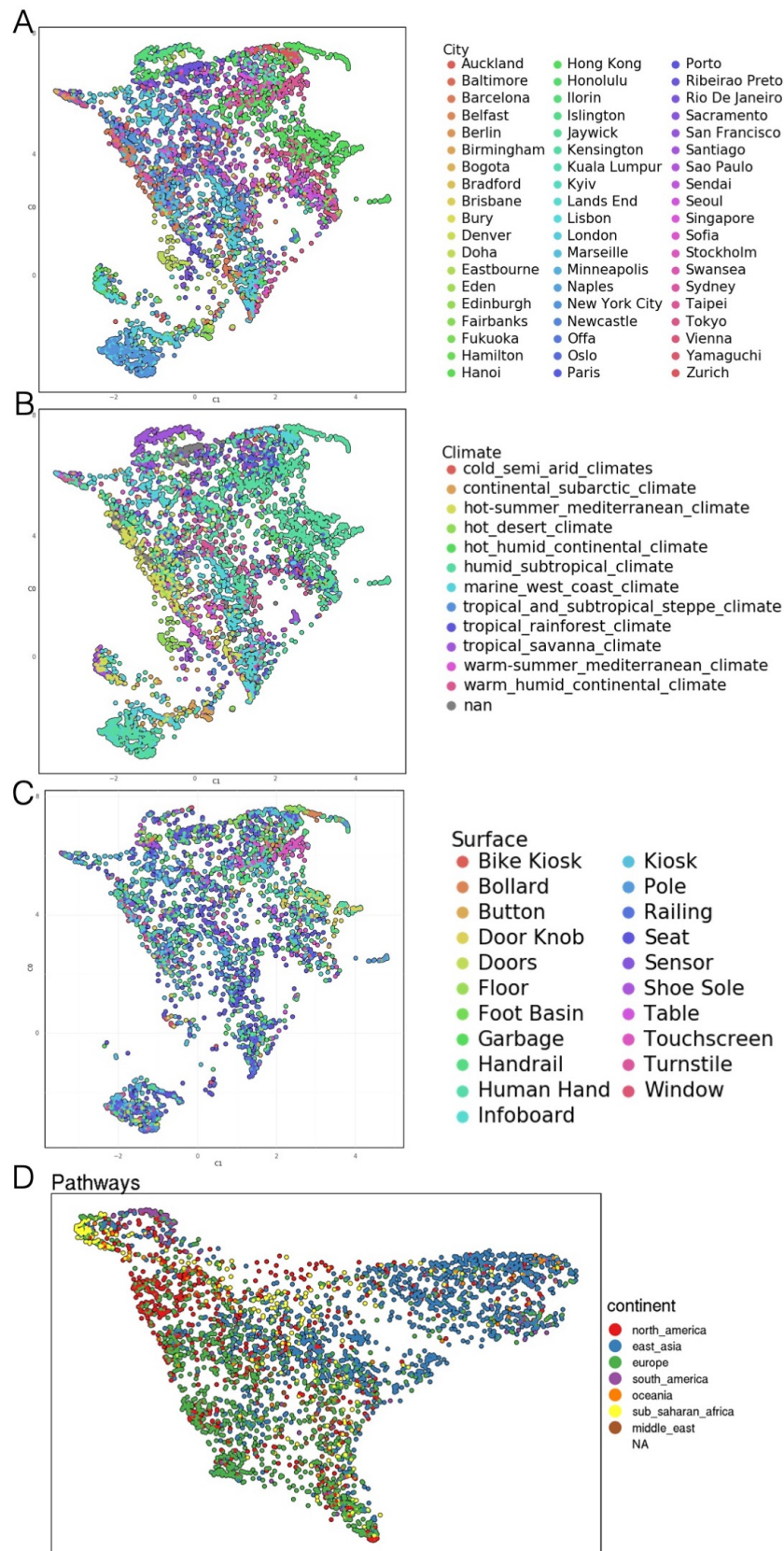


Figure S5: A) UMAP of taxonomic profiles colored by city B) UMAP of taxonomic profiles colored by climate classification C) UMAP of taxonomic profiles colored by surface type D) UMAP of functional profiles colored by region

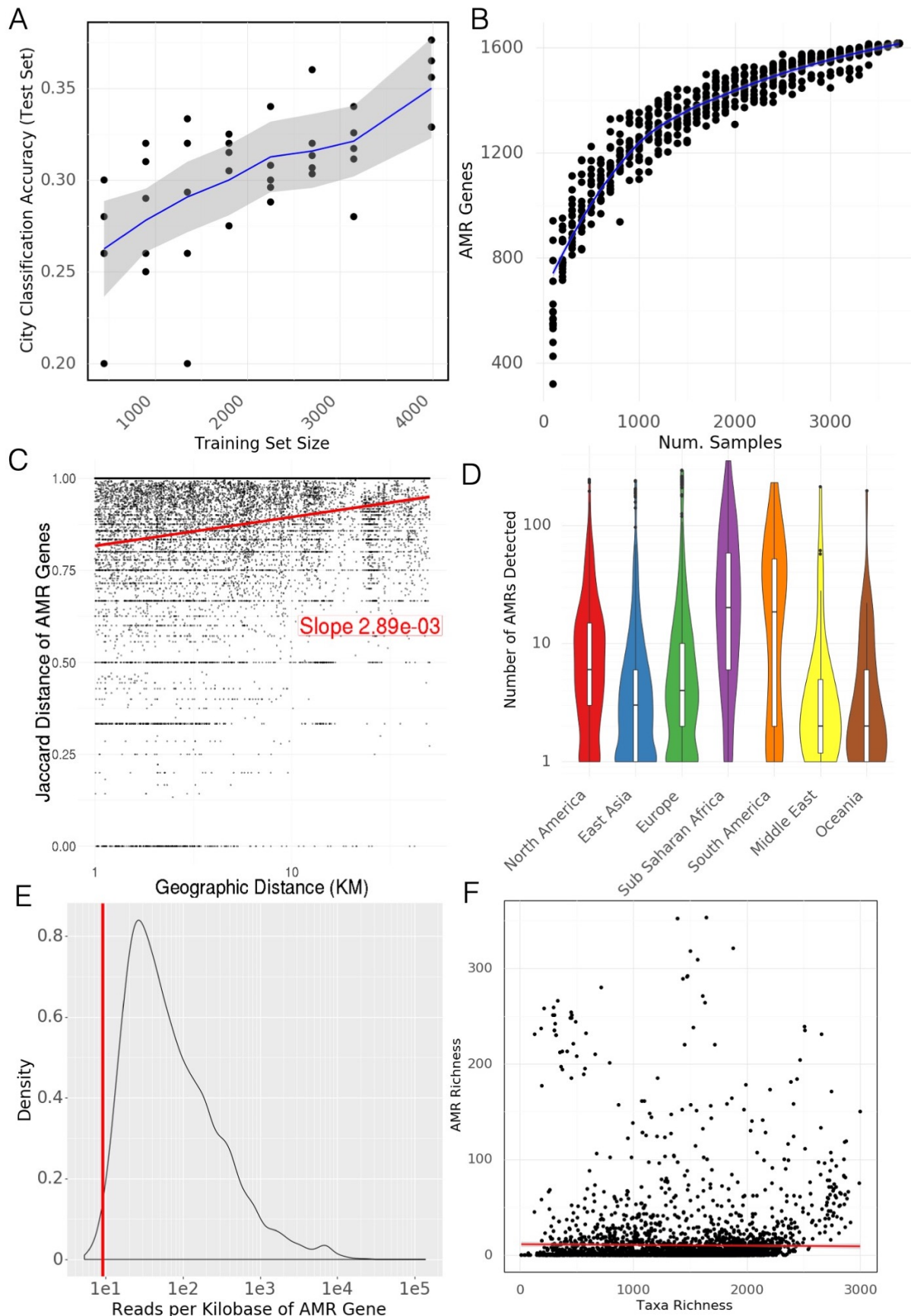


Figure S6: Antimicrobial Resistance Genes, supplemental. A) Classification accuracy of a random forest model predicting city labels for held out samples from antimicrobial resistance genes. B) Rarefaction analysis of antimicrobial resistance genes. Curve does not flatten suggesting we would identify more AMR genes with more samples. C) Neighbourhood effect. Jaccard distance of AMR genes weakly correlates with geographic distance within cities. D) Number of AMR genes detected for samples in each region. E) Distribution of reads per gene (normalized by kilobases of gene length) for AMR gene calls. The vertical red line indicates that 99% of AMR genes have more than 9.06 reads per kilobase and would still be called at a lower read depth.

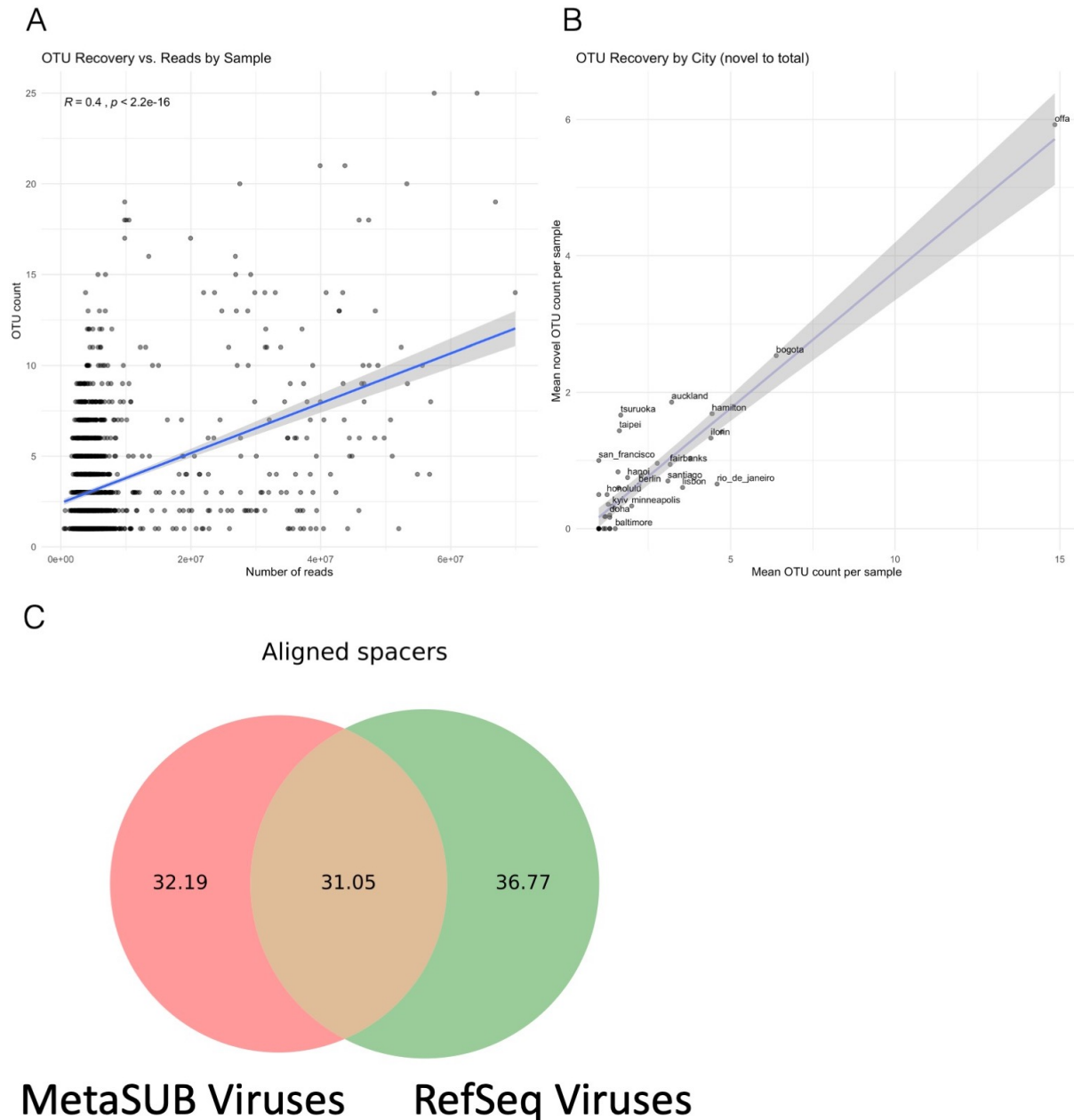


Figure S7: Novel biology, supplemental. A) Relation of read depth to the number of identified bacterial Metagenome Assembled Genomes (MAGs) in a sample. B) Discovery rate for bacterial MAGs in each city. C) Total fraction of CRISPR spacers aligned to MetaSUB viral MAGs and viral genomes in RefSeq.

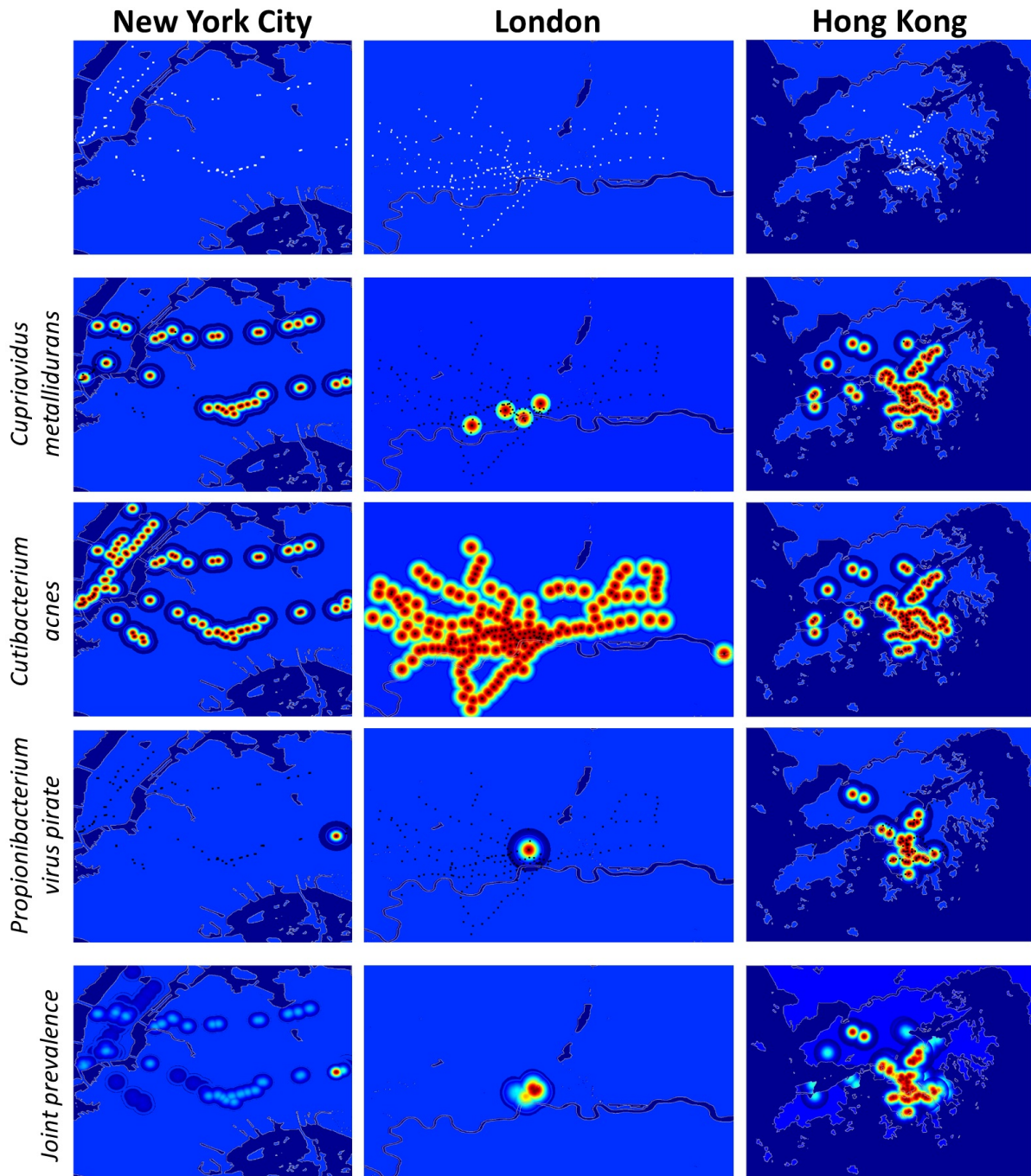


Figure S8: Example Geographic taxonomic Distributions. Distributions of taxa were estimated by fitting Gaussian distributions to sampling locations where the taxa was found with standard deviations based on the geographic distance between observations. Top Row) Sampling sites in three major cities Rows 2-4) Estimated distribution of different example species in major cities Row 5) Estimated distribution of three species together in major cities

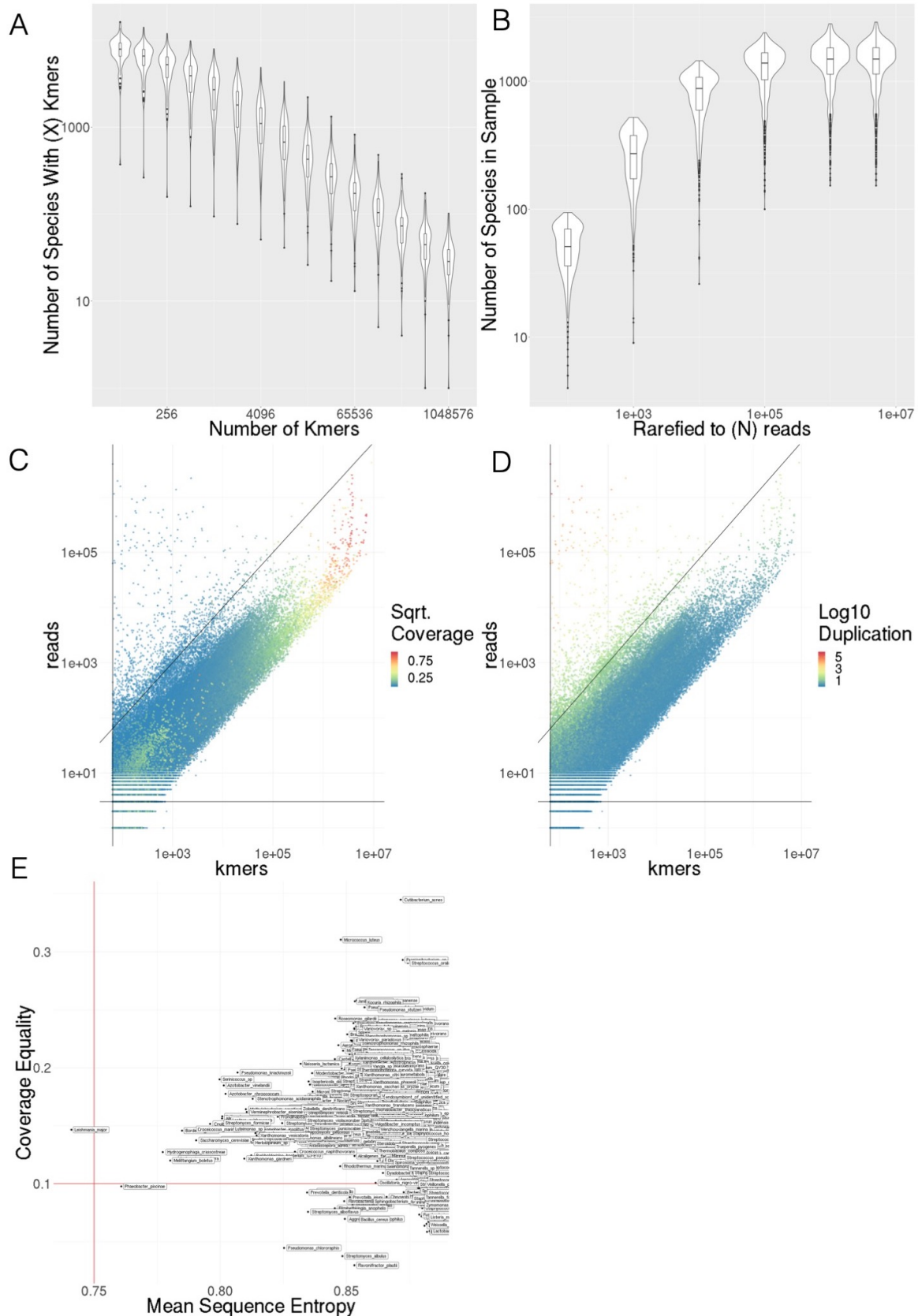


Figure S9: A) Number of species detected as k -mer threshold increases for 100 randomly selected samples B) Number of species detected as number of sub-sampled reads increase C) k -mer counts compared to number of reads for species level annotations in 100 randomly selected samples, colored by coverage of marker k -mer set D) k -mer counts compared to number of reads for species level annotations in 100 randomly selected samples, colored by average duplication of k -mers E) Comparison of Mean Sequence Entropy and Coverage Equality for core and sub-core taxa. Thresholds are shown by red lines.

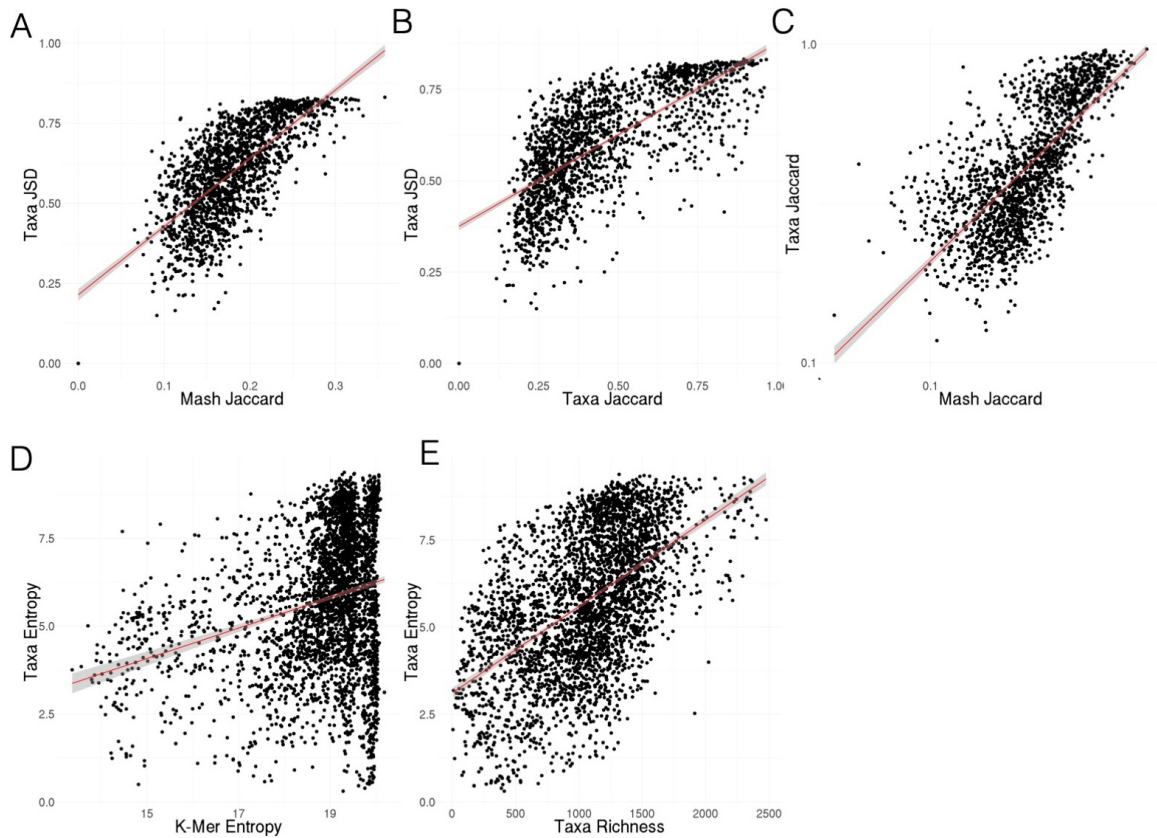


Figure S10: A) Jensen-Shannon Divergence of taxonomic profiles vs MASH Jaccard distance of k -mers B) Jensen-Shannon Divergence of taxonomic profiles vs Jaccard distance of taxonomic profiles. C) Jaccard distance of taxonomic profiles vs MASH Jaccard distance of k -mers D) Shannon's Entropy of taxonomic profiles vs Shannon's Entropy of k -mers E) Taxonomic richness (number of species) vs Shannon's Entropy of taxonomic profiles

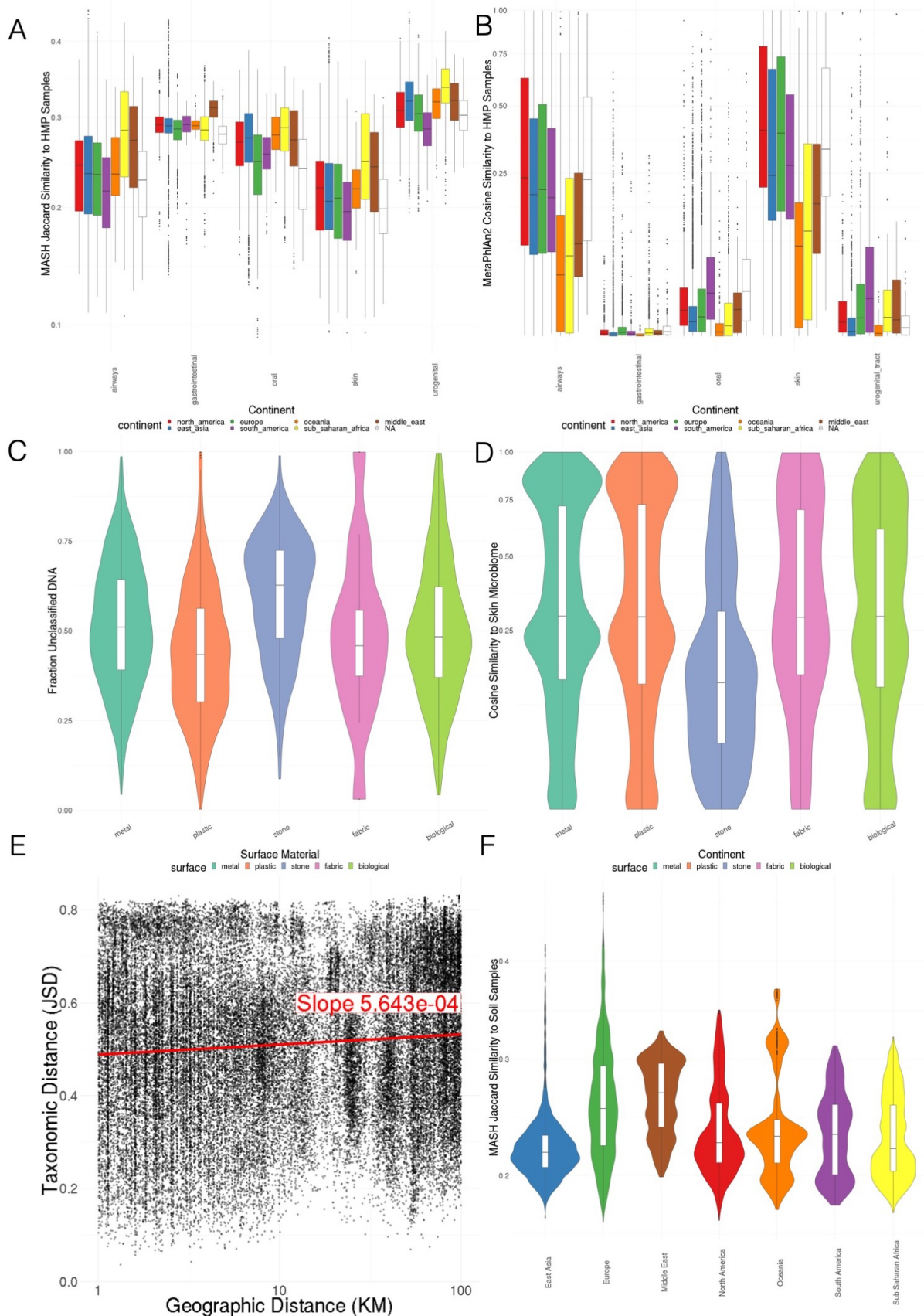


Figure S11: A) MASH *k*-mer Jaccard similarity to representative HMP samples, colored by continent B) MetaPhlan v2.0 cosine similarity to representative HMP samples, colored by continent C) Fraction unclassified DNA by surface material D) Cosine similarity to MetaPhlan v2.0 skin microbiome profile by surface E) Jensen-Shannon distance between pairs of taxonomic profiles vs Geographic Distance F) MASH *k*-mer Jaccard similarity to representative soil samples, colored by continent

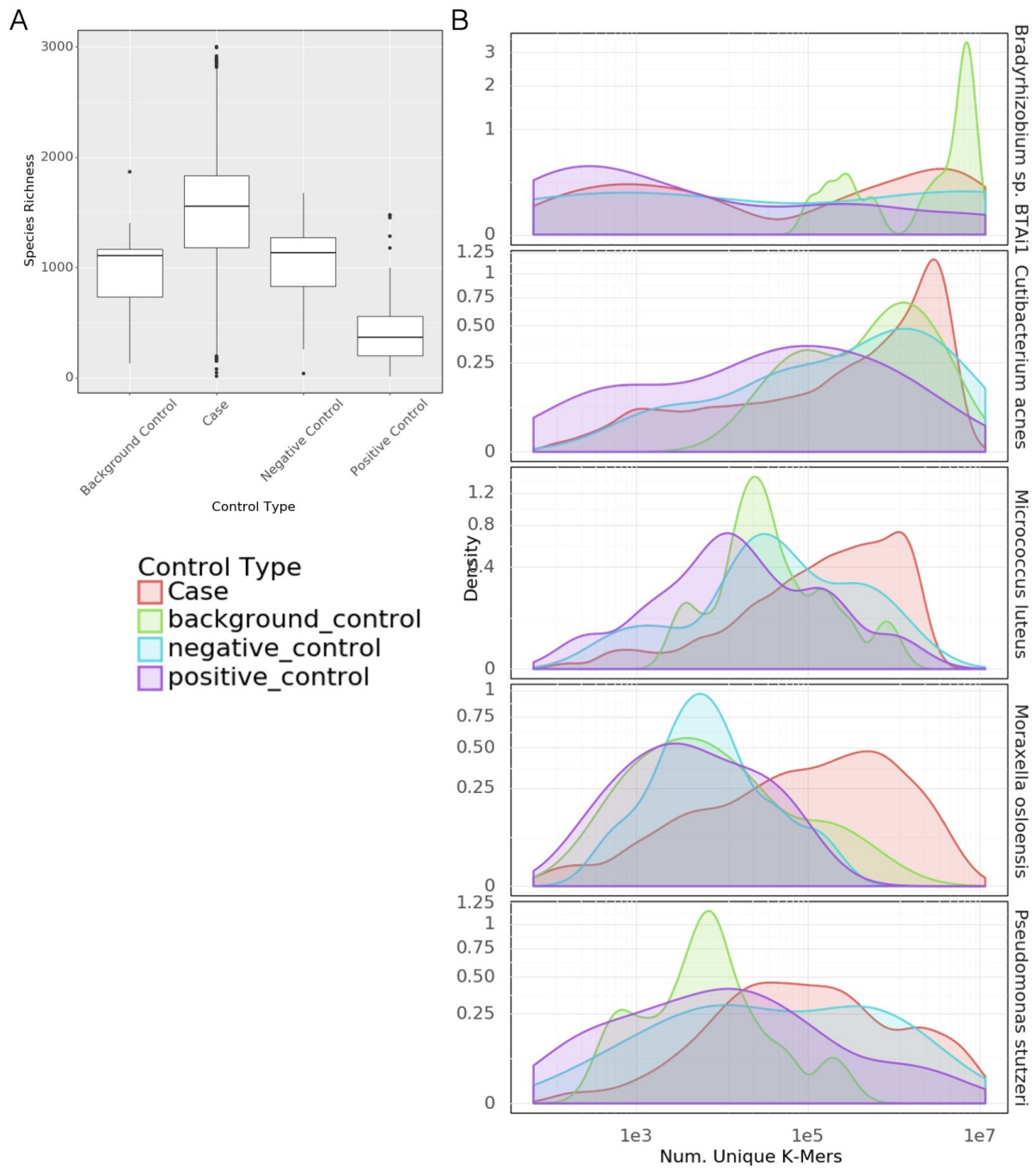


Figure S12: A) Taxonomic Richness in Cases vs. Types of Controls B) Distributions of k -mer counts in control types vs cases for 5 most abundant taxa. k -mer count is a marker of assignment confidence.

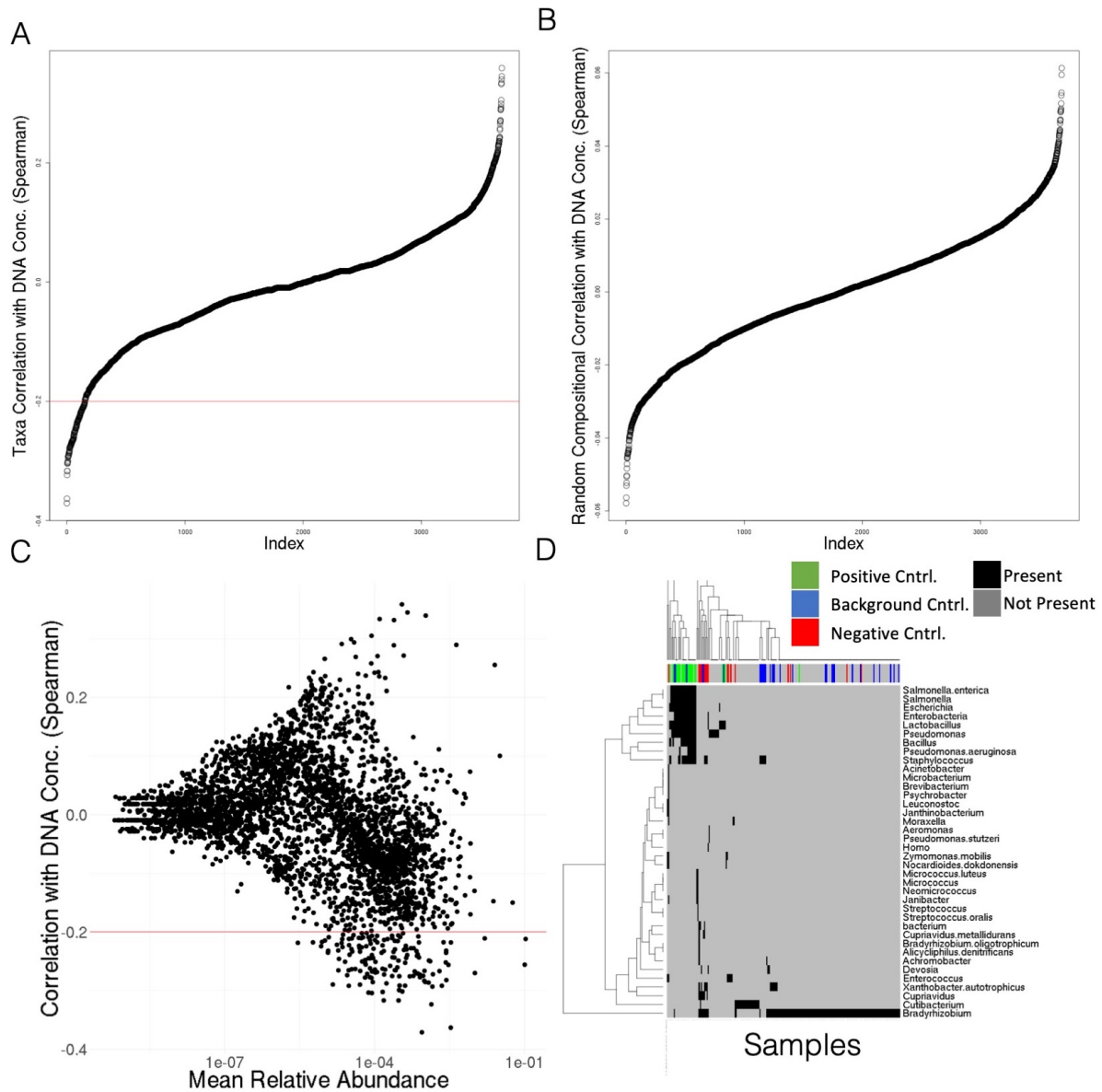


Figure S13: A) Correlation of taxonomic (species) relative abundances with DNA concentration B) Correlation of randomly generated compositional vectors with DNA concentration. Note the same shape but lower magnitude C) Correlation of taxa with DNA Concentration vs the mean relative abundance of that taxa D) Presence (black) absence (grey) heatmap of taxa found in controls and other samples. Colored bar at top, red are negative controls, blue are background, green are positive. Case samples with homology are grey. Case samples without homology to control sequences are not shown.

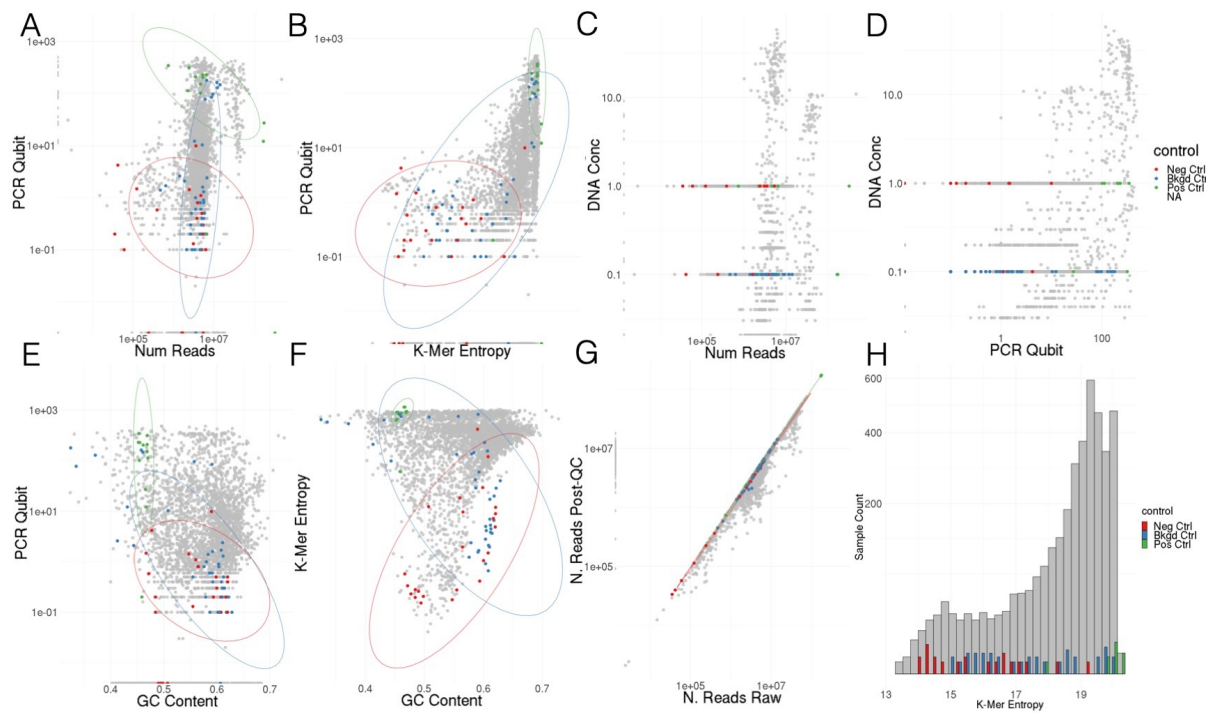


Figure S14: Comparisons of different sequencing quality control metrics with controls marked. A-F) Comparisons of the raw reads, PCR Qubit scores, manually recorded DNA concentrations, *k*-mer Shannon entropy, and GC fraction of quality controlled reads G) Comparison of read counts before and after quality control but before human reads were removed H) Histogram showing the number of samples with different *k*-mer entropies.

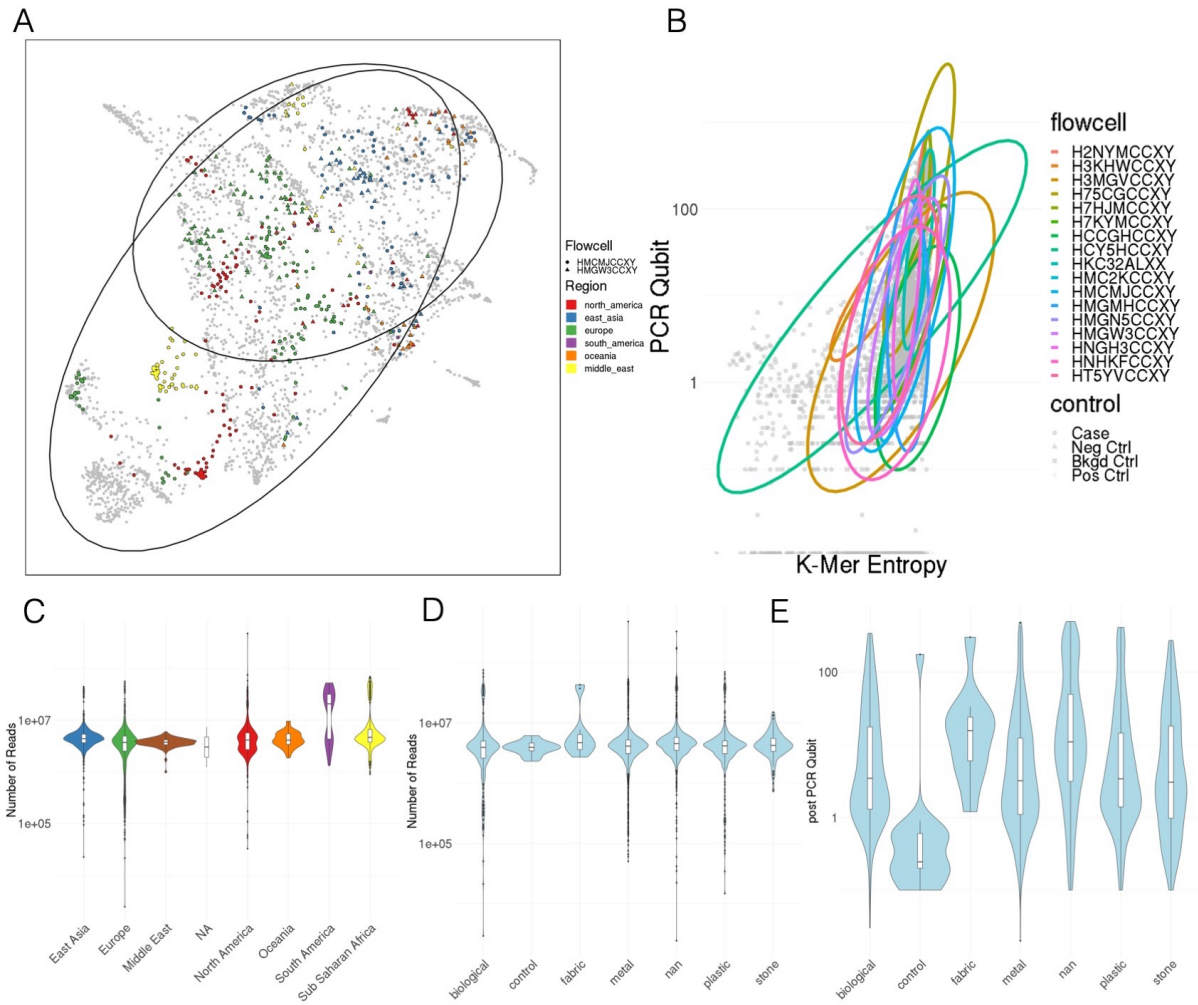


Figure S15: A) UMAP of taxonomic profiles from geographically diverse flowcells B) Flowcells vs quality control metrics C) Number of reads by region D) number of reads by surface material E) PCR Qubit by surface material